GOI ESKOLA
POLITEKNIKOA
ESCUELA
POLITÉCNICA
SUPERIOR

Ph.D. THESIS DISSERTATION

Submitted for the degree of EUROPEAN DOCTOR
in MONDRAGON UNIBERTSITATEA

Experimental and numerical analysis of the elastic behaviour of the TRIP 700 steel for springback predictions

JOSEBA MENDIGUREN

Supervisors:
Dr. Lander Galdos
Dr. Fernando Cortés

October 2012

Preface

Declaration

I hereby declare that this thesis is the result of my own work and that, to the best of my knowledge and belief, no part of this dissertation has previously been submitted for any similar qualification or degree.

Joseba Mendiguren (October 2012)

Copyright and reproduction

I would like to dedicate my thesis to my friend Jagoba.

Acknowledgement

Parece que fue ayer cuando empecé con las derivadas fraccionarias, los *yield criteria*s y los *hardening models*, y cuando nos preguntábamos si esto de la tesis se terminaría algún día o seguiríamos hasta la eternidad leyendo artículos y más artículos, pero finalmente el día parece ser que llega y es momento de mirar hacia atrás y reflexionar.

Estos últimos cuatro años ha habido buenos y malos momentos y he aprendido más sobre muchas cosas que en el resto de mi vida (según Newton supongo que habré aprendido mucho menos de otras...), pero recordaré esta época con felicidad y como una llena de ilusión.

Nunca habría podido llegar a donde me encuentro hoy sin el apoyo de todas esas personas que me han rodeado este tiempo y es a ellos a los que quiero dar las gracias por estar a mi lado.

En primer lugar me gustaría agradecer a mis directores el Dr. Lander Galdos y el Dr. Fernando Cortés por la dedicación personal y profesional a la dirección de esta tesis.

I would like to acknowledge Dr. Gilormini, Dr. Balan and Dr. Trujillo for their disinterested advices to help me in my research work and personal life as researcher. They showed me the importance of the balance between work and personal life.

To Dr. Berveiller and Dr. Weiss for giving me the chance to join their groups and learn from them. Thanks to Nico, David, Busch, Cassie, Jascha, Razane, Danny and others for welcoming me into their lives and helping me with my language issues.

Eskerrik asko tailerreko teknikari taldeari, Gotzon, Iñaki eta Arkaitz eduki duzuen pazientziagatik eta erakutsitako guztiagatik. Eskerrak ere Larraitzeri, laborategian eginiko lanagatik eta Winston zubiari atera diogun probetzu guztiagatik.

Ildo berean, Nagore Elexpururen lana eskertu nahiko nuke. Bertan bera egongo ez balitz ezinezkoa izango litzatekelako egin beharreko burokrazia burutzea.

Agradecer a Eneko y Rafa por todo el apoyo que me han ofrecido y por los trabajos que juntos hemos desarrollado. Felicitar a Elena por su rápida conversión a la mecánica y agradecerle todo el trabajo experimental y numérico que ha realizado en mi ausencia. Igualmente, agradecer al grupo de doctorandos por hacer el día a día tan agradable: Josu, Pablo, Trini, Nagore, Alaitz, Jon Ander (siento no poder poneros a todos) y especialmente a Christian, Aitor, Zurbi, Asier, Haritz y Jon. Muchas gracias a Luis por las interminables horas que hemos pasado juntos trabajando, traduciendo y divagando sobre tensores, interpolaciones y potenciales; ha sido un placer trabajar contigo.

Muchas gracias a toda la "cuadri" y a los chicos (Dani, Zalaka y Lasa) por recibirme y despedirme en cada estancia con tanto cariño y por hacerme sentir querido. Gracias Itzi por tus traducciones de Grünwald-Letnikov, entre otras, y por estar ahí para desahogarme cuando las cosas no iban bien.

Eskerrik asko Maitane, Bego, Aita eta Ama por todo el apoyo que me habéis dado durante todo este tiempo y por todos los favores que me habéis hecho. Sin vosotros no hubiera llegado este momento, eskerrik asko por estar cuando os he necesitado.

Pero sobre todo muchas gracias a Ainhoa por haberme animado a embarcarme en todo esto, por estar a mi lado en los momentos duros en los que gruño, por haberme dejado poner una pizarra en casa y por aguantarme cuando hay algo en mi cabeza que no sale y no existe nada más en ese momento. Benetan eskerrik asko.

Laburpena

Ingurumen legediak errespetatzeko ibilgailuen pisua gutxitze beharra eta merkatuaren lehiakortasuna dela eta, automobil industriak material berriak erabiltzera eta produkzio prozesuak hobetzera behartua izan da.

Gaur egun, elementu finitu bidezko kalkuluak ezinbestekoak bihurtu dira automobil industrian prozesuen konplexutasuna ikertzeko eta hauek optimizatzeko, horrela kostuak gutxitzen direlarik. Elementu finituetako softwareen zehaztasuna industriagatik berretsia izan da. Kode hauek xehetasunez iragarri dezakete landutako materialaren forma eta honetan agertuko diren akatsak prozesuaren konfigurazioaren arabera. Hala eta guztiz ere, materiala landu ostean gertatzen den berreskuratze elastikoa (springback) aurresatea oraindik lortugabeko erronka bat da. Zehaztasun falta honek garestia den test-akats teknika bat burutzera behartzen du industria, behar den forma lortzeko fabrikazio prozesua egokitzen delarik.

Ikerketa lan honen helburu nagusia springbacka iragartzeko erabiltzen diren material modeloak eta teknika matematikoak hobetzea da. Hobetze honen bitartez, gaur egungo prozesuen optimizazioa hobetzea espero da, iragarpenen zehaztasuna areagotuz, modu honetan kostuak murrizteko.

Burututako bibliografia ikerketaren bitartez, materialaren portaera elastikoaren garrantzia springbacka aurreikusteko ezarri egin izan da. Karakterizazio zehatz bat lortzeko trakzio, trakzio-erlaxazio eta trakzio-konpresio saiakuntzak burutu dira.

Portaera elastikoaren zehaztasunaren eragina aztertzeko helburuarekin lege elastiko klasikoaren luzapen bat proposatu da. Luzapen honen bitartez, modelo elastiko berria, portaera lineala zein ez linealak irudikatzeko gai da. Luzapen hau erabiliz zehaztasun desberdineko portaera elastikoak sartu ahal izan dira springback iragarpen simulazioetan.

Modelo elastiko zehatz batek springback iragarpenean egindako hobekuntza zenbakiko modelo desberdinak saiakuntza sartu esperimentalekin alderatuz aztertua izan da. Modelo bakoitzak zehaztasun desberdinekin adierazi du portaera elastikoa, lege

elastikoaren luzapena erabiliz. Iragarpen hauek alderatu dira erresistentzia handiko altzairu baten burututako V-bending saiakuntza baten datu esperimentalekin.

Lan honetatik ondorioztatzen da springback iragarpenentzako portaera elastikoaren irudikapen zehatzaren garrantzia.

Abstract

The demand for lightweight fuel-efficient vehicles and the increasing industrial competitiveness between constructors have motivated the automotive industry to introduce new materials and to reinforce the accuracy of metal forming processes with the aim of reducing costs.

Steady advancements in technology, combined with shortened product cycle times and continual demand to reduce costs, have resulted in the dependence on finite element (FE) codes for the simulation of sheet metal forming processes in the automotive industry. It is generally accepted that commercially available FE programs can be successfully utilised to predict formability and the likelihood of splits and wrinkles, even for complex part geometry.

However, the prediction of the elastically-driven change of shape after forming a product (springback) remains a challenge. This inaccuracy of springback prediction involves a need to use expensive and time consuming experimental try-outs to determine the proper tool geometry and all other parameters which can lead to the desired final shape.

The main objective of the research presented in this thesis has been to improve the current numerical algorithms and material modelling techniques that allow the industry to reach a more accurate springback predictions in sheet metal forming.

The literature review shows the relevance of the elastic behaviour on springback predictions. Therefore, first, a material characterisation of the elastic and elastoplastic behaviours has been performed. Aiming at accurately characterising the material, tensile tests, loading-unloading cyclic tests and tension-compression tests have been carried out.

In order to improve the elastic behaviour model's accuracy, the classical elastic law has been extended. By means of this extension the elastic model is able to represent both linear and non-linear behaviours. Therefore, it has been possible to introduce the

elastic behaviour with different levels of accuracy to predict the springback.

Aiming at analysing the improvement introduced by modelling more accurately the elastic behaviour of the sheet, different simulations have been compared with experimental data. V-free bending experimental tests have been conducted in an AHSS sheet steel. Each numerical simulations has been provided with different particularisation of the extended model, representing each one the elastic behaviour of the material with different levels of accuracy.

The results show the importance of an accurate modelling of the elastic behaviour for springback prediction.

Resumen

La necesidad de aligerar los vehículos para reducir el consumo y el aumento de la competitividad ha motivado a la industria del automóvil a introducir nuevas familias de materiales y reforzar la precisión de los procesos de fabricación con el objetivo de reducir gastos.

La complejidad de los procesos de conformado, junto con la demanda de disminución de costes, ha conllevado a la dependencia de códigos de elementos finitos para la simulación y optimización de los procesos en la industria de la automoción. La precisión de los software comerciales de elementos finitos ha sido ampliamente validada industrialmente. Estos son capaces de predecir con exactitud la conformabilidad, defectos y secciones críticas incluso para piezas complejas.

Sin embargo, la predicción de la recuperación elástica que se produce tras el conformado(también llamado springback) aún es un desafío sin resolver. La inexactitud en la predicción de springbcak conlleva la necesidad de un costoso método de prueba-error para la puesta a punto de los procesos y de los utillajes.

El principal objetivo de esta tesis es la mejora de los algoritmos numéricos y de los modelos de material para la predicción de springback a nivel industrial en el conformado de chapa.

De la revisión bibliográfica se desprende la importancia del comportamiento elástico en la predicción del springback. Con la intención de realizar una caracterización exhaustiva se han llevado a cabo ensayos de tracción, ensayos de ciclos de tracción-relajación y ensayos de tensión-compresión. A fin de analizar la influencia de la precisión del modelo de comportamiento elástico se propone una extensión de la ley elástica clásica. Mediante esta extensión el modelo elástico es capaz de representar tanto comportamientos lineales como no-lineales. Haciendo uso de este nuevo modelo, ha sido posible introducir diferentes niveles de precisión del comportamiento elástico en las simulaciones de springback.

La mejora introducida en la predicción del springbak debida a la precisión del modelo elástico ha sido analizada comparando diferentes modelos numéricos con datos experimentales. Cada modelo ha representado el comportamiento elástico con diferentes precisiones haciendo uso de la extensión de la ley elástica. Estas predicciones han sido comparadas con los datos experimentales de un ensayo de V-bending realizado empleando un acero de alta resistencia.

De este trabajo se concluye la importancia de una representación precisa del comportamiento elástico para predicciones de springback.

Contents

Nomenclature

$\bar{\varepsilon}^{\mathrm{p}}$	Acumulated plastic strain strain
$\bar{r}$	Averaged Lankford coefficient
$\boldsymbol{\alpha}$	State variables
$\boldsymbol{\sigma}$	Stress tensor
$\boldsymbol{\upsigma}$	Vector representation of the stress tensor
$\boldsymbol{\upvarepsilon}$	Vector representation of the strain tensor
$\boldsymbol{\varepsilon}^{\mathrm{e}}$	Elastic strain tensor
$\boldsymbol{\varepsilon}^{\mathrm{p}}$	Plastic strain tensor
$\boldsymbol{\varepsilon}^{\mathrm{t}}$	Total strain tensor
$\boldsymbol{\varphi}$	Extended elastic strain tensor
$\boldsymbol{\xi}$	Spacial variable tensor
$\boldsymbol{F}(\boldsymbol{\varepsilon}^{\mathrm{e}})$	Elasticity tensor function
$\boldsymbol{N}$	Flow vector
$\boldsymbol{s}(\boldsymbol{\sigma})$	Deviatoric stress tensor
$\Delta(\cdot)$	Variation of $(\cdot)$. Increment of $(\cdot)$. Typically, $\Delta(\cdot) = (\cdot)_{n+1} - (\cdot)_n$
$\dot{\gamma}$	Plastic multiplier
λ, μ	Lamé coefficients
$\mathbf{D}$	Fourth order elasticity tensor
K	Kernel functions vector
$\mathsf{K}(\cdot)$	Kernel function

ν	Poisson's ratio
Φ	Yield function
$\mathbf{f}$	Objective functions vector
$\mathbf{u}$	Variables vector
σ	True stress
σ_0	Stress initial condition
σ_q	von Mises equivalent stress
σ_macro	Macroscopic stress
σ_r	Maximum stress
σ_y	Yield stress
σ_i	Stress of the i-th phase
θ	Springback angle
δ_{ij}	Kronecker delta
ε	True strain
ε^e	Elastic strain
ε^e	Plastic strain strain
ε^t	Total strain
ε_l	True longitudinal strain
ε_t	True strain in thickness
ε_w	True strain in width
ε_pr	Pre-strain
ξ	Spacial variable
A	Elongation
$A_{1,2}$	First coefficient of the extended elastic laws

A_{y}, B_{y} Yu's model's parameters

$B_{1,2}$ Second coefficient of the extended elastic laws

b_{with} Width of the sheet

C, γ Chaboche's kinematic parameters

$C_{1,2}$ Third coefficient of the extended elastic laws

CD Process nature variable

E Young's modulus or elastic modulus

E_0 Initial elastic modulus

E_{ch} Chord modulus

E_{ins} Instantaneous elastic modulus

E_{sat}, q Yoshida's model's parameters

f_i, u_i Objective functions and variables

h Thickness of the sheet

J Jacobian matrix

$J_2(\cdot)$ Second invariant of the deviatoric part of stress

Q, b Chaboche's isotropic hardening parameters

R Curvature radius of the midline plane

r Lankford coefficient, anisotropy coefficient

$r0$ Lankford coefficient at 0^{o} RD

$r45$ Lankford coefficient at 45^{o} RD

$r90$ Lankford coefficient at 90^{o} RD

V Volume

V_i Volume fraction of the i-th phase

z Distance in the $\vec{z}$ direction

List of Figures

List of Algorithms

List of Tables

Chapter 1

General introduction

The present thesis work *Experimental and numerical analysis of the elastic behaviour of the TRIP 700 steel for springback predictions* is enshrined in the Metal Forming Research Area of the Mechanical and Manufacturing Department of Mondragon Unibertsitatea.

1.1 Motivation and background

The demand for lightweight fuel-efficient vehicles and the increasing industrial competitiveness between constructors have motivated the automotive industry to introduce new materials and to reinforce the accuracy of production processes with the aim of reducing costs.

A large number of parts of car bodies are obtained by forming processes. For example, B. Osgurg (2012) shows that the number of hot stamping parts in a Volvo car body have augment 50 times in the last ten years. These forming processes comprise, forging, rolling, extrusion, sheet metal forming, among others. Sheet metal forming is a special class of deformation process where the sheet pieces are formed into the desired shape by plastic deformation.

In sheet metal forming, blanks, with the thickness being much smaller than the other dimensions, are placed between two tools, the upper die or punch and the lower die, the blank being placed in contact with one die and the die set-up is closed imposing a specific shape to the blank by plastic deformation.

A wide range of geometries are obtained by sheet metal forming, from simple bending sheets until complex automotive components geometries such as the door part illustrated in Fig. 1.1.

Steady advancements in technology, combined with shortened product cycle times and continual demand to reduce costs, has resulted in the dependence on finite element (FE) codes for the simulation of sheet metal forming processes in the automotive industry. It is generally accepted that commercially available FE programs can be successfully

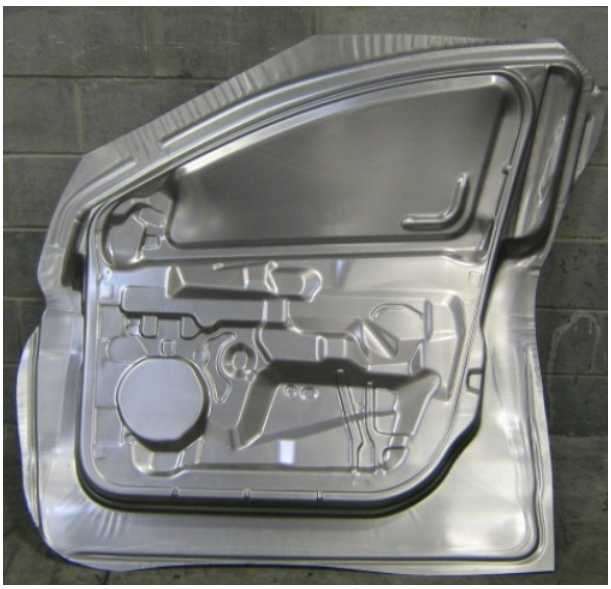

Figure 1.1. Deep drawn door part, taken from Maki (2012).

utilised to predict formability and the likelihood of splits and wrinkles, even for complex part geometry. However, the phenomenon of springback, remains a challenge (Eggertsen and Mattiasson, 2011).

Springback can be defined as an elastically-driven change of shape of a deformed product that takes place during removal of external loads. It is a complex physical phenomenon which is mainly governed by the stress state obtained at the end of a deformation.

This inaccuracy of springback prediction involves a need to use expensive and time consuming experimental try-outs to determine the proper tool geometry and all other parameters that can lead to the desired final shape. Changes in geometry after springback are a big and costly problem in the automotive industry. The assembling process cannot handle parts with too much deviation in geometry and therefore adjusting operations are required. These are extra operation costs, both time and money, in the production process and should be reduced to a minimum. Therefore, research in this field is necessary to improve the reliability of numerical simulations in industrial sheet metal forming.

An accurate numerical prediction will allow to diminish the try-outs process and thus reduce the cost, time and environmental impact of the process.

1.2 Objective and outline of this thesis

The main objective of the research presented in this thesis is to improve the current numerical algorithms and material modelling techniques that will allow the industry to reach more accurate springback predictions in sheet metal forming.
In order to understand the state of knowledge about the springback phenomenon simulation in sheet metal forming processes, first of all a bibliographical review is carried out. Taking the conclusions of the review of the state of the knowledge as a basis, a material characterisation is performed in order to provide accurate data for the numerical simulation.

The literature review shows the relevance of the elastic behaviour accurate modelling for a correct springback modelisation. Therefore, a numerical model, first in one-dimensional state and then extrapolated to the three dimensional space, is developed in order to evaluate the impact of the elastic behaviour on the final shape after springback.

With the aim of analysing the improvement introduced by modelling more accurately the elastic behaviour of the sheet, V-bending experimental tests (Fei and Hodgson, 2006) are conducted in an advanced high strength steel (hereafter AHSS) and compared with different numerical approaches. The AHSS family of steels is composed by different microstructural variations, such as martensitic steel, (MS), dual phase steel, (MS) and transformation induced plasticity steel, (TRIP) among others.

The general outline of the thesis is composed into seven chapters including this first introductory chapter:

Chapter 2
In this chapter a bibliographical review of the state of the knowledge about numerical simulation of springback phenomenon in sheet metal forming is carried out.

By means of this review, the most important concepts to take into account springback prediction are stated. These conclusions are taken as a basis for the subsequent thesis work, and the functional objectives and specific thesis tasks are presented.

Chapter 3
The third chapter deals with the experimental characterisation of the selected AHSS steel for this work. This experimental characterisation covers the mechanical phenomena that have been stated as relevant for springback prediction in Chapter 2, e.g. anisotropy and hardening. The aim of this chapter is to provide material behaviour data for an accurate parameter identification of the numerical material modelling.

Chapter 4

Once the material has been characterised, a new extended elastic law is proposed in order to introduce a wide range of elastic behaviours in an elastoplastic material model. In this context, after developing the extended elastic law, this is introduced into a one-dimensional isotropic hardening von Mises elastoplastic model. In order to analyse the influence of the elastic behaviour accuracy from a theoretical point of view a pseudo-analytical bending test is performed with different levels of accuracy.

Chapter 5

Both, the extended elastic law and the elastoplastic behaviour model presented in Chapter 4 have been developed under an one-dimensional state assumption. Nevertheless, industrial springback processes have to be numerically analysed in a three-dimensional state. Therefore, in the fifth chapter the three-dimensional extrapolation of the extended elastic law is performed. In the same way, following the conclusions obtained from the bibliographical review in Chapter 2, the extended three-dimensional elastic law is introduced in an elastoplastic three-dimensional model. In order to analyse the influence of the elastic law accuracy in a finite element springback prediction, V-free bending process is simulated using solid element model with different accuracy levels of the elastic behaviour.

Chapter 6

Aimed at comparing the numerical predictions with experimental results, in this chapter V-free bending experimental tests are carried out and compared with simple elastic behaviour model's predictions using a shell element model. In this model, only the classical linear elastic and linear elastic with variable elastic modulus behaviours are compared with experimental.

Chapter 7

After analysing the improvement introduced in springback prediction, in Chapter 7 the main conclusions of this thesis work are presented and future works are proposed. In this chapter, the extended elastic law proposed in this thesis work is critically analysed and the advantages and disadvantages of the proposed law are exposed.

Chapter 2

Springback simulation

Synopsis

In this chapter, a bibliographical review of some of the most important works about springback simulations is presented. On the one hand, a summary of the most used springback characterisation techniques is exposed. On the other hand, in order to stablish the evolution of the state of knowledge about the springback simulation, a brief review of some of the most important publications about the springback phenomenon simulation of the last decade is carried out.

From the springback characterisation experimental methods review it can be pointed out how different approaches exist for the springback measurement. These approaches go from the more theoretical loading-unloading cyclic test until industrial springback characterisations. Each test has its advantages and disadvantages, and the correct test has to been chosen depending on the objective of the analysis.

From the historical review of the springback publications it can be stated that each forming and therefore springback process leads to a different optimal numerical model configuration, e.g. hardening, yield criteria and element type. The number of integration points thought the thickness and the stiffness degradation have shown to be the major parameters to be taken into account for springback predictions.

2.1 Introduction

In this chapter, a bibliographical review of some of the most important works about springback simulations is carried out.

On the one hand, a summary of the most used springback characterisation techniques is exposed. These springback characterisation methods go from the most theoretical loading-unloading cyclic test until industrial part springback optimisation through classical V-free bending test.

On the other hand, in order to stablish the evolution of the state of knowledge about the springback simulation, a brief review of some of the most important publications about the springback phenomenon simulation of the last decade is carried out. In this literature review, both sensitivity analysis and numerical simulations publications are reviewed in order to obtain the global point of view of the state of knowledge.

At the end, the main conclusions of the review are exposed in order to be taken as a basis for the rest of the thesis work.

2.2 Experimental methods for springback characterisation

The main experimental tests can be differentiated into five different groups. The first group is composed by the free bending tests. In these processes the test set-up is usually only composed by a lower die and a punch.

The second group is composed by restricted bending-drawing tests, where the sheet is not more free to move and a blank holder is added to the experimental set-up to impose a controlled blank holding force.

Complex drawing processes compose the third group. The formed part is not longer a short width but a three dimensional one has to be taken into account. These tests are divided into those having a straight width and those where the geometry in width takes a complex shape.

The fourth group is composed by particular test methods, e.g. loading-unloading cyclic tests, draw-bending tests and Demeri cup test.

The last group is formed by industrial characterisations where an industrial part is analysed to optimise its springback, e.g. B-pillar forming.

2.2.1 Free bending tests

Among the five groups of springback testing methods existing in the literature, the free bending test is the most simple test able to put in evidence the springback phenomenon. The test is basically composed by a die and a punch, where the sheet is bent until a

specific forming angle, θ, and then the force of the punch is removed, allowing the sheet to recover elastically until the stable state, θ'. The springback is measured with the angle difference before and after the elastic recovery. In Fig. 2.1, the V-free bending method is schematically represented. One of the main advantages of this method is the few process

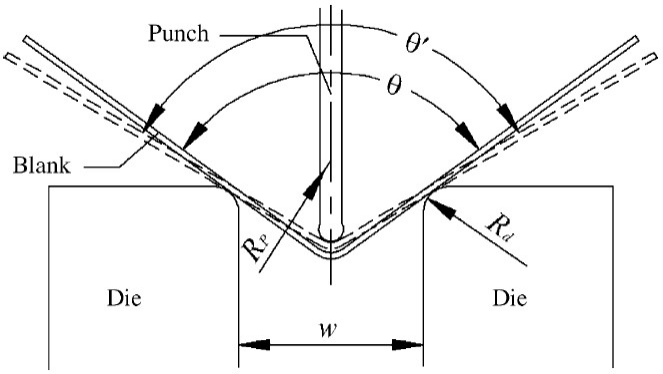

Figure 2.1. Schematic representation of the V-free bending method (Fei and Hodgson, 2006).

variables, i.e. die radius R_d, punch radius R_p, die gap w, forming angle θ, punch velocity and die friction. The other one is that this test is very sensitive to springback and the slightest angle change is possible to be measured by increasing the blank.

Apart from the V-bending method, different free bending methods exist in the literature depending on the geometry of the die and the punch, e.g. U-free bending method.

Among the different free bending methods a special attention has to be paid to the L-free bending method. In Fig. 2.2 the L-free bending test performed by Chatti and Hermi (2011) is shown. In this test, even if a holder is introduced and one side of the sheet is not free to move, when the punch is removed, the sheet will recover elastically changing the angle between the deformed side and the other static side of the sheet. This test is used to represent the tangential bending, very often used as a post process operation in deep drawn sheet metal parts.

2.2.2 Restricted bending-drawing tests

As it has been previously introduced, in the restricted bending-drawing tests, a holder is introduced in the experimental set up. In this case, contrary to the L-free bending test, a relative displacement is allowed between the sheet and the die-holder. In Fig. 2.3 a schematic representation of the U-drawing test is presented. This test is also known as Numisheet'93 benchmark problem.

On the one hand, these tests are more close to an industrial part forming process,

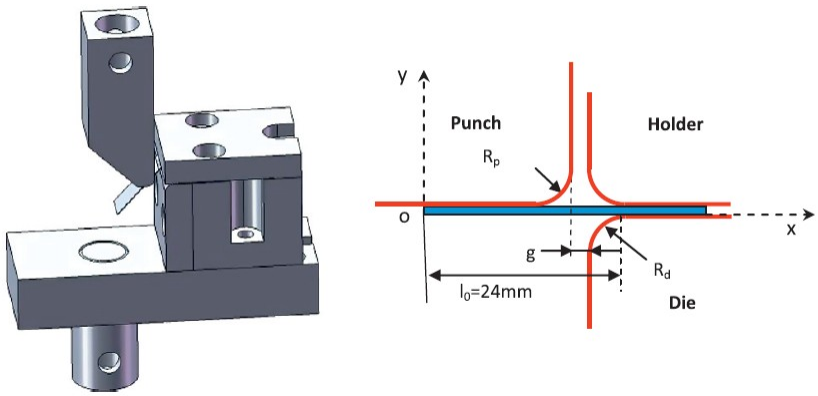

Figure 2.2. Schematic representation of the L-free bending method (Chatti and Hermi, 2011).

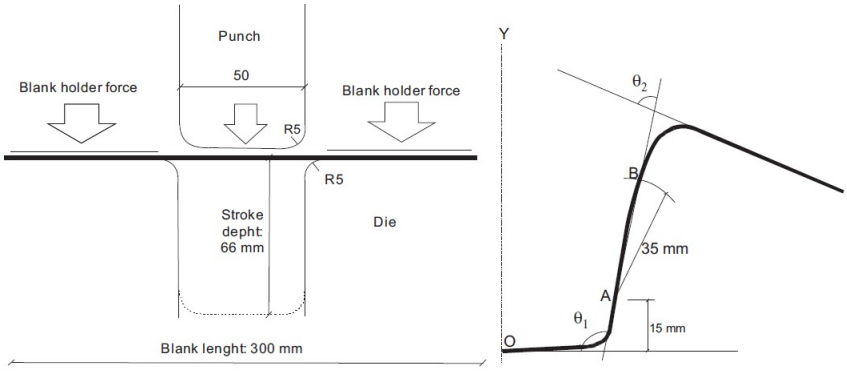

Figure 2.3. Schematic representation of the U-drawing test (Eggertsen and Mattiasson, 2009).

and due to the blank holder addition, a higher strain state can be reached. On the other hand, the analysis of these tests become more difficult because new parameters are introduced. The blank holder force is a new process parameter that has to be taken into account. The friction between the sheet and the holder-die is a relevant variable in these kind of tests, which is always a problematic issue due to the difficulties of measuring friction coefficients. In Fig. 2.4 experimental test results of DP 600 and DP 1000 are exposed, where the difference of springback between them is shown.

As it has been shown in Fig. 2.3, in these tests two different springback angles are measured, the side wall curl angle, θ_1, and the blank angle, θ_2.

In the literature review, different kind of restricted bending-drawing tests are shown, being differentiated by its punch and die geometry. In Fig. 2.5 another type of U-drawing test is schematically represented.

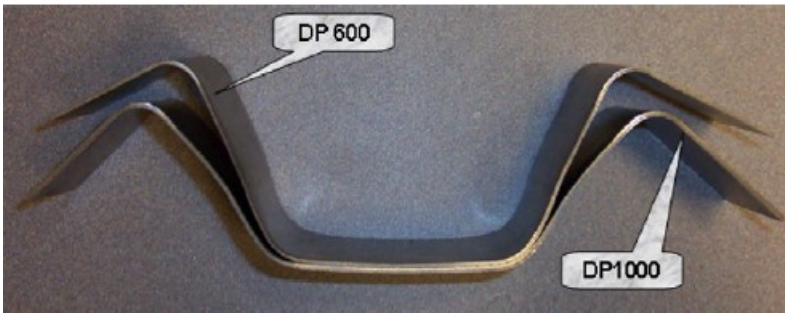

Figure 2.4. Experimental test results of DP 600 and DP 1000 of the U-drawing test (Koc and Chen, 2007). Both materials have been formed using the same process.

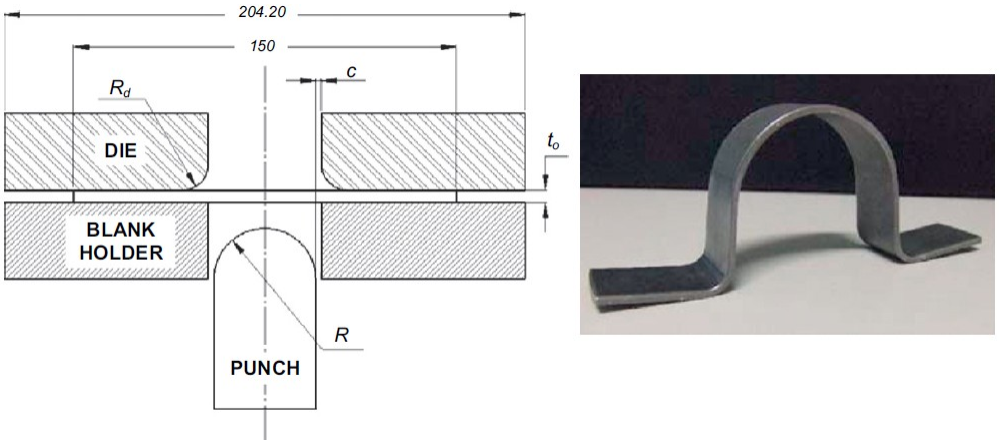

Figure 2.5. U-drawing test schematic representation (Souza and Rolfe, 2010). In this test, a U-shape geometry punch has been used for the forming step.

2.2.3 Complex drawing processes

In the restricted bending-drawing tests, the test samples have a short width. Therefore, tests can be considered almost bi-dimensional. In the complex drawing tests, samples do not have a short width and usually are formed into final complex geometries. In Fig. 2.6 a complex drawing shape is shown. In this kind of tests the stress and strain fields are no longer bi-dimensional but three-dimensional. A common test is the S-rail test. A U-shape S-rail test is illustrated in Fig. 2.7. These tests are still more close to real industrial part forming but the springback angle become difficult to be measured and the number of process parameters and variables augment considerably.

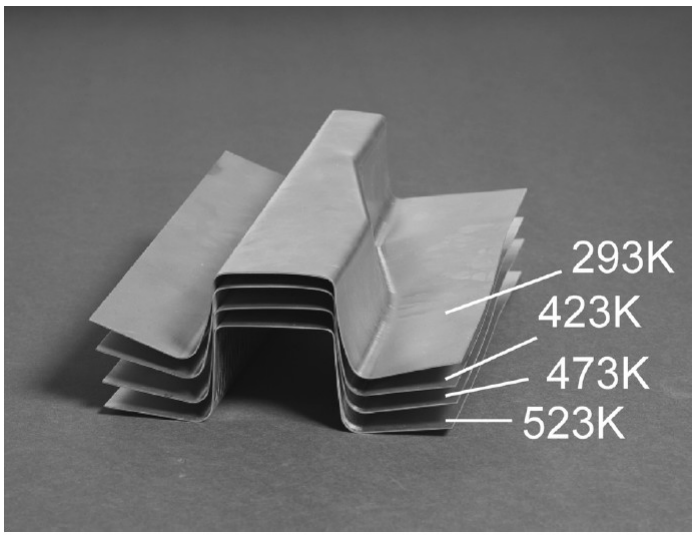

Figure 2.6. Complex U-drawing test schematic representation (Souza and Rolfe, 2010). In this figures the influence of the forming temperature on the recovery of the material is shown.

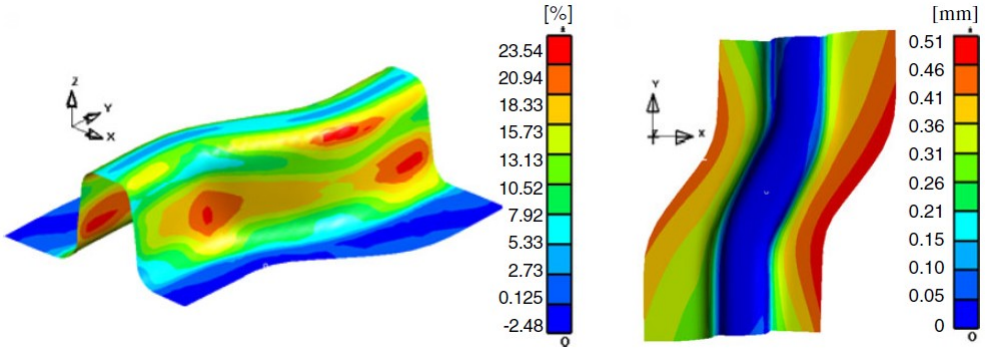

Figure 2.7. U-shape S-rail test numerical representation (Marretta and Di Lorenzo, 2010).

2.2.4 Particular test methods

In this group, special test methods are placed. Basically it is composed by three testing methods, being all of them widely used in literature for springback characterisation. The fist one is the draw-bend test, the second one is the loading-unloading cyclic test and the last one is the Demeri cup (split-ring) test.

In the draw-bend test, the sample is bended around a cylinder to 90º. Then, a resistant force is applied during the test on one side of the sample and a 40 mm/s of displacement is imposed on the other side. Finally, the sample is relaxed and the final

shape after springback is reached. A schematic representation of this method is shown in Fig. 2.8. The main advantage of this test is the accurate control of the process pa-

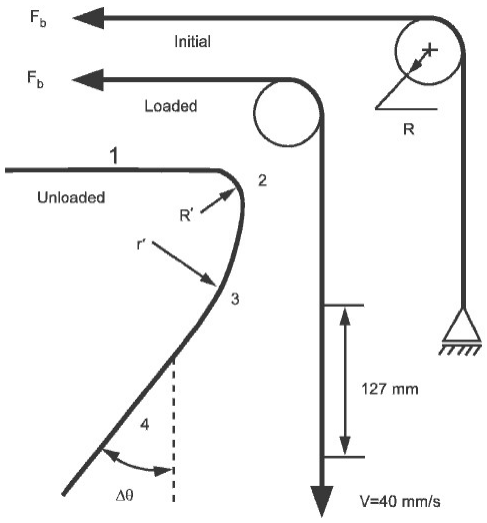

Figure 2.8. Schematic representation of the draw-bend test (Gan et al., 2006).

rameters, e.g. velocity, resistant force, cylinder radius and the sensitivity of the test to springback. In Fig. 2.9 test results for both DP 780 and TRIP 780 are shown. In this figure the influence of the resistant force is noticed for each material.

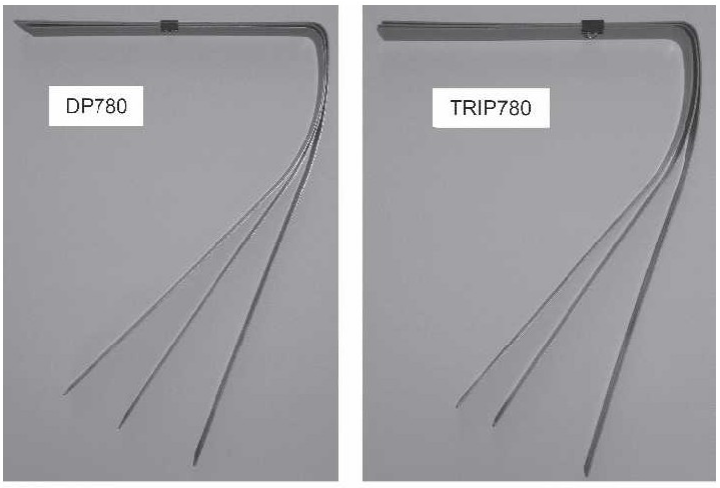

Figure 2.9. Experimental results of the draw-bend test (Gan et al., 2006).

The second particular springback test, is the loading-unloading cyclic test. In this test, a

standard tensile sample is loaded until a predefined pre-strain and subsequently relaxed. Once that the first loading-unloading cycle is performed the sample is reloaded until the next pre-strain and relaxed again, this procedure is repeated until the last cycle is performed. Figure 2.10 shows the schematic representation of the loading-unloading test result.

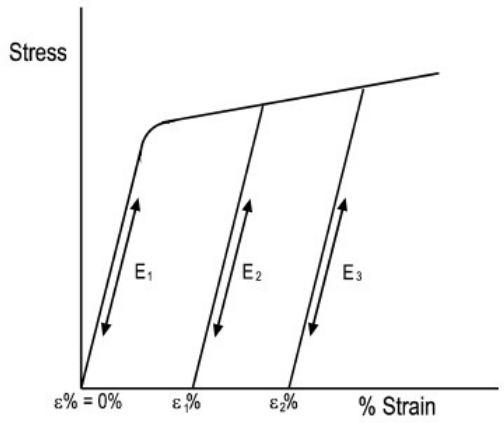

Figure 2.10. Loading-unloading cyclic test strain path scheme (Perez et al., 2005).

Figure 2.11 shows the unloading behaviour exposed by the loading-unloading cyclic test for a TRIP 700 steel (Perez et al., 2005). In this context, this test method provides an accurate measurement of the elastic behaviour for an uni-axial springback. In the same way, the process parameters can be accurately controlled by performing the test in a standard tensile test machine. The only trouble of this testing method is that it is far away from an industrial forming process.

The last test method of this section is the Demeri cup test also known as split-ring test. This test was conceived to put in evidence the springback after deep-drawing operations. Figure 2.12 shows the numerical approach of the Demeri cup test. First, a piece of sheet is formed. Then, from the resulting piece a cylindrical ring is cut. After cutting the ring, a transversal cut is performed and the ring is split measuring the distance between both edges. The experimental procedure is summarised in Fig. 2.13, where a numerical simulation of the test is illustrated.

The advantage of this test is that it is highly sensible to springback and the measurement of the distance between both edges is easy to perform. The disadvantages that it poses are that a deep drawing and the subsequent cutting have to be carried out.

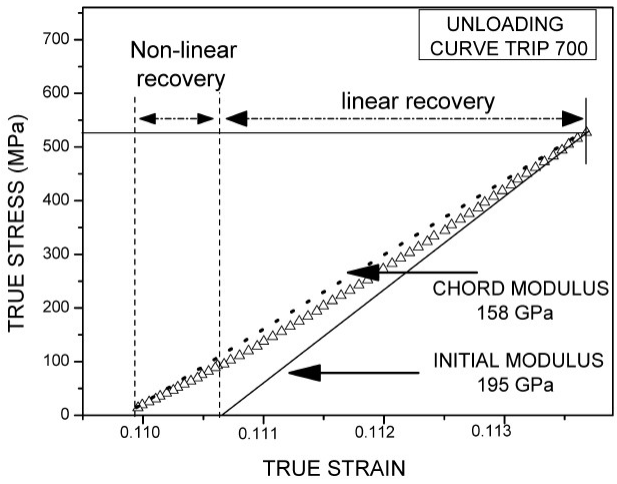

Figure 2.11. Loading-unloading cyclic test results (Perez et al., 2005). In this figure two different unloading modulus, chord modulus and initial modulus are represented together with the experimental data.

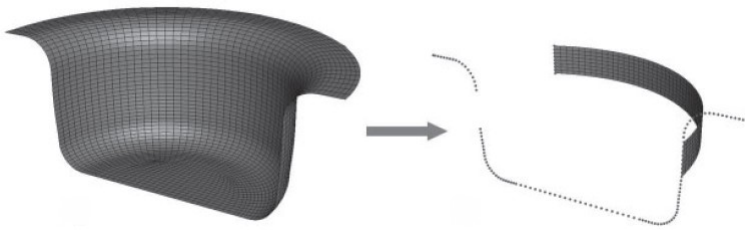

Figure 2.12. Demeri cup test or split-ring test, numerical implementation (Vrh et al., 2008).

Figure 2.13. Demeri cup, split-ring test, experimental procedure (Laurent et al., 2010).

2.2.5 Industrial part

The last group is composed by industrial part tests, being the automotive sector the most interested in the springback phenomenon, these parts usually are A, B, C-pillars

or engine suspensions brackets.

In Fig. 2.14 an high strength low alloy engine suspension upper bracket is shown as example of industrial part used as springback test. The main objective of these test is not the understanding of the springback phenomenon but the optimisation of the industrial process.

Figure 2.14. Engine suspension upper bracket. (Firat et al., 2010).

Figure 2.15 shows the numerical simulation of the upper bracket's forming.

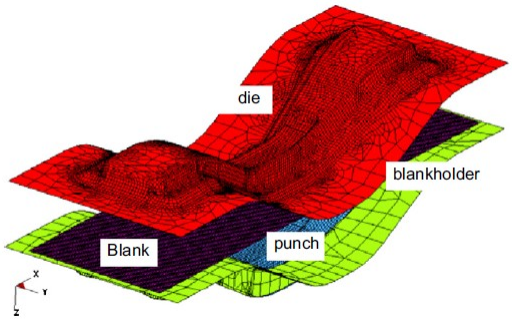

Figure 2.15. Numerical simulation of the engine suspension upper bracket (Firat et al., 2010).

The advantage of this test is the direct industrial application of the test results. Nevertheless, the disadvantage from a technical point of view is the high number of process parameters and variables that usually lead to a complex sensitivity analysis. This complexity implies that the test results and conclusions are rarely applicable to another case.

2.3 Bibliographical review of springback prediction

In this section, some of the most important works published in the last decade about the springback phenomenon are reviewed. The objective of this section is to give a brief chronological review of the springback phenomenon study evolution.

Among all the springback characterisation tests reviewed in the previous section, Li et al. (2002b) by means of the V-free bending test analysed the influence of both hardening model and elastic modulus evolution on springback simulation accuracy. They concluded that the material's hardening model directly affects the accuracy of the springback calculation. The greater the veracity of the hardening model, the greater the springback accuracy. In the same way, elastic modulus was found to be very important for springback accuracy.

At the same time, by means of draw-bend test, Carden et al. (2002) analysed the role of typical process variables on springback. In particular, the role of friction coefficient and R/t (ratio between the punch-die radius and the sheet thickness) were studied. They found that friction in the range normally encountered in sheet forming practice had little effect on springback and that springback decreases for large tool radius (R/t greater than about 5).

Due to the importance of the hardening model in springback simulation, Wagoner and Geng (2002) implemented the Geng-Wagoner hardening law in conjunction with three different yield criteria: von Mises, Barlat's three parameter yield function and Barlat's YLD96, in order to evaluate the importance of anisotropic yield criteria and hardening model on springback and anticlastic curvature prediction. These models were compared with experimental data obtained by draw-bend test. While the new hardening model represented well the three principal characteristics of strain hardening following a reversal of uni-axial stress of an 6022-T4, only Barlat YLD96 faithfully reproduced experimental data.

Comparing the draw-bend test experimental data with a wide range of numerical simulations, Li et al. (2002a) carried out probably one of the most relevant works about numerical simulation of springback by finite element method. Numerical simulations over a typical range of numerical variables, e.g. element type, integration points through-thickness, contact nodes and equilibrium convergence tolerances, among others where conducted. They concluded that whereas typical forming simulations are acceptable accurate with 5-9 through-thickness integration points, springback analysis within 1% numerical error required up to 51 points and more typically 15-25 points, depending on R/t, sheet tension and friction coefficient. In the case of springback simulation, more contact nodes were necessary, one node per 5^o of turn angle versus 10^o recommended for forming. Equilibrium convergence tolerances must be enforced carefully. Analysing the element type, they concluded that 3D shell and non-linear solid elements were preferred for $R/t <$ 5-6. However, due to the excessive computational cost of these elements, shell

elements were more appropriated for $R/t >$ 5-6.

From an empirical point of view, Greisert and Wesemann (2002) analysed the influence of different die radii and constant and variable restraining forces on springback and the possible benefits of a "shape set" process. The investigation showed that the restraining force and the material behaviour have a major impact on springback. The "shape set" process was found a suitable tool to reduce springback, maintaining formability of the material.

Traditional approaches for the prediction of springback strain from the formed state are based on an over-simplification of the unloading behaviour as a linear elastic unloading. This phenomenon was investigated by Cleveland and Ghosh (2002) and they concluded that this over-simplification can cause appreciable errors in the final shape, reaching the 10-20% error for certain part geometries.

Doege et al. (2002) analysed why the springback level of TRIP steels was significant higher than in other steels, concluding that it was mainly conditioned on yield strength and the reduction of Young's modulus for this materials.

In order to analyse the accuracy and sensitivity of FEM tools in predicting the forming behaviour and post-formed geometric shape of a conventional steel and AHSS grades, Pereira et al. (2005) carried out different numerical simulations with commercial FEM packages of an industrial part. The sensitivity variables taken into account in that work were the friction, the blank holder force and the material model characterisation. They concluded that even if an accuracy over 90% for thickness prediction was achieved, an average springback error of approximately 50% was shown. For the analysed industrial part it was found that the springback was not particularly sensitive to the sensitivity variables examined.

In the same context, Andersson (2005) showed how a greater springback was achieved for TRIP steels than other materials. He compared the same industrial part forming for three different steel grades: mild steel, Rephos steel and TRIP steel.

Gelin et al. (2005) stated that the variation on Young's modulus in TRIP steels was due to the change of microstructure that they suffered during forming processes. Therefore, a more important recovery was obtained by implementing this microstructural change in springback simulations.

In order to obtain a better understanding of springback deformation in high anisotropic steels, a combined numerical and experimental investigation was presented by Gomes

et al. (2005). A U-shape geometry was selected for experimental and numerical analysis of an high strength steel. Among all the evaluated numerical models it was shown that Barlat's model gave the closest correlation to experimental results. They stated the importance of using the yield stress at 0^o, 45^o and 90^o rather than using the r anisotropic values. They concluded that an anisotropic model able to capture the existing differences between the springback behaviour at different rolling direction clearly could improve the springback simulations.

Following the same idea of sensitivity analysis as Pereira et al. (2005), a what-if type analysis of the accuracy of two forming simulation solvers was performed by Asgari et al. (2005). The two solvers were commercial software and the objective was to investigate variations in the default input parameters when TRIP steel was used in simulation. Four input factors were analysed: number of integration points through the thickness, tool offset, Young's modulus and friction. This analysis was conducted in an industrial part front cross member component. They realised that the increase of number of integration points through the thickness gave a sudden increase in the correlation for both springback and forming stages. The increase of the gap between tools from 10% to 21% deduced the correlation values for both softwares. In contrast to previous studies, a change in the friction coefficient and the Young's modulus did not have found a strong effect on the accuracy of the predictions.

On the other hand, the work presented by Fei and Hodgson (2006) analysed the influence of geometrical parameters in a V-free bending process, i.e. die gap, punch radius, punch velocity and blank thickness. They concluded that the springback for TRIP steel in this test configuration depends strongly on the blank thickness and die gap, while the influence of punch radius and velocity on springback was negligible. The decrease in Young's modulus during forming was experimentally shown and they concluded that taking it into account in numerical simulations gave better correlation between numerical analysis for the springback simulation and experimental results. On the other hand, simulation results showed that friction coefficient could influence on the punch force but not on the springback angle in the V-free bending process, which agrees with Asgari et al. (2005).

In the work presented by Gan et al. (2006), the finite element method was applied to simulate the springback behaviour of dual phase DP 780 and TRIP 780 steel sheets during draw-bend testing. The observed springback behaviour was compared with computational models. The effect of through thickness property variation on sheet springback was studied and concluded that this variation has a significant impact on the springback

behaviour of sheet metal. It could modify the springback prediction by more than 20%.

From a more experimental point of view, Yanagimoto and Oyamada (2006) conducted a quasi-isothermal sheet V-free bending experiments on high strength steel sheets, aluminium alloy and mild steel sheets. They concluded that a marked decrease in springback was observed when the forming temperature of TRIP and DP steels as well as for mild steels was higher than 750 ^{o}K.

Two combined isotropic-kinematic hardening models, the classical Chaboche model and the microstructural Teodosiu-Hu model, were compared in the paper presented by Haddag et al. (2007) in order to analyse the impact of the transient hardening on springback. The authors concluded that the choice of hardening law is less important than the uncertainty of other simulation parameters, e.g. mesh size, element type and number of integration points.

The effect of the yielding behaviour of a material on springback prediction in bending under tension while maintaining a constant initial sheet thickness and tensile strength was investigated by Matlock et al. (2007). They stated that using only the tensile strength and initial thickness of a material to estimate curl in bending under tension can lead to discrepancies in predicted results depending on the low strain deformation characteristics of the material such as the yield stress.

In the same context, Andersson (2007) evaluated the springback prediction of a flex-rail, which generates a complex geometry containing flange change, side wall curl and twist. The author concluded that simulations under predicts the springback for all analysed materials.

Following the previous works about the influence of the hardening on springback predictions, Oliveira et al. (2007) evaluated several work-hardening models in a U-shape forming process. They concluded that, even if in general the springback results show some sensitivity to the work hardening, despite the high levels of equivalent plastic strain attained in the analysed process it was shown that the springback predictions were not significantly higher than those reported in previous studies, for which the equivalent plastic strain levels were clearly lower than in their work. Nevertheless, differences between the results were found and the authors attributed to the predicted through-thickness stress gradient.

In the same context of sensitive analysis using finite element method (Pereira et al., 2005; Asgari et al., 2005), the effects of blank holder force, material and friction on

springback were analysed parametrically using finite element method and DOE with random number generation by Koc and Chen (2007). They conclude that the side wall curl was very sensitive to the contact condition in simulation.

In order to introduce damage theories in springback simulations, Halilovic et al. (2007) presented an improved material parameters' identification method, including damage models, using neural networks. From the comparison of the numerical results of springback behaviour they concluded that not only porosity but also the shape of voids had a significant influence and therefore can not be neglected if a damage model would be implemented.

Following the previously mentioned works on sensitivity analysis, Asgari et al. (2008) statistically studied the effect for a range selected input parameters in forming and springback simulations. It was shown that the tool offset and the number of integration points through the thickness were of significant importance when modelling a TRIP steel. The effect of variation in Young's modulus and Poisson coefficient were insignificant in increasing the accuracy of predictions. On the contrary, Vrh et al. (2008) showed the importance of considering the stiffness degradation in the calculation of the final shape of a draw part. They carried out Demeri springback cup tests and compared with numerical simulations.

Loading-unloading cyclic tests were performed by Yu (2009) in order to study the inelastic recovery behaviour of cold-rolled TRIP 600 steel since it was seen that the elastic modulus had been stated as an important factor in springback simulations. The author concluded that the strain recovery during unloading process was a combination of elastic recovery and inelastic recovery. The inelastic recovery could reach more than 20% of the total recovery at some cases. In the same context the author stated that the springback angles simulated with variable elastic modulus were larger than those simulated with constant elastic modulus, concluding that the inelastic recovery on springback needs to be considered so as to get a more precise springback simulations.

Other important phenomenon that it was seen to be relevant for springback simulations was the hardening model, that is why Taherizadeh et al. (2009) simulated both forming and subsequent springback stages of the Numisheet'05 benchmark3 with different hardening models. To model the material behaviour, Hill48 yield function was used with two different hardening models, isotropic and combined. Also, as effective parameter in springback simulation, the decrease in unloading modulus was taken into account. They

concluded that for almost all cases, the simulation results using the isotropic hardening models overestimated the experimental data. However, the combined model predicted more accurately the experimental data.

In the same context, Eggertsen and Mattiasson (2009) investigated five different hardening laws: pure isotropic, mixed, Amstrong-Frederick, Geng-Wagoner and Yoshida-Uemori. In addition, three different yield conditions were evaluated: Hill 48, Barlat-Lian, and Banabic-Aretz. The authors concluded that the choice of hardening law was proved to be highly significant for the accuracy of the fitting procedure of the model to the experimental data. Since the study dealt with an almost-uniaxial problem, the influence of the yield condition was very small. It turned out that the influence of the stiffness degradation was even bigger than that of the choice of hardening law. Among the five hardening laws, the Yoshida-Uemori gave the best results for this particular case.

Based on the statistical analysis of the most relevant process parameters carried out before them, Ingarao et al. (2009) investigated a S-shape U-channel component stamping operation using two DP in order to analyse two of the most important process parameters: lubrication and blank holder force. The authors presented a methodology based on Pareto frontier and Response Surface Methodology to optimise industrial processes.

Chatti (2010) analysed the effect of the elastoplastic formulation on forming process and springback at finite strain, concluding that a hypoelastoplastic formulation leads to numerical errors for the springback process.

In contrast to the conclusions stated by Fei and Hodgson (2006), Firat et al. (2010) observed that the punch velocity and the element size of both blank and contact segments may remarkably influence predicted springback deformations.

At the same time Panthi et al. (2010) stated that the springback highly depends on material properties, and geometrical parameters. They found that friction had negligible effect on springback.

In order to provide a springback calculation method for engineering applications, Zhou et al. (2010) proposed a curvature based analytical method of springback prediction and tool shape compensation. The results showed that the calculation accuracy was satisfying for engineering applications, but it was limited to 2D pure bending cases.

In the same context, Souza and Rolfe (2010) developed a new methodology to construct process robustness response windows, by analysing changes in the effective stress and effective strain for a critical region of the stamped component. They conclude that material's mechanical property variation had the primary effect on the stress component

of the response window and on springback prediction.

Coming back to the numerical simulation parameters, Laurent et al. (2010) studied the influence of mesh size, numerical integration formulation and yield criterion for springback simulations by Demeri cup springback test. They concluded that element type but also yield criteria are critical in determining the distribution of the stress. Among the tested elements the C3D8I element was found to be the optimum for springback simulations. As stated by Li et al. (2002a), a fine mesh was necessary to obtain opening results close to the experimental springback value.

Following their own work (Eggertsen and Mattiasson, 2009), Eggertsen and Mattiasson (2011) analysed the influence of the hardening models using a tension-compression test to fit the mixed hardening models. They concluded that even if the Yoshida-Uemori hardening model accurately fitted the tension-compression test data, it was not guaranteeing a good springback prediction.

Following the theory of Gelin et al. (2005) in which Young's modulus decreases during deformation due to the microstructural changes, Li and Tikun (2011) introduced the variation of the Young's modulus associated with the retained austenite transformation, leading to better correlation with experimental, compared to constant Young's modulus. The same kind of model was implemented by Shan and Liu (2011) concluding that the Young's modulus played and important role on springback prediction for TRIP steel.

Chatti and Hermi (2011) followed the investigation about the hardening model and variation of the Young's modulus in springback simulations concluding that the combination of the modified Yoshida-Uemori elastic modulus evolution law combined with a non-linear kinematic hardening model leads to accurate prediction of L-bending springback test.

2.4 Conclusions

In this chapter the state of knowledge about springback phenomenon simulation is exposed. First, the most important springback test methods have been reviewed separating them into five different groups. Then, a brief review of some of the most important publications about springback of the last decade has been performed.

In the following lines, the most important concepts and conclusions of this chapter are summarised next.

From the springback characterisation experimental methods review, it can be pointed out that different approaches exist for the springback measurement. These approaches go from the more theoretical loading-unloading cyclic tests until industrial springback characterisations. Depending on the the objective of the springback analysis, one test or another should be chosen.

From the literature review it is shown, how the free-bending tests and the draw-bend tests are the most used due to their sensibility to springback and because of the grate agreement between process variables, springback sensitivity and parameter control accuracy.

It should be emphasised that even if the industrial part characterisation provides very useful data, usually carries out a complex sensibility analysis. Prove of that are the process robustness response window analysis and the statistical analysis that are exposed in the bibliographical review.

From the historical review of the springback publications two kind of conclusions can be stated. On the one hand, conclusions related to the sensitivity of the springback phenomenon to process variables or parameters. On the other hand, conclusions about the numerical simulation to predict springback in metal forming processes.

Focusing on the sensitivity of the springback phenomenon to process variables, these results are dependent on the test type. It has been concluded by some authors how the friction do not affect the springback phenomenon and it only affects to the forming forces. On the contrary, other authors concluded that the springback is sensitive to the friction coefficient. The effect of the friction on the springback will be negligible on free-bending type test but it will affect the strain flow for the restricted bending-drawing tests and industrial tests. The same phenomenon occurs with the punch radius, punch velocity, among others. The sensitivity results depend on the analysed test configuration.

Analysing the numerical prediction of springback, different conclusions are stated into the review. These conclusions are divided into two groups. First, the purely numerical aspects, e.g. element type, mesh size or integration points through the thickness. Then, the material modelling, e.g. hardening, yield function and stiffness degradation.

The main conclusions of the numerical aspects of the springback simulations are summarised in the work of Li et al. (2002a). The most important aspect for springback simulation is the number of integration points through the thickness. Being the metal sheet in bending state, a high stress gradient is imposed through the thickness. This high gradient needs a good discretisation and therefore the increase of the integration points. It is concluded that a minimum of 25-50 integration points are needed for an

accurate springback prediction.

Assuming that the final forming state has to be carefully evaluated, the contact between die-punch and the metal sheet has to be accurately analysed. Therefore, the number of nodes in contact through the contact radius has to augment for a more precise discretisation.

About element types, for $R/t <$ 5-6 solid elements are necessary and for $R/t >$5-6 shell elements are preferred. The non-linear solid elements and the solid elements with incompatible modes are preferred in front of the linear ones, due to the element shape and the number of integration points.

The material formulation for springback simulations has been widely analysed during the last decade. In the literature review different hardening models are proposed, emphasising the importance of taking into account the Baushinger effect by means of mixed or kinematic hardening models. Most of the authors concluded that, even if an accurate hardening representation does not imply a good springback prediction, the choosing of an appropriate hardening model leads to a better springback simulation.

The yield criteria phenomenon has been also deeply studied by some authors. They conclude the necessity of a correct yield criterion selection for anisotropic materials. Nevertheless, it is also concluded that if the forming and springback processes have a preferential sheet direction, the inclusion of an anisotropic yield criteria is not going to improve the springback prediction.

The main conclusion about the material modelling is that, still remaining important the correct selection of hardening an anisotropic yielding, taking into account the elastic modulus degradation has been shown to be crucial for springback predictions. Not all de metallic materials suffer elastic modulus degradation, but in those cases where microstructural change, dislocation pile-ups or other mechanisms occur, the elastic behaviour changes during forming and it has been proven to be the main variable to take into account to improve springback predictions. In the same context, it is stated by some authors that the over-simplification of taking the unloading behaviour as a linear elastic unloading cause appreciable errors, reaching the 10-20% error for certain part geometries.

Concluding, it can be stated that each forming and therefore springback process leads to a different numerical configuration (e.g. hardening, yield criteria and element type) depending on its properties and material. From a testing point of view, it has been shown that each testing method is suitable for a specific objective, e.g. industrial process optimisation, material modelling or process sensitivity. Therefore, the springback simulation is highly dependent on the process to be analysed.

2.5 Structure of the thesis work

From the literature review presented in the previous section it can be concluded, that different action lines exist in order to improve the springback prediction by numerical methods.

These action lines are divided into two main groups. On the one hand, actions related with numerical methods, e.g. element type, convergence algorithms or contact algorithms. On the other hand, lines associated with material behaviour modelling, e.g. hardening models, elastic behaviour or anisotropic yielding. In the context of numerical methods, different research groups are improving the springback simulation (e.g. Schwarze et al. (2011) are developing solid-shell finite element where a high number of integration points can be used in thickness).

In the material modelling field, it has been noted in the literature review that the hardening model is an active research line for improving springback. The anisotropic yielding is being deeply analysed by different authors and they are improving the existing yield criteria for springback predictions. In the same way, some publications are concerned about the elastic behaviour modelling, but it seams to be less developed than the others, even if it has been stated by different authors the importance of a correct representation of the elastic behaviour for springback prediction.

Taking all this into consideration, the functional objective of this thesis work is stated as: *Improve the current springback predictions by representing more accurately the elastic behaviour of the material.*

In order to reach this functional objective a three-steps research program is stabilised. In regard to provide accurate material behaviour data for the model, in the first step a material characterisation is conducted. In the second step, a numerical model able to represent with different levels of accuracy the elastic behaviour is developed. The third step consist on the comparison of experimental tests and numerical simulations with different elastic behaviours, some more accurate than other, with the aim of analysing the influence of the accuracy of the elastic behaviour. This three step program is summarised in Fig. 2.16.

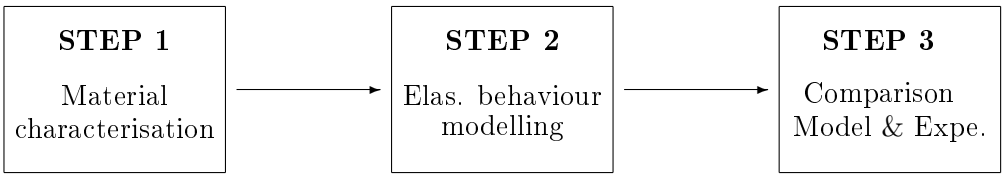

Figure 2.16. Three-steps research program to reach the functional objective.

Following the three-step programs, the research work is divided in four different tasks:

Task 1
In this task, the material is characterised taking into account the most important phenomena in springback prediction stated in the literature review.

Task 2
An one-dimensional elastoplastic model able to represent, with different accuracy levels, the elastic behaviour of the analysed material is developed.

Task 3
The comparison between experimental and numerical requires a three-dimensional elastoplastic model. Therefore, this third task consist on establishing the three-dimensional elastoplastic model extrapolating the previously developed one-dimensional model taking into account the particularities exposed in the literature review, e.g. yield criterion. Implementing this model into solid element formulation commercial FEM software.

Task 4
In this forth task, springback tests and numerical simulations are performed and the influence of the elastic behaviour is analysed. In order to emphasise the elastic behaviour's influence and to diminish other phenomena involved in a springback test, the V-free bending test is selected as experimental test, where the die support are bearings to eliminate the friction phenomenon.

Previously developed model is able to represent, with different accuracy, the elastic behaviour of the characterised material. Therefore, a comparison between the predicted springback angles with different elastic behaviour accuracy levels is performed.

In Fig. 2.17 the graphical representation of the task program with the three-steps is shown.

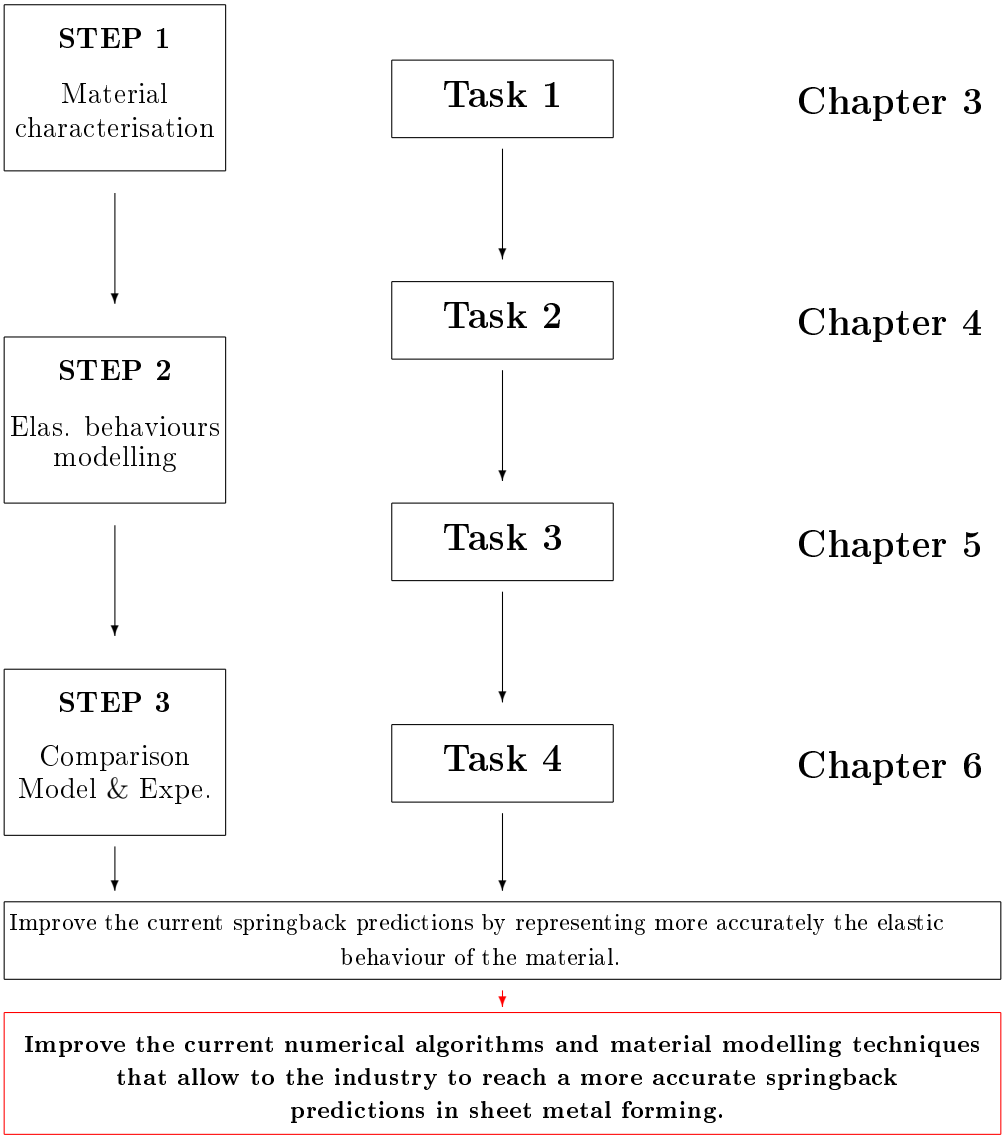

Figure 2.17. Task program coupled with the three step program and their corresponding chapters.

Chapter 3

Material characterisation

Synopsis

In this chapter the material characterisation of the selected TRIP 700 steel is performed. The material characterisation covers the most important properties for springback simulations at room temperature (i.e. tensile behaviour, anisotropic behaviour, kinematic hardening and Baushinger phenomenon and the elastic behaviour evolution during plastic deformation) analysing the influence of the strain path in this elastic behaviour evolution.

From the results it can be emphasised that the TRIP 700 steel can reach around 25% of strain before necking and its yield limit is around 490 MPa. It exhibits an anisotropic behaviour in which a more important reduction is expected in thickness than in width. The hardening behaviour is close to a pure kinematic hardening but definitely the mixed hardening represents better the hardening behaviour. The elastic modulus during loading as well as the chord modulus during unloading decrease as pre-strain increases. This decrease could reach the $15-20\%$ at 12% of pre-strain. The non-linearity of the unloading can be explained by dislocation bending while the unloading non-linearity is composed by different phenomena where the main one is the microplastic strain. The strain path seams to have no influence on the elastic behaviour neither at macro nor micro level.

3.1 Introduction

In the last years, and mainly due to the constantly increasing market competitiveness, it has been a trend towards design lightwight structures which means the use of more complex geometries and new materials. The AHSS steels are taking acceptance in the market due to their good mechanical properties to weight ratio. Among these, TRIP steels present a good drawability associated with a high resistance; their advantageous properties are due to the presence of residual austenite that can be transformed into martensite when stress is applied. The TRIP steel is specially suitable for our research group due to the high interest of our industrial partners on analysing this material.

As it has been emphasised in the previous chapter, the correct modelisation of the material behaviour become crucial for springback simulations.

The TRIP steels have already been characterised under different conditions in the last decade. Among all the published works, Doege et al. (2002), analysed the forming limit curves at different forming temperatures. On the other hand, Huh et al. (2008) characterised the dynamic response of different TRIP steels at intermediate strain rates ranging from 0.003 to 200 s^{-1}. The importance of the non-linear elastic behaviour of the TRIP steels have been analysed for different authors too. Morestin and Boivin (1996) exposed that the diminution of the value of the elastic modulus can reach more than 10% of the initial value after only 5% plastic strain in some cases. Cleveland and Ghosh (2002) presented a model based on physical mechanisms for strain recovery after studying the non-linear recovery of the 6022-T4 Al and a high strength steel. The decrease of the elastic modulus in TRIP steels was introduced in finite element codes by Gelin et al. (2005), relating this reduction to the martensite volume fraction variation, and comparing to deep drawing of a cylindrical cup, concluding that this variation during forming process has a strong influence on the resulting behaviour of the parts considering springback.

The implementation of this change in the elastic modulus has been developed in different ways. Fei and Hodgson (2006) simulated a V-bending process with elastic modulus variation, while Halilovic et al. (2007) included this material parameter evolution as stiffness degradation. In the same year, Vrh et al. (2008) and Asgari et al. (2008), analysed the influence of the material parameter change in the springback prediction precision, the first one by Demeri springback cup test and the second one by DOE approach using an industrial case. Both authors concluded that the variation of the elastic modulus and the friction coefficients were found to be significant to improve the springback simulations. Chatti, in two different works (Chatti, 2010; Chatti and Hermi, 2011), Shan and Liu

(2011) and Eggertsen and Mattiasson (2011) presented the implementation of the elastic modulus change mixed with more complex material models, e.g. kinematic hardening, metal anisotropy, concluding that the inclusion of this kind of complex models improves the accuracy of springback simulations.

From the bibliographical review it can be concluded that there are two different theories about why the elastic modulus decreases during plastic deformation. On the one hand, the theories related with the TRIP effect and the austenite content decrease when the plastic strain increases. Thibaud et al. (2002) formulated an exponential expression of the elastic modulus dependent on martensite volume fraction based on the fact that elastic properties of austenite and martensite are quite different. On the other hand, Perez et al. (2005) analysed the same elastic modulus reduction phenomenon concluding that the decrease of the elastic modulus is related with the dislocation behaviour instead of the austenite volume fraction.

Therefore, taking all this into account, in this chapter the material characterisation of the selected TRIP steel for this thesis work is performed.
The material characterisation covers the most important properties for springback simulation at room temperature (tensile behaviour, anisotropic behaviour, kinematic hardening and Baushinger phenomenon) and the elastic behaviour evolution during plastic deformation.

First, tensile tests are conducted in order to analyse the quasi-static behaviour of the material under uni-axial state. As the analysed TRIP steel has been cold rolled, an anisotropic behaviour is expected . Therefore, tensile tests are performed for 0^o, 45^o and 90^o regarding the rolling direction, in order to analyse the anisotropy of the material.

In the previous chapter it has been stated that the Baushinger phenomenon during hardening has a big importance on the springback simulations. Therefore, in the second section, tension-compression tests are presented in order to analyse the hardening behaviour of the studied TRIP steel. It should be noted that as the main objective of this thesis work deals with the elastic behaviour characterisation, not a deep study is performed about the kinematic hardening. In the model developed in next chapters the kinematic hardening is not going to be taken into account. This phenomenon can be neglected because the process that is going to be modelled is a bending process without change of the bending direction. Therefore, strain reverses don't occur during the process and the kinematic hardening is assumed to be not a relevant phenomenon.

The third section deals with the elastic behaviour characterisation. In this context, this characterisation is carried out by means of classic loading-unloading cyclic tests (Perez et al., 2005; Sun and Wagoner, 2011; Yu, 2009).

Once the elastic behaviour is characterised, the strain path influence in this elastic behaviour is analysed. Both macroscopic and microscopic measurements techniques are performed to stablish the influence of the strain path in the elastic behaviour of the TRIP steel.

3.2 Material and specimens

3.2.1 Material

TRIP steels are made of a complex structure with several phases, which all together result in its outstanding mechanical properties. They are made of a ferrite matrix with retained austenite and martensite islands. The retained austenite turns to martensite during ductile tensile strain, which is known as TRIP effect (Tomita and Iwamoto, 1995). These phases can be distinguished metallurgically. By increasing tensile strain, the proportion of martensite increases and that of the retained austenite decreases. This is the result of the tensile strain-inducing transformation of retained austenite into martensite. This effect increases the work hardening rate, postpones the onset of necking and thus, increases the formability of the material (Li and Tikun, 2011).

The material analysed in this thesis work has been a cold-rolled TRIP 700 steel with a thickness of 1.5 mm. The chemical composition obtained by optical emission spectroscopy is shown in Table 3.1.

Table 3.1
Chemical composition (wt%) of the TRIP 700 steel.

C	Si	Mn	P	S	Cr	Ni	Mo	Al	Cu
0.22	0.29	1.82	0.012	0.002	0.03	0.02	0.04	0.86	0.03

Figure 3.1 shows the microstructure of the TRIP 700 steel analysed in this thesis work. Optical micrograph has been obtained from the material as received. The samples prepa-

ration consists of embedding the sectioned specimens in phenolic resin, grinding them up to 4000 grit SiC paper and finally polishing with 1 µm diamond suspension.

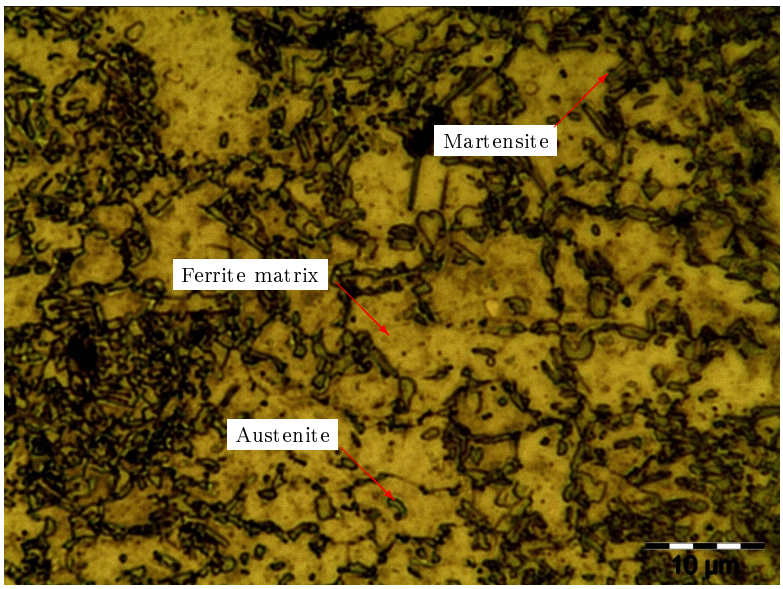

Figure 3.1. Microstructure of the TRIP 700 as received material.

After polishing, the specimens have been chemically etched in order to be analysed in an OLYMPUS SC30 optical microscope equipped with BX 60M, V-CMAD-2 camera for image acquisition. The etchant used to reveal grain boundaries is nital 2% and the etchant used to identify different phases is a 10% of a sodium metabisulfite, 10 g $Na_2S_2O_5$ in 100 ml H_2O (Bramfitt and Benscoter, 2002).

The entire etching process is divided in several steps. First, the specimens have been etched in nital 2% (2 s). Then, the surfaces have been cleaned with compressed air and ethanol. Once the specimens have been cleaned, the surfaces have been etched with 10% of metabisulfite (10 s), and subsequently cleaned with compressed air and ethanol. This last step (metabisulfite etching and cleaning) has been repeated two times more during 4 s and 3 s.

3.2.2 Uniaxial test specimens

Three different specimen shapes have been used in this characterisation:

Standard tensile test specimen

The standard tensile test specimen shape selected for this work it has been obtained following the EN 10 002-1 standard. In Fig. 3.2 the geometry of the specimen defined

by the EN 10 002-1 standard is shown. In order to minimise the influence of the cutting in the microstructure and behaviour of the specimens the cutting has been carried out in a wire EDM (Electrical Discharge Machine).

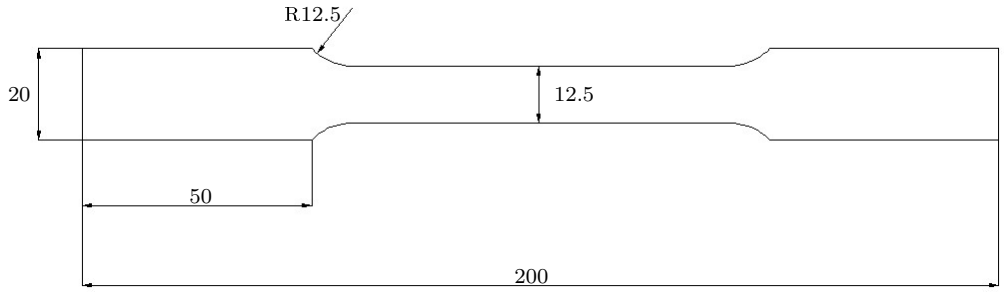

Figure 3.2. Geometry of the specimen employed at room temperature tensile test.

Tension-compression test specimen

For the tension compression tests, due to the buckling phenomenon, the specimen's geometry did not follow the EN 10 002-1 standard. Figure 3.3 shows the non-standard geometry of the samples used in the tension-compression tests. Wire EDM has been also used in this case to cut the specimens. It has been confirmed that both tension-compression and EN 10 002-1 standard samples give the same tensile result.

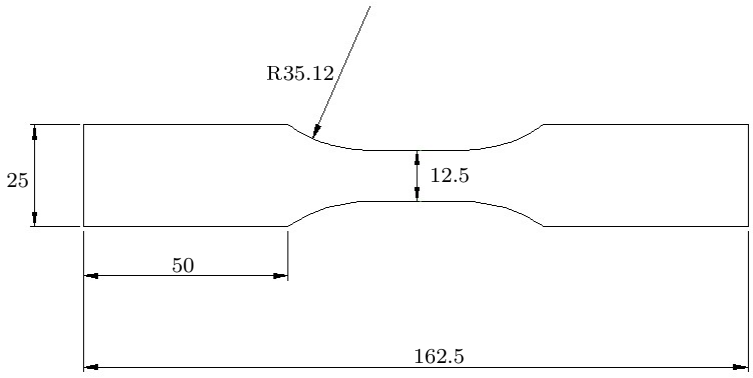

Figure 3.3. Tension-compression test sample geometry.

Micro analysis test specimen

The micro analysis test have been conducted in a in-situ tensile test machine. Therefore, the geometry of the sample needed for these tests does not follow any standard because it has to be introduced into a micro-tensile machine inside the XRD machine. Figure 3.4 shows the non-standard geometry of the micro analysis specimens. These specimens have been also cut by wire EDM.

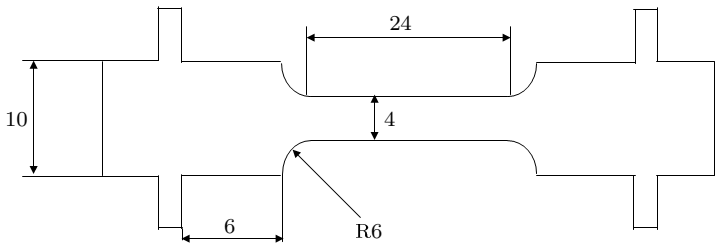

Figure 3.4. Micro analysis test sample geometry.

3.3 Quasi-static tensile test at room temperature

In this section, the tensile test behaviour of the TRIP 700 is analysed. First, the experimental procedure is exposed. Apart from the tensile procedure, the strain measurement technique as well as the anisotropy Lankford coefficients calculation method are shown.

Then, the results of the tests are pointed out. By means of this characterisation, the isotropic hardening behaviour of the material is analysed. In the same context, the Lankford coefficients that define the anisotropy of the material are obtained.

3.3.1 Experimental procedure

The tensile tests have been performed following the EN 10 002-1 standard. The specimens have been cut from the as-received sheets in the rolling direction (0^o RD), 90 degrees from the rolling direction (90^o RD), and 45 degrees from the rolling direction (45^o RD).

Tensile test experiments have been carried out in an Universal 5 t Instron-Zwick/Roell

machine. The length of the reduced section of the specimen is around 50 mm. In order to obtain approximately 1×10^{-3} s^{-1} of strain rate, the tests have been developed under 3 mm/min test machine speed. In order to get a sufficient data, four specimens have been tested in each direction.

Strain measurement technique

In order to obtain an accurate measurement of the strains during the tests, high elongation strain measurement EP-08-250BF-350 type gages, from Vishay Micro-Measurement have been used. High elongation strain measurement places severe demands on the gage installation, and needs special adhesive selection and surface preparation procedures (NC, 2010). The selected gage for this work is a specially fully annealed constantan foil with high elongation polyimide backing. In theory, a properly bonded and wired gage is capable to elongate around a 20%.

The strain gage installation consists on cleaning and abrading the surface, conditioning and neutralising the surface, bonding the gage and wiring it.

Degreasing has been performed to remove oils, greases, organic contaminants, and soluble chemical residues. Once the surface has been degreased, it has been abraded to remove any loosely bonded adherents, e.g. scale, rust, paint, galvanised coatings or oxides, and to develop a surface texture suitable for bonding. The abrade has been performed in 0^o, $+45^o$, -45^o and 90^o using at first 120-grit silicon-carbide paper and then 400-grit paper. When the surface had the desired roughness, approximately 6.4 μm, the surface has been conditioned and neutralised to an optimum alkalinity of 7.0 to 7.5 pH.

Once the surface has been prepared, the strain gages have been glued using a 100% solid epoxy system adhesive. The strain gages have been then cured for 2 hours at 74^oC (NC, 2010).

In Fig. 3.5 the strain gages layout for the tensile test is shown. The strain measurement has been carried out using a quarter Wheatstone bridge, and the data acquisition has been conducted using NI cDAQ-9178 and NI 9219 tools from National Instrument and LabVIEW® software, with approximately 20 Hz of reading rate.

Strain anisotropy calculation, Lankford coefficients

The plastic anisotropy coefficient r is defined by the UNE-36-404-88 as the relation between the true strain in width direction and the true strain in thickness direction during

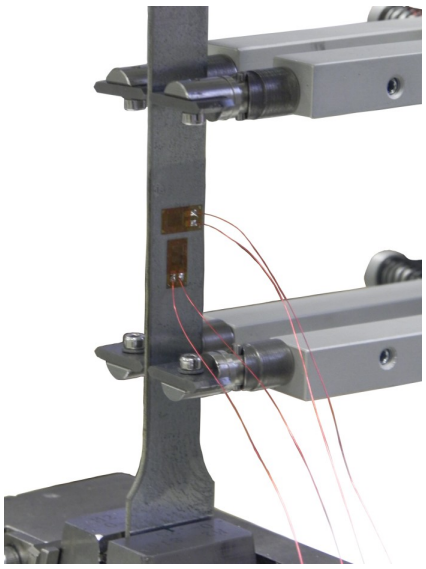

Figure 3.5. Strain gages layout for the tensile test.

a uni-axial tension testing. The mathematical expression that defines the coefficient is

$$r = \frac{\varepsilon_{\mathrm{w}}}{\varepsilon_{\mathrm{t}}}, \tag{3.1}$$

where ε_{w} and ε_{t} represent the true strain in width and thickness respectively, and r is the anisotropy coefficient.

Due to the difficulty associated to thickness strain measurement, the volume constancy law has been used to calculate the thickness true strain. The volume constancy law satisfies

$$\frac{\Delta V}{V} = \varepsilon_{\mathrm{w}} + \varepsilon_{\mathrm{t}} + \varepsilon_{\mathrm{l}} = 0, \tag{3.2}$$

where ε_{l} represents the longitudinal true strain, ΔV is the variation in volume, and V is the volume. Therefore, the Lankford coefficient can be expressed as

$$r = \frac{\varepsilon_{\mathrm{w}}}{-\varepsilon_{\mathrm{l}} - \varepsilon_{\mathrm{w}}}. \tag{3.3}$$

The anisotropic Lankford coefficient shows the resistance of the sheet to thinning during uniaxial tension test.

3.3.2 Experimental results

Figure 3.6 shows the stress-strain curves of the performed tensile tests (only one representative sample for each direction). Even if in the Fig. 3.6 only one sample is shown for each direction, results of the four specimens have been taken into account for Young's

modulus calculation.

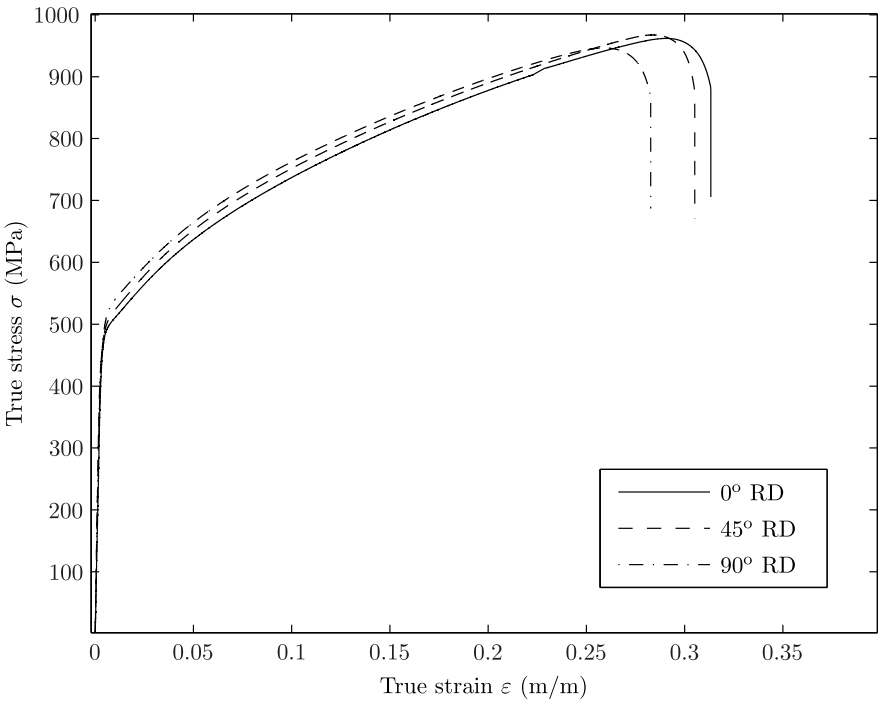

Figure 3.6. Tensile test results for 0° RD, 90° RD and 45° RD.

In order to obtain the Young's modulus, the mean value of the tested four specimens has been taken. The Young's modulus has been obtained by curve fitting following the E111-97 standard, taking 100 MPa, and 350 MPa as lower and upper limits. The averaged Young's modulus is 204 GPa, with a deviation of ±5.25 GPa. Table 3.2 shows the mechanical properties of the TRIP 700 steel obtained from the tensile tests. The resultant Lankford coefficients are exposed in Table 3.3.

Table 3.2
Mechanical properties of the TRIP 700 steel.

Young's modulus E	Yield stress (0.2%) σ_y	Maximum stress σ_r	Elongation A
204 ± 5.25 GPa	490 MPa	940 MPa	25%

Table 3.3
Lankford coefficients for three material orientation, 0° RD, 45° RD and 90° RD, and the averaged coefficient obtained following the UNE 36-404-88 standard ($\varepsilon = 8\%$ strain).

$r0$	$r45$	$r90$	$\bar{r}$
0.7934	0.6957	0.6306	0.7038

The exposed Lankford coefficients are lower than one, $r0, r45, r90 < 1$, which means that when the specimen is deformed in the longitudinal direction a more important reduction occurs in thickness than in width.

3.4 Kinematic hardening

In this section, the experimental characterisation of the kinematic hardening of the TRIP 700 steel is exposed. In Chapter 2, it has been emphasised the relevance of an accurate hardening model selection for springback simulations.

From the tensile test, isotropic hardening models can be obtained, however this kind of hardening models are not able to represent the Baushinger phenomenon in cyclic plasticity (Chun et al., 2002). The Baushinger phenomenon is responsible of an early yielding when the strain path is reversed. Strain path reversal is quite common in sheet metal forming processes, e.g. bending-unbending processes.

In steel characterisation the tension-compression test is commonly used to obtain the kinematic hardening behaviour of the material (Madej et al., 2011). The problem of the sample's buckling that appears in this kind of tests has been differently overcome, e.g. using bending test instead of tensile test, using special tools to block the buckling (Eggertsen and Mattiasson, 2011). In this thesis, experimental tension-compression tests have been performed using a tool that avoids the buckling.

First, the test procedure is presented where the tool to avoid the buckling is presented. Next, the results are exposed and some conclusions about the hardening of the TRIP 700 are pointed out. Finally, a parameter identification procedure is carried out and a mixed hardening (isotropic + kinematic) model is fitted to the experimental data.

3.4.1 Experimental procedure

A servo-hydraulic fatigue MTS 810 Material Test System has been used for tension-compression test. In order to obtain an accurate strain measurement CEA-09-125UN-350 type strain measurement gages, from Vishay Micro-Measurement, have been used.

In Fig. 3.7, the special tool used to block the bucking is shown as well as the experimental set-up of the test.

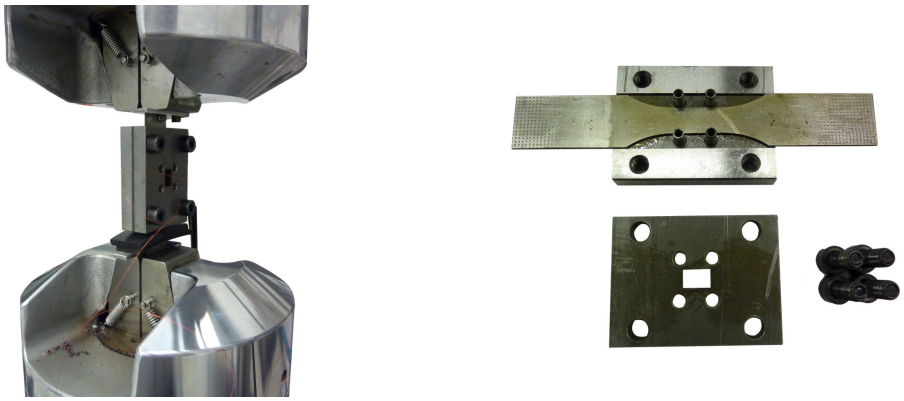

(a) (b)

Figure 3.7. Experimental set-up used in tension-compression cyclic test to obtain the kinematic hardening behaviour: (a) test equipment; (b) special tool to avoid buckling.

Three specimens have been used for this tests. The specimens have been clamped between the two holders leaving a 0.1 mm gap and they have been lubricated by Rhenus Fe-1300 lubricant (Galdos et al., 2006) in order to eliminate the influence of friction during the test. One of the holders has a hole where the strain gage has been placed for measuring.

3.4.2 Experimental results

In Fig. 3.8 the result of one representative sample of the tension-compression test performed with the TRIP 700 steel is shown. In this figure it is shown that the first yield point, which agrees with the tensile test results is around $400 - 500$ MPa. After 2% of deformation, the yield stress of the material increases to 600 MPa. When the strain path is reversed the new yield stress in compression is around -400 MPa.

Assuming and purely isotropic hardening behaviour, after 2% of strain the yield sur-

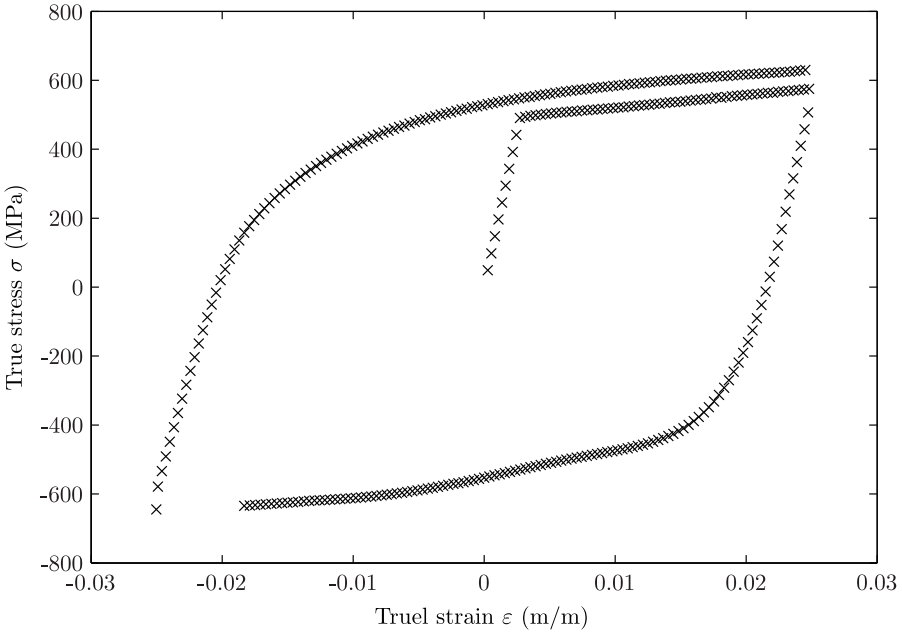

Figure 3.8. Result of the tension-compression test performed with the TRIP 700.

face has expanded from around ±490 MPa to around ±600 MPa, therefore the yield stress in compression should be around −600 MPa. However the new yield stress has been found around −400 MPa. On the other hand, the hardening behaviour seams to be closer to purely kinematic hardening, where the dimension of the elastic range remains constant while it moves with the hardening evolution. However, under a purely kinematic behaviour assumption the reloading tension data should fit the first loading data and in Fig. 3.8 the reloading tension data expose higher stress values than the first loading data.

Therefore, mixed hardening model, which is able to reproduce both expansion and motion of the elastic range, represents more accurately than any pure behaviour models, isotropic or kinematic, the hardening behaviour of the TRIP 700 steel.

3.4.3 Hardening parameter identification

In order to represent the mixed hardening showed by the TRIP 700 steel, the Chaboche hardening model (M. Chaboche, 1983), with one back stress tensor, has been fitted to the experimental data.

The numerical procedure carried out for the parameter identification and an exhaustive analysis of the hardening model is detailed in Mendiguren et al. (2012c) and the

material hardening parameters are sumarised in Table 3.4.

Table 3.4
Chaboche, (M. Chaboche, 1983), hardening parameters for the TRIP 700 steel.

Q MPa	b	C MPa	γ
184.45	2.705×10^{-13}	6692.8	32.9219

From the results shown in Table 3.4, it can be confirmed the predominant kinematic hardening behaviour. In Fig 3.9 the experimental data with the fitted Chaboche's model is shown. A deeper analysis of the results is exposed in Mendiguren et al. (2012c).

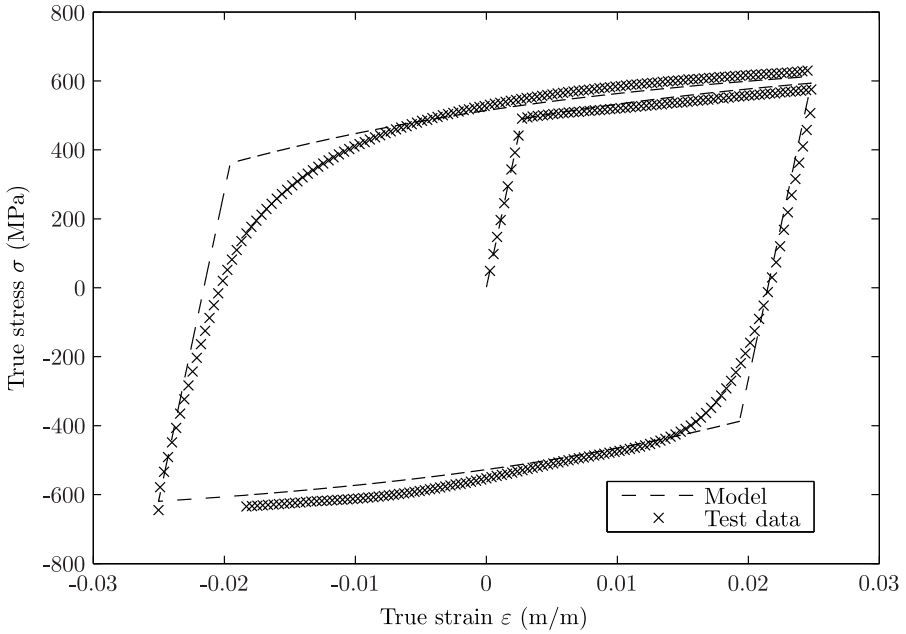

Figure 3.9. Result of the tension-compression test performed with the TRIP 700 and the fitted Chaboche's model (M. Chaboche, 1983).

3.5 Loading-unloading elastic characterisation

In this section, the elastic behaviour of the TRIP 700 steel is analysed. This characterisation has been carried out by means of loading-unloading cyclic tests (Perez et al., 2005; Sun and Wagoner, 2011; Yu, 2009).
Perez et al. (2005) and more recently Yu (2009) have performed elastic unloading characterisations of TRIP steels by means of the loading-unloading test. In the former work the strain was measured by classical strain gages, which implies that a new gage had to be bonded at each cycle. For the latter, Yu measured the strain by an extensometer. In this work, the strain has been measured with high elongation gages, which give the precision of a gage but can hold theoretically a 20% of deformation, an provide more accuracy than the extensometer. Using this measurement technique, it has been possible to make accurate measurements along the test without having to manipulate the specimen at each cycle.

First, the experimental procedure is presented, detailing the loading-unloading cyclic test. Then, the results of the loading-unloading tests are exposed, and some conclusions are outlined.

3.5.1 Experimental procedure

The loading-unloading cyclic tests are widely used in the literature in order to analyse the behaviour of the material during elastic recovery (Perez et al., 2005; Sun and Wagoner, 2011; Yu, 2009). The test consist on loading the tensile specimen until a defined specific strain, called hereafter pre-strain, and then removing the load until reaching the relaxed state (zero stress). Once the first loading-unloading cycle is performed, the specimen is reloaded again until the next pre-strain and subsequently unloaded. This procedure is repeated until the last cycle is performed. The pre-strains defining each cycle are shown in the Table 3.5.

Table 3.5
Pre-strain values for the loading-unloading cyclic test.

Cycle	1	2	3	4	5	6	7	8
$\varepsilon_{\mathrm{pr}}$	0.015	0.030	0.045	0.060	0.090	0.120	0.160	0.190

The loading-unloading tests have been conducted in a Universal 5 t Instron-Zwick/Roell machine under the EN 10 002-1 standard. These tests have been conducted also at 3 mm/min in order to obtain the same strain rate as in the tensile tests. In this case, three specimens obtained by wire EDM have been tested at each direction (0º RD, 90º RD and 45º RD).

As in the tensile tests, EP-08-250BF-350 type high elongation strain measurement gages, from Vishay Micro-Measurement, have been used in these tests in order to get an accurate strain measurement.

3.5.2 Experimental results

In Fig. 3.10 the result of the loading-unloading test in the rolling direction is shown. Maximum strain is 18.5%, because the gages didn't resist higher strains. Similar results have been found for the other rolling directions. From this figure different appreciations can be emphasised. On the one hand, when the specimen is reloaded after an unloading step, an increase in the upper yield point is shown. On the other hand, from the elastic part of the cycles it can be deduced that the loading and unloading stress-strain curves do not follow the same path.

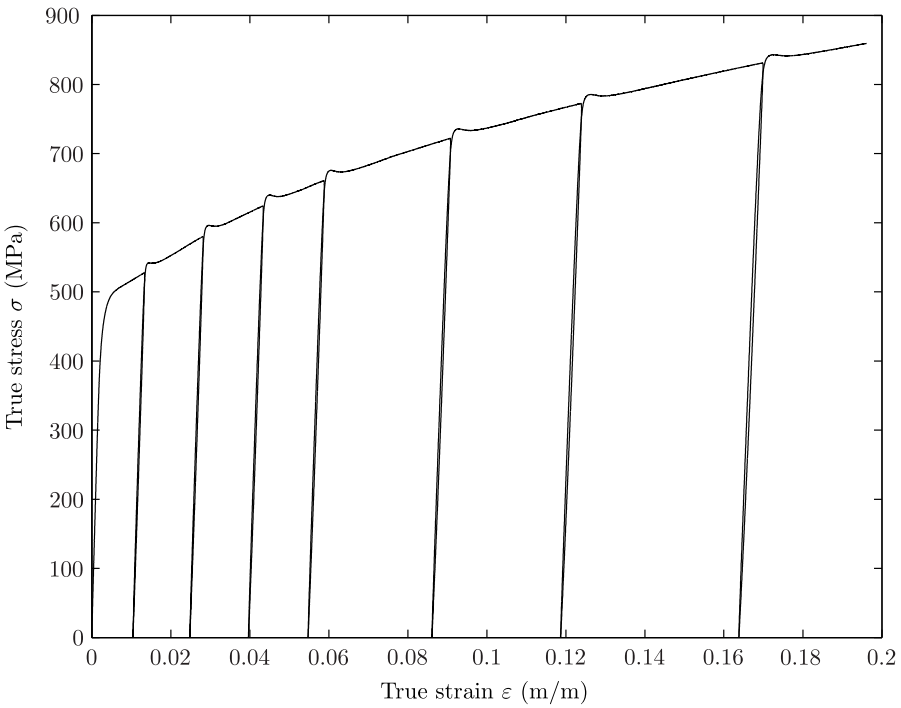

Figure 3.10. Loading-unloading cyclic test behaviour performed in the rolling direction (0º RD).

The hardening behaviour shown by the loading-unloading cyclic test, Fig. 3.10, is similar to the one shown by tensile test, 3.6, apart from the increase in the upper yield point in the loading steps.

Loading behaviour

First, the loading steps of the loading-unloading test are analysed. From each loading step, the elastic modulus has been obtained following the same strategy as followed to obtain de Young's modulus with the tensile tests.

From each material orientation, three specimens have been tested, and the mean value and deviation have been obtained. In Fig. 3.11, the elastic modulus for each loading step versus the pre-strain of the previous unloading step is represented, i.e. first loading step has gone from $\varepsilon = 0$ to $\varepsilon = 0.015$, so the first elastic modulus is represented at $\varepsilon = 0$, but the second loading step goes from $\varepsilon < 0.015$ to $\varepsilon = 0.03$, therefore the second elastic modulus is represented at $\varepsilon = 0.015$. In this figure the main value and the standard deviation are shown. Only the results until 0.12 are exposed because up to this strain some strain gages have been failed.

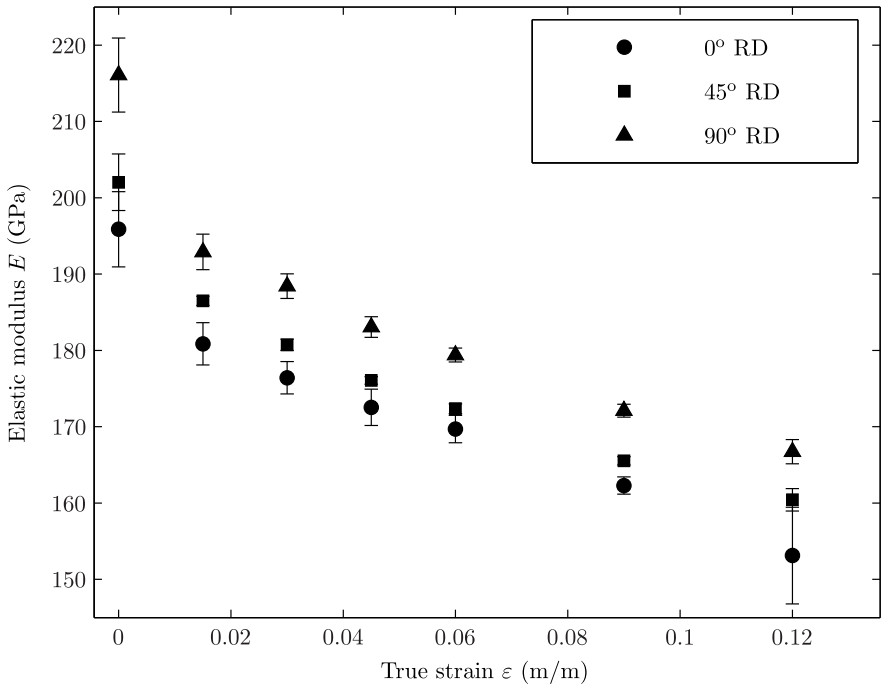

Figure 3.11. Loading elastic modulus at different pre-strains for the three material directions.

Figure 3.11 shows how the elastic modulus measured during loadings decreases at each loading-unloading cycle. On the one hand, Yu (2009) arrives to the same conclusion

for the TRIP 600 steel, measuring a decrease on 20% for 30% of plastic pre-strain. On the other hand, Perez et al. (2005) analysed this phenomenon with the TRIP 700. They concluded that the elastic modulus for the TRIP 700 diminishes quickly in the first stage of deformation, followed by a slight and constant drop as strain increases, where the final decrease in elastic modulus at 20% of pre-strain is about $5-6\%$. In this case, the decrease of the elastic modulus reaches the $15-20\%$ for a 12% of pre-strain.

In the same way, the instantaneous elastic modulus, represented by the derivative $\mathrm{d}\sigma/\mathrm{d}\varepsilon$, of each loading steps is shown in Fig. 3.12, choosing a 0º RD specimen. This analysis has been carried out only for this representative specimen to the point out non-linearity of the loading steps.

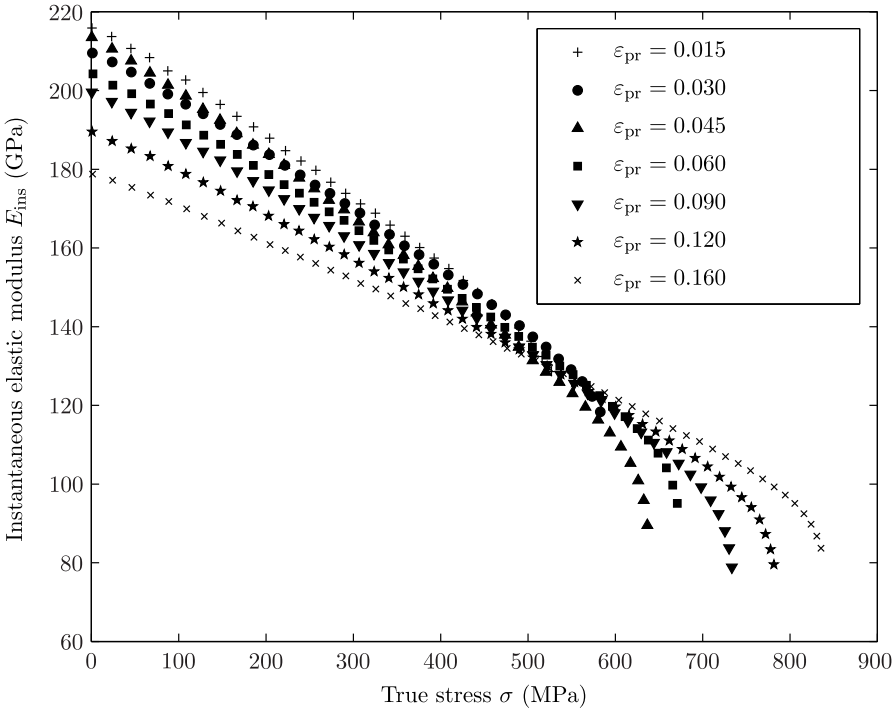

Figure 3.12. Loading instantaneous elastic modulus for each loading step. Results from the 0º RD specimen.

In this figure it can be appreciated that the instantaneous elastic modulus decreases when the stress increases. This phenomenon is related to different mechanisms. On the one hand, the difference between plastic properties of each step. On the other hand, the mechanism of bowing of the existing dislocation lines between pinning points (Foreman, 1967) contributes to the non-linearity of the loading step of the TRIP steel.

Unloading behaviour

After analysing the loading behaviours, the unloading steps of the loading-unloading tests are analysed. Figure 3.13 shows a representative unloading step after a 0.16 pre-strain loading step ($\varepsilon_{\mathrm{pr}} = 0.16$). The unloading stress-strain curve is not a straight line but a curve. The slope of the straight line that links the first and the last stress-strain points is defined as the chord modulus, E_{ch}. As it is shown in Fig. 3.13, the chord modulus is lower than the Young's modulus, obtained following the E111-97 standard on the first loading step.

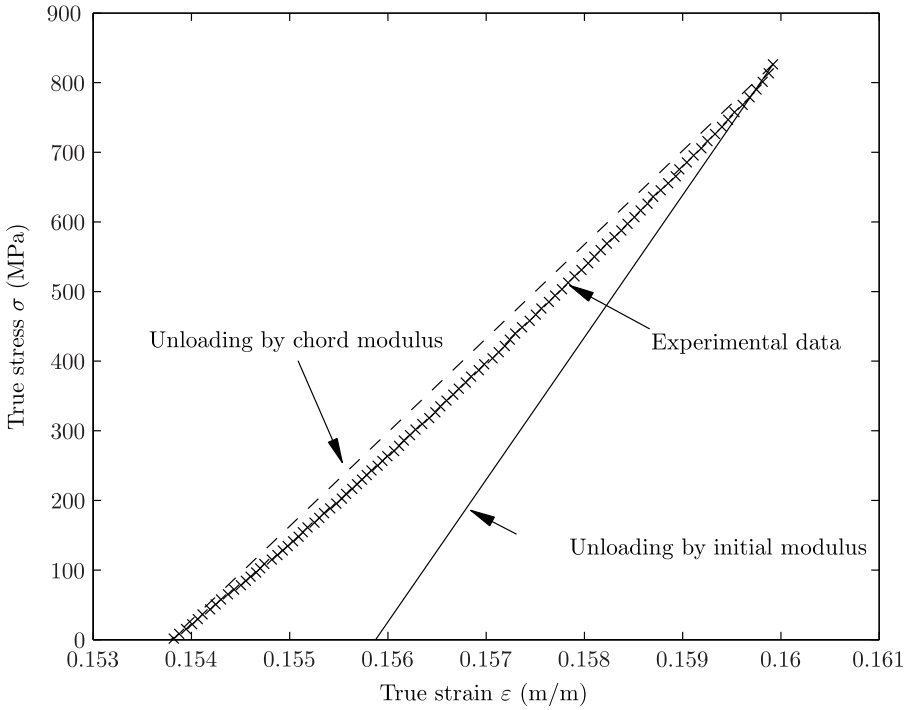

Figure 3.13. Unloading stress-strain curve obtained experimentally and curves calculated with chord modulus and initial elastic modulus when strained to 0.16.

From the three specimens tested at each material direction, the averaged chord modulus has been taken as representative value. In Fig. 3.14 the averaged results of the chord modulus are shown. In Fig. 3.10 is shown how despite the unloading and subsequent loading steps do not follow the same path, both start and finish approximately at the same point. Therefore, the chord moduli obtained from the unloading steps are very close to the elastic modulus obtained from loading steps.

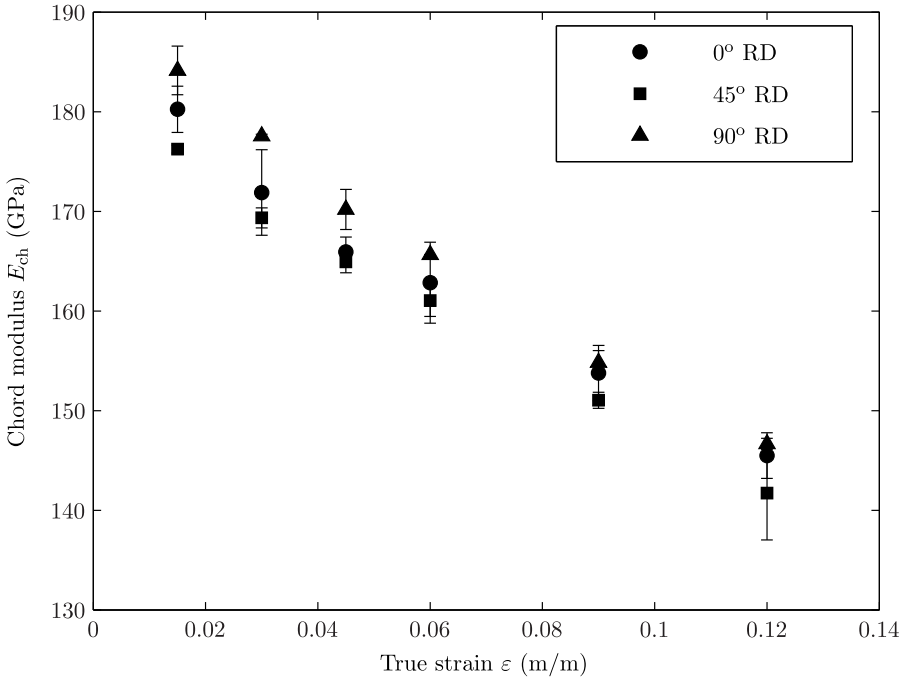

Figure 3.14. Chord modulus evolution at different pre-strains for three material directions.

As it has been shown in Fig. 3.13, the stress-strain experimental curve follows a non-linear path. This part has a concave shape, and thus the instantaneous elastic modulus during an unloading step decreases when the stress decreases. Figure 3.15 shows the unloading instantaneous elastic modulus of the 0º RD specimen previously analysed for the non-linear loading. The conclusions exposed in other publications (Perez et al., 2005), agree with this results. This non-linear unloading path can be explained in terms of microplastic strain (Cleveland and Ghosh, 2002; Perez et al., 2005), i.e. during plastic deformation, dislocations move through the grain and at the same time new dislocations are created. Under stress, despite these dislocations are repellent one to another, they form pile-ups in the grain boundaries. Therefore, when stress is removed, dislocations tend to adopt a configuration corresponding to an equilibrium state. This go back of dislocations, produces an extra strain converting unloading path in non-linear. Apart from the micropastic strain recovery the unloading step recovery is also composed by the classical interatomic planes relocation and the bended dislocations unbending.

From the loading instantaneous elastic modulus results it can be appreciated that the modulus decreases with stress from around 200 GPa to 90 GPa. On the contrary to the loading behaviour, each unloading step starts and finish with different instantaneous

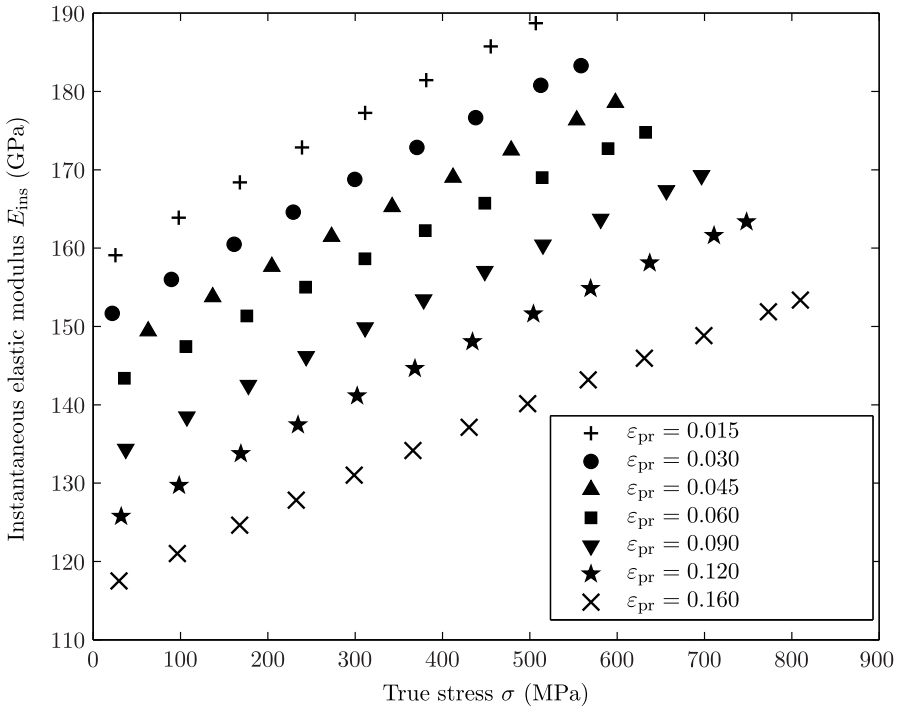

Figure 3.15. Unloading instantaneous slope for each unloading step. Results from the 0°RD specimen.

elastic modulus value but all of them decreases with a 50 Pa/Pa ratio.

From Fig. 3.12 and Fig. 3.15, it can be concluded that both loading and unloading steps follow non-linear paths. As a representative value of the loading steps, the Young's modulus is obtained, Fig. 3.11, where the deviation value takes into account the non-linearity of the curve. On the other hand, in the unloading steps, which are more non-linear than the loading steps, the chord modulus is taken as a representative value. Other authors took the same value in order to quantify the unloading module (Perez et al., 2005; Yu, 2009).

Perez et al. analysed the retained austenite volume fraction evolution during deformation process, concluding that during the first part of deformation process the total amount of transformed austenite is high, but the rate slows as the strain increases reaching an amount of untransformed austenite around $2-3\%$.
Taking into account the retained austenite evolution and the chord modulus evolution shown in Fig. 3.13, it can be concluded that the main reason for which the chord modulus decreases with the pre-strain is the microplastic strain. In Fig. 3.13 it is shown how after

a 10% of deformation, which is where Perez et al. established the end of the austenite transformation, the chord modulus continues decreasing. In the same way in Fig. 3.11 is shown that after a 10 % of deformation, the initial elastic modulus continues decreasing, and that can be explained because the increase in dislocations with the plastic strains.

Reloading behaviour

As it has been previously mentioned, when the specimen is reloaded after an unloading step, an increase in the upper yield point is shown (see Fig. 3.10). This phenomenon could be explained by stage ageing process (Farías, 2006). Strain ageing can be divided in three stages in time. In the first stage, short time Snoek rearrangement process, is an effect of the stress-induced rearrangement of the interstitial atoms in the stress field of dislocations. The medium time dislocation pinning by Cottrell effect composes the second stage. The last stage of the ageing process, long time process, is the precipitation of carbides at dislocation regions. However, the loading-unloading cyclic tests have been performed at room temperature and a long time is required for the diffusion of the carbon atoms towards the dislocations lines at this temperature. That is why it can be concluded that the short time Snoek rearrangement process (which is an effect of the stress-induced rearrangement to the interstitial atoms in the stress field of dislocations) is the mechanism responsible for the increase of the upper yield limit during reloading (Farías, 2006).

In order to prove that the increasing of the upper yield point phenomenon is related with the iteration between carbon atoms and dislocation, the loading-unloading cyclic test has been carried out for a mild steel. The carbon content of the mild steel is lower than that of the TRIP 700 one. Therefore, the increase of the upper yield limit in the mild steel has to be lower than the one of the TRIP 700.

Table 3.6
Chemical composition (wt%) of the mild steel.

C	Si	Mn	P	S	Cr	Ni	Al	Cu
0.06	0.02	0.22	0.15	0.007	0.03	0.02	0.05	0.01

In Table 3.6 the chemical composition of the tested mild steel, obtained by optical

emission spectroscopy, is shown. In Fig. 3.16 the increase in the upper yield limit of both TRIP 700 steel, Fig. 3.16(a), and mild steel, Fig. 3.16(b), are shown. By means of this comparative, the hypothesis that the increase in the upper yield point is due to the Snoek short time rearrangement is confirmed.

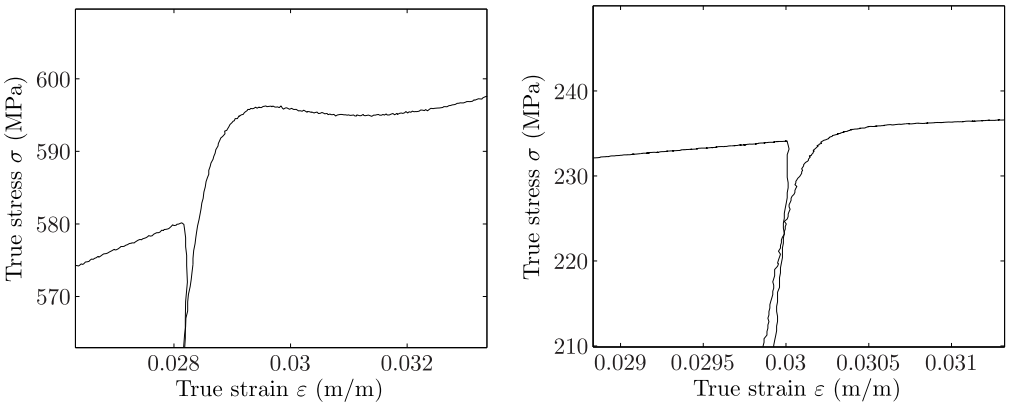

Figure 3.16. Snoek phenomenon comparative. On the one hand the increase in the upper yield limit in the TRIP 700, and on the other hand the increase in the upper yield limit in the mild steel: (a) increase in the upper yield limit in the TRIP steel; (b) increase in the upper yield limit in the mild steel.

3.6 Strain path influence

In the previous section it has been stated that cyclic testing using loading and unloading at some equivalent strains is a suitable test to characterise the inelastic behaviour of the TRIP 700. However, no study has been found in the literature review in which the influence of the strain path is analysed. This is essential, since the metal strip or the blank suffers different loading and unloading steps when being formed using conventional metal forming techniques, e.g. multi-step drawing or roll forming, and not always the material is relaxed in between steps.

Therefore, this section deals with the strain path's influence on the elastic behaviour of the TRIP 700 steel in order to validate the cyclic testing method for the characterisation of the inelastic behaviour of the AHSS having different paths. The cyclic testing method is developed at macroscopic scale, but during a loading cycle, the microstructure

evolves as austenite is transformed into martensite and it can induce a load transfer between phases (Pereira et al., 2005). Therefore, in this section the influence of the strain path is analysed at both macroscopic and crystallographic phase's levels. First of all, the different macroscopic cyclic tests are presented, in which the strain path is changed from test to test. Secondly, the macro and micro measuring methods are explained. High strain elongation strain gages have been used to compare the inelastic behaviour of the specimens at macro level. In-situ stress measurements have been carried out for different cyclic testing using XRD technique for the micro analysis. Ferrite and austenite phases stress has been measured at different points of the loading-unloading cycles. Finally experimental results and conclusions are pointed out.

3.6.1 Experimental procedure

Macro measurements

Three different cyclic tests have been compared in order to stablish the influence of the strain path at macroscopic level. The baseline test is the loading-unloading cyclic test previously performed in Section 3.5, which is composed by eight loading-unloading cycles. In the second variant, only two loading-unloading cycles have been performed: the final maximum strain is the same as in the baseline test. Finally, in the third variant, eight loading-unloading cycles have been performed, like in the baseline test, but unloading has been limited to 80 MPa. The different variant tests are shown in Fig. 3.17. The different test conditions are summarised in Table 3.7.

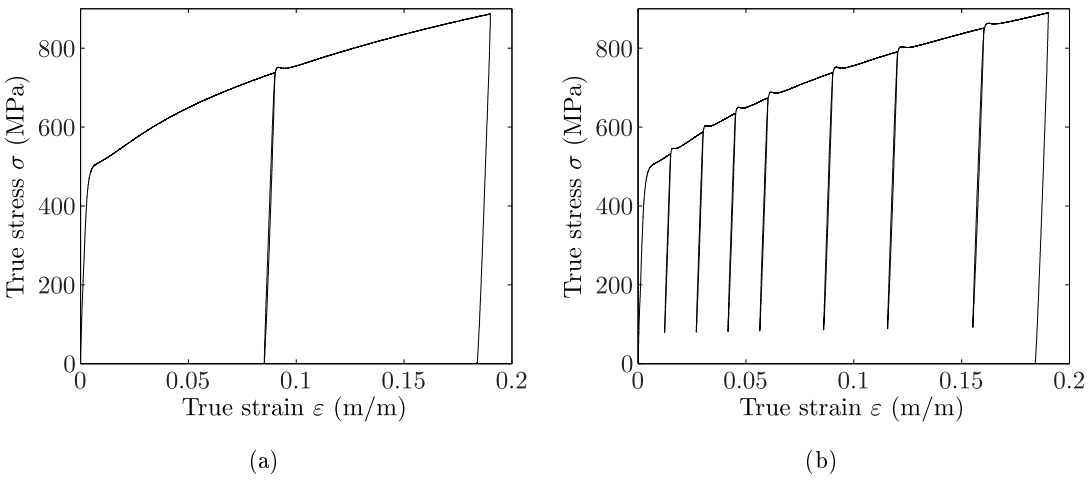

Figure 3.17. Two variants of the baseline test, Fig 3.10: (a) second variant test with two unloading-loading cycles; (b) third variant with eight uncompleted unloading-loading cycles.

Table 3.7
Strain path influence test summary. Reached pre-strain and unloading type.

Test id.	Pre-strain								Unloading type
Baseline	0.015	0.03	0.045	0.06	0.09	0.12	0.16	0.19	relaxation
2nd variant	−−	−−	−−	−−	0.09	−−	−−	0.19	relaxation
3rd variant	0.015	0.03	0.045	0.06	0.09	0.12	0.16	0.19	80 MPa
Micro cyclic	−−	−−	0.04	0.06	−−	−−	−−	−−	relaxation

Cyclic tests have been performed using specimens according to EN 10 002-1 standard. As in previous tests, samples have been cut by wire EDM, the rolling direction being parallel to the tensile direction. Experimental tests have been carried out in a 5 t Instron-Zwick/Roell universal machine and at 10^3 s^1 strain rate.

In situ X-ray diffraction micro measurements

In order to evaluate stress evolution in each phase, in-situ stress measurements using a tensile micromachine have been performed. The set up has been installed in a X-Ray goniometer (Proto iXRD). As X-ray diffraction can only distinguish between crystallographic phases, the mean stress in austenite can be determined; for ferrite, the stress is an average value of pure α-ferrite and the one contained in bainite. The X-Ray Diffraction machine equipped with the in-situ tensile test machine is shown in Fig. 3.18. The macroscopic stress and strain have been calculated from force and displacement sensors directly attached to the tensile machine. Phase stress measurements have been performed using the classical $\sin^2\phi$ law (Hauk, 1997). X-Ray measurements have been carried out on $\{3\,1\,1\}$ crystallographic planes of austenite using Mn Kα radiation and on $\{2\,1\,1\}$ crystallographic planes of ferrite using Cr Kα radiation, as given in the standard NF-EN 15305.

As in macroscopic tests, stress analysis has been performed at different loading and unloading points. As both phases cannot be analysed with the same radiation, the anticathod has to be changed at each measurement point. That way, the macroscopic loading (given by the force sensor) and the local stress in each phase has been obtained.

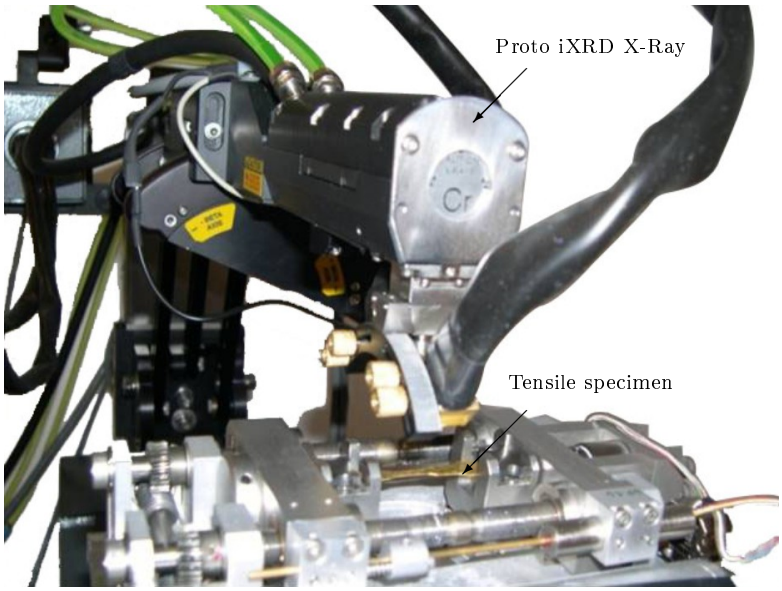

Figure 3.18. Proto iXRD X-Ray diffraction machine equipped with in-situ tensile test machine.

Comparing stresses before unloading and after loading the influence of cycling and the strain path can be analysed from a microscopic point of view (Berveiller et al., 2004; Weidner et al., 2010; Jatczak, 1980).

3.6.2 Experimental results

Macro strain path influence analysis

The baseline test has been compared with second and third variants in order to study the influence of the strain path on the recovery behaviour of the material. The elastic unloading-loading behaviours after 9% and 19% of pre-strain have been analysed for each test and compared. Figure 3.19 shows the comparison between the baseline test and the second variant (fewer cycles) at 9% pre-strain. Similar results are obtained for 19% of pre-strain and are not plotted. The differences between both elastic unloading-loading paths stress-strain are lower than the 2%.

Third variant and baseline tests have been compared aimed at analysing if unloading up to a fixed stress (not reaching total relaxation) could affect the loading-unloading behaviour. Figure 3.20 represents the comparison between the elastic unloading-loading of the baseline test and third variant test at 9% pre-strain. Similar results are obtained for 19% of pre-strain and are not plotted. It can be noted that the stress values for third variant do not go until zero, but finishes around 80 MPa, according to the stress

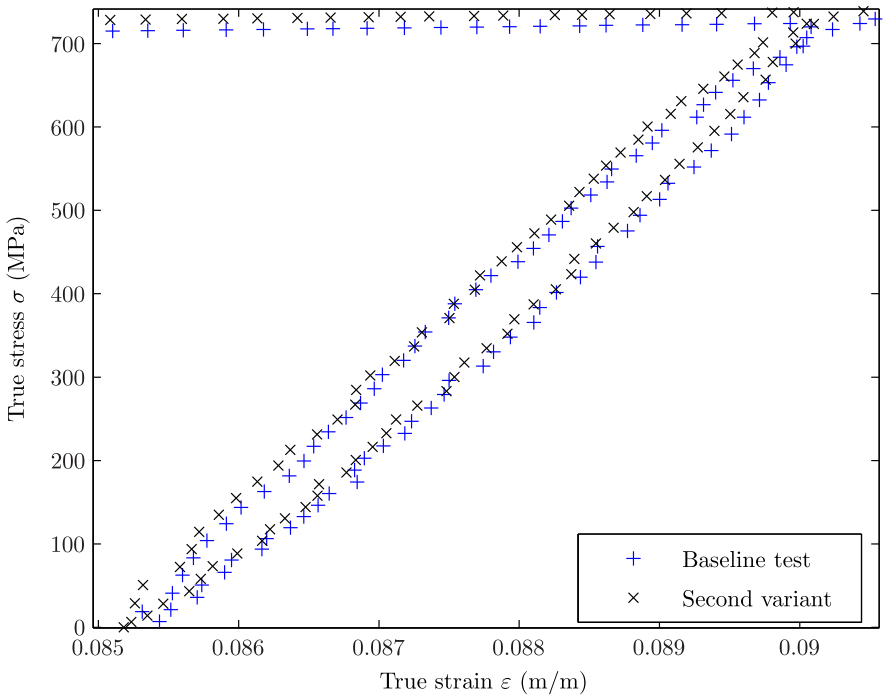

Figure 3.19. Comparative between the unloading phase after 9% of pre-strain of the baseline test and second variant.

for the relaxation force. Like in previous comparison, the difference between both elastic unloading-loading paths stress-strain is lower than the 2% (loading is not compared due to different relaxation stresses).

Micro X-Ray Diffraction results

- *Micro Strain path influence analysis in austenite.* No influence of the elastic path in the unloading-loading behaviour has been observed in the macro tests. In order to understand if the strain path influences at micro level micro cyclic tests have been performed as explained before.

  Figure 3.21 shows the results of in-situ X-ray diffraction measurement of micro-stress in the austenite phase. Macro stress curve is plotted in solid line. To analyse the influence of the change in the elastic path the micro-stress state has been measured before and after unloading, as well as in the middle of the unloading and in the middle of the loading. The comparable measurements are rounded by dashed circles. It has to be keep in mind that this is a surface measurement.

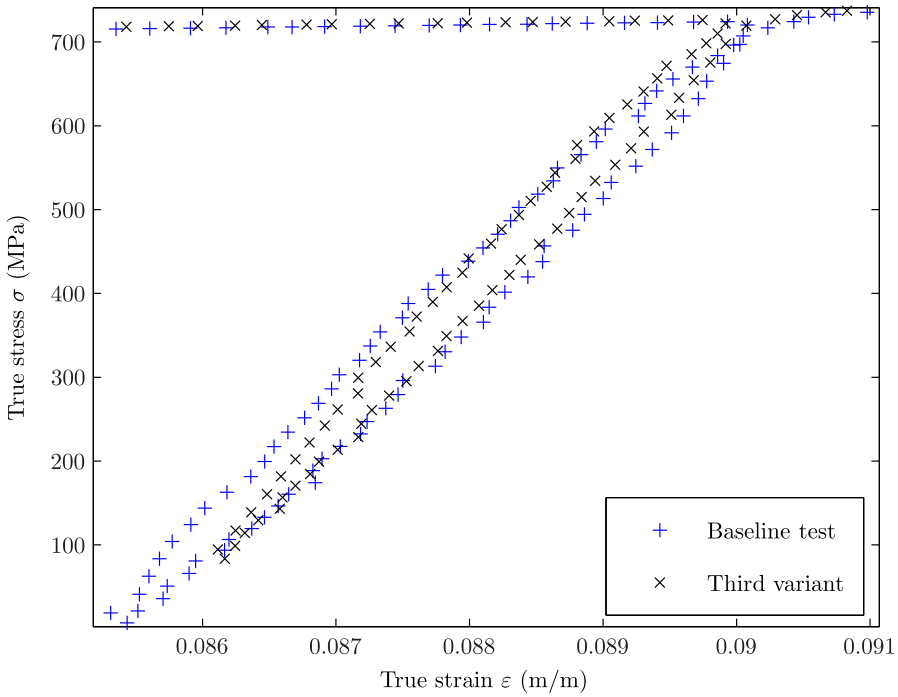

Figure 3.20. Comparative between the unloading phase after 9% of pre-strain of the baseline test and third variant.

It is noticed that the austenite phase is in tension during the tensile test except at the initial state where the stress value is negative due to surface preparation (Berrahmoune et al., 2004) and the skin-pass in coll rolling.

The micro stress values of the austenite phase are higher than the macroscopic ones, between 50 MPa and 70 MPa. This means that austenite is harder than the other phases. Phase rigidity is assumed to be the reason for this effect. Stress values inside the circles fall in same values before and after unloading-loading cycle, thus no influence of the strain path on the stress state of the austenite phase is revealed.

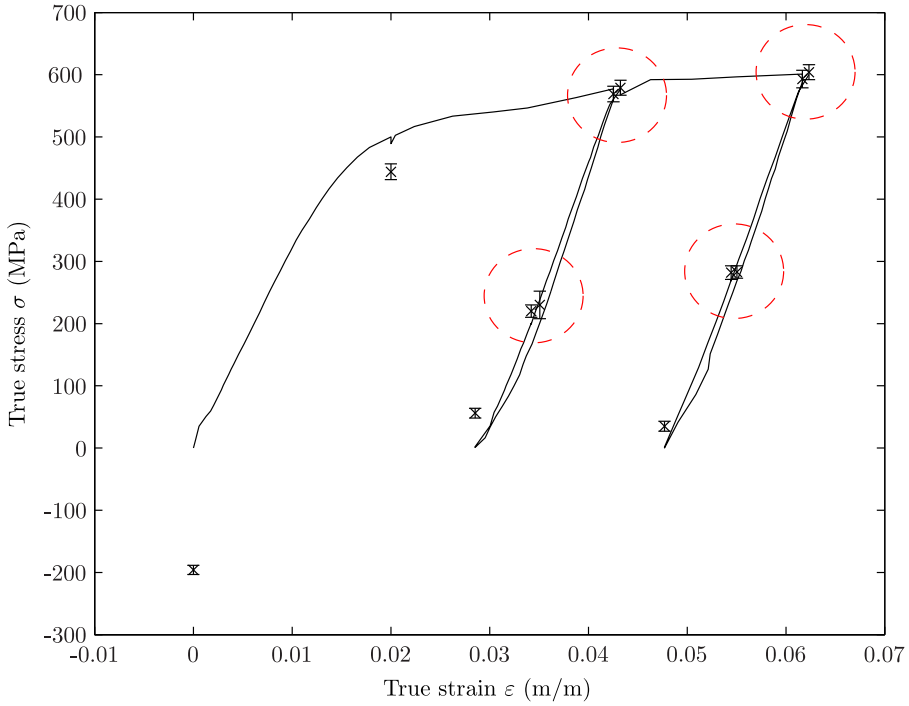

Figure 3.21. X-ray diffraction measurements in austenite.

- *Micro Strain path influence analysis in ferrite.* Following the same technique, micro stress values have been measured in the ferrite phase, using the {2 1 1} crystallographic planes. Results are shown in Fig. 3.22. Macro stress curve is plotted in solid line. The comparable measurements are rounded by dashed circles.

  The stress value at the initial state shows that the ferrite phase is in compression around 200 MPa. Both phases are in compression at the initial stress whereas there is no applied stress in the sample. As previously mentioned, this phenomenon could be due to the sample polishing and the skin-pass in cold rolling.

  The ferrite stress values are lower than the macroscopic stress values for low strains, around 50 MPa at the yield stress, and seem to converge to the macroscopic stress in larger strains than 3-4%. The microstructure of TRIP steels is retained austenite embedded in a primary matrix of ferrite. In addition to a minimum of around 7 volume percent of retained austenite, hard phases such as martensite and bainite are present in varying amounts. When the plastic strain increases the TRIP transformation occurs and the percentage of residual austenite decreases. The

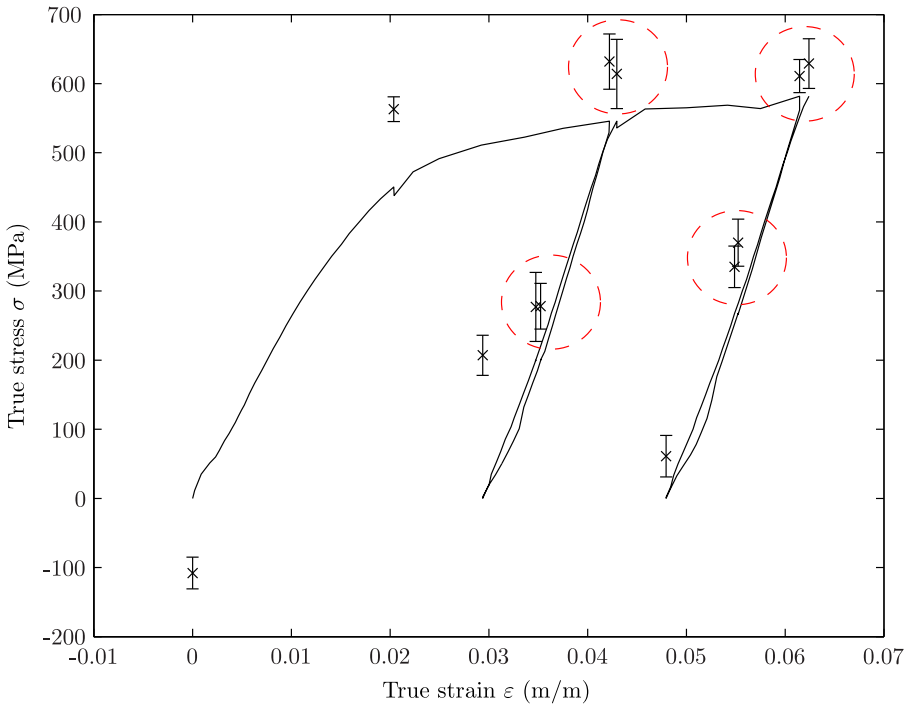

Figure 3.22. X-ray diffraction measurements in ferrite.

stress addition theory (Kouznetsova and Geers, 2008) states that the stress value supported by each phase is dependent on its volume fraction,

$$\sigma_{\text{macro}} \cdot V = \sum \sigma_i \cdot V_i, \tag{3.4}$$

where σ_i is the stress of the i-th phase with V_i volume fraction. Therefore, as low percentage of residual austenite is expected at high strains, the microscopic-stress value of ferrite should converge with the macroscopic stress-value.

Comparing the micro measurements before and after unloading cycle it can be noted that the unloading-loading cycle has not changed the ferrite stress value.

Summarising, not remarkable differences have been found when changing the elastic strain path at macroscopic level (first three variants). Considering the present results, the number of elastic unloading-loading cycles performed before an unloading phase is not relevant for the elastic unloading behaviour. Elastic behaviour is independent of the strain path for the selected steel and conditions.

At the same time, micro stress states before and after the elastic unloading-loading cycles fall in the same value (taking into account the measurement uncertainty) during

the X-Ray Diffraction measurements. Therefore, no influence of the elastic strain path is shown at microscopic level.

By means of this analysis the no influence of the elastic strain path on the unloading-loading of the TRIP steel has been confirmed. These results prove that conventional cyclic testing (baseline test in this paper) is a valid methodology for a detailed characterisation of the elastic modulus and reliable numerical modelling of springback.

3.7 Conclusions

In this section the main conclusions of the conducted material characterisation of the TRIP 700 steel are exposed.

- The tensile tests reveal that the TRIP 700 steel has an initial yield stress around 490 MPa while it could be elongated up to a 25%. In the same way from the Lankford coefficients can be concluded that during a longitudinal deformation a more important reduction occurs in thickness than in width. This conclusion could be crucial for a complex bending springback simulation, where the reduction in thickness plays a very important role.

- The hardening behaviour of the TRIP 700 steel is more close to a pure kinematic hardening than to a pure isotropic. However, the mixed hardening behaviour represents more accurately the behaviour of the material.

- The elastic modulus during loading phases as well as the chord modulus during unloading phases decrease as pre-strain increases. This decrease could be of about $15\% - 20\%$ at 12% of pre-strain.

- The non-linearity of the loading phases can be explained by the dislocation bending phenomenon while the unloading non-linearity is composed by different phenomena, in which the main one is the microplastic strain.

- The reduction of the unloading elastic modulus is related to both TRIP phenomena and dislocation rearrangement effect. The dislocation rearrangement is the main reason of the elastic modulus decrease.

- The increase in the upper yield point shown in the reloading phases could be explained by the short time Snoek rearrangement process.

- About the strain path influence, no remarkable differences have been found when changing the elastic strain path at macroscopic level. Considering the present results, the number of elastic unloading-loading cycles performed before an unloading

phase is not relevant for the elastic unloading behaviour. Elastic behaviour is independent of the strain path for the selected steel and conditions.

- Micro stress states before and after the elastic unloading-loading cycles fall in the same value during the X-Ray Diffraction measurements. Therefore, no influence of the elastic strain path is shown at microscopic level.

The results prove that the baseline test is a valid methodology for a detailed characterisation of the elastic behaviour.

Chapter 4

One-dimensional extended elastic law

Synopsis

This chapter deals with the influence of the elastic behaviour modelling in sprinback simulations. An extended elastic law is proposed. The extended elastic law is particularised for the TRIP 700 steel using three different modelling techniques: classical behaviour, linear elastic with variable elastic modulus and non-linear elastic behaviours. In order to analyse the influence of the elastic behaviour on the springback prediction, a pseudo-analytical bending test is performed.

The comparative of the numerical loading-unloading test performed between the three modelling techniques and the experimental data shows that the unloading occurs until complete relaxed point, both linear elastic with variable elastic modulus and non-linear elastic behaviour leads to the same point even if only the second one follows the experimental data. Nevertheless, when the unloading does not reach the complete relaxed point, the linear elastic with variable elastic modulus behaviour is not able to fit the experimental data as accurately law as the non-linear elastic behaviour. On the contrary the classical linear elastic does not fit neither the case of complete unloading neither the case with partial unloading.

The pseudo-analytical test shows the differences between springback predictions between the different elastic behaviours.

4.1 Introduction

In the previous chapter the TRIP 700 steel has been experimentally characterised in order to provide experimental data for an accurate modelling of the springback phenomenon.

In Chapter 2, the most important phenomena to be taken into account in order to carry out an accurate springback simulation have been presented.

From a material modelling point of view, anisotropic behaviour, kinematic hardening and elastic behaviour have been proven to be the most important phenomena to be taken into account. Therefore, in Chapter 3 the three phenomena have been characterised.

Even if the three phenomena have been characterised, in this thesis work, only the modelling of the elastic behaviour phenomenon will be studied. In this context, an isotropic hardening with isotropic von Mises yield criteria elastoplastic model is developed. Consequently, the experimental test to be performed, to validate the model, has to be simple and not sensitive to the cyclic plasticity and the anisotropic yielding.

This chapter deals with the influence of the elastic behaviour modelling in springback simulations. First, a review of the most used modelling techniques is performed. As the existing elastic behaviour modelling techniques do not represent the elastic behaviour of the TRIP 700 steel between others, an extended elastic law is proposed.

Next, the formulation of that extended elastic law is developed detailing the numerical implementation scheme.

After the identification of the parameters of each modelling technique for the TRIP 700 steel, the accuracy of each modelling technique is analysed comparing the uniaxial numerical results with those obtained experimentally in the previous chapter.

Finally, a pseudo-analytical bending test is carried out in order to evaluate the influence of the elastic behaviour accuracy on a theoretical springback prediction.

4.2 Elastic law definition

In this section, an extension of the classical elastic law (for the uni-axial case) able to represent both linear and non-linear elastic behaviour is presented.
The experimental results exposed in the previous chapter show how the TRIP 700 steel does not maintain a linear behaviour during successive elastic unloading-loading cycles.

In Fig. 4.1 a representative elastic unloading-loading cycle extracted from the experimental data obtained in the previous chapter is exposed.

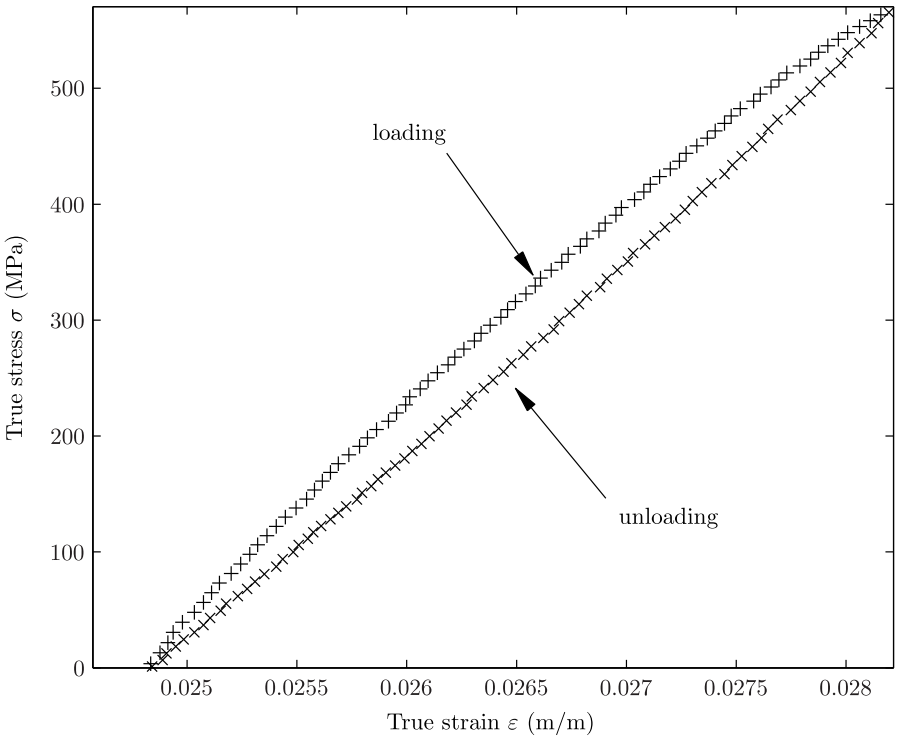

Figure 4.1. Representative elastic unloading and subsequent loading cycle extracted from the springback tests performed in Chapter 3.

Different kind of modelling techniques are shown in the literature in order to represents the non-linear elastic behaviour in metals. Following the idea that the change in microstructure induces the change of the elastic modulus, Thibaud et al. (2002) established a model of evolution of the elastic modulus in function of the percentage of retained austenite for materials with metastable phases. On the other hand, Halilovic et al. (2007) introduced the variation of the elastic modulus by means of stiffness degradation. However, the most extended modelling technique is making the elastic modulus dependent of the accumulated plastic strain (Yoshida et al., 2002; Yu, 2009). All these techniques involve a linear elastic model where the elastic modulus changes in function of an internal variable. It has been concluded in the bibliography review that this kind of over-simplification of taking the unloading behaviour as a linear elastic unloading cause errors reaching the $10 - 20\%$ at some cases.

The extra strain introduced during the non-linear elastic unloading draws a concave

shape of the unloading path. The modulus of the straight line that relies the first and last unloading points (chord modulus) is usually taken as equivalent elastic modulus. The use of this modelling technique gives an accurate result as long as the unloading reaches the zero stress state. However, it creates significant accuracy limitations when the unloading does not reach the zero stress value. After unloading a standard bending process, the residual stresses can be of the same magnitude as the stresses in loading. This is why large differences between the experimental test and numerical simulation are achieved even when the elastic modulus evolution is taken into account.

Sun and Wagoner (2011) presented an elastoplastic formulation based in two yield surface models, where a new "Quasi-Plastic-Elastic" strain was introduced. By means of this new strain the model was able to represent a non-linear unloading behaviour, differentiating between elastic strains and "Quasi-Plastic-Elastic" strains.

In view of the state of understanding of the modelling of non-linear elastic behaviour, in this work, an extension of the classic elastic law is proposed. The main objective of the proposed law is to augment the capability of the elastic law to represent non-linear elastic behaviours, as well as classical linear elastic and linear elastic with variable elastic modulus behaviours.

First, the theoretical basis of the extension of the classical elastic law is developed. In this context, the special technique that is needed to recover the extended law parameters is presented.

Once the extended elastic law is defined, an one-dimensional isotropic hardening von Mises elastoplastic formulation coupled with the extended elastic law is presented. In order to provide a useful tool, the numerical implementation of the elastoplastic model is also detailed.

Aimed at comparing the different elastic law formulations, a parameter identification procedure is conducted for the TRIP 700 steel characterised in the previous chapter. In this context, the parameters for three different behaviours are obtained, i.e. classical elastic law, Yu and Yoshida (Yu, 2009; Yoshida et al., 2002) type linear elastic law with evolution of the elastic modulus and extended elastic law where the non-linear elastic behaviour is taken into account.

Once the parameter identification is carried out, the loading-unloading test in different configurations is performed with the three different behaviours in order to analyse the differences between them.

4.2.1 Unidimensional extended elastic law

Taking into account the limitation of the classic elastic law to represent only linear elastic behaviour, in this section an extended formulation is proposed, which is able to represent both classical linear and non-linear behaviours.

This kind of classical model extensions have been widely developed in other science areas as thermal conductivity or population dynamics among others (e.g., Luchko et al., 2010; Rivero et al., 2010; Kilbas et al., 2006).

Theoretical basis

The classical elastic law relates the macroscopic elastic strain and macroscopic stress (hereafter named elastic strain and stress, respectively) by means of a differential equation written as

$$\mathrm{d}\sigma = E\,\mathrm{d}\varepsilon^{\mathrm{e}}, \tag{4.1}$$

where σ represents stress ε^{e} represents the elastic strain and E is the Young's modulus. A more deeper explanation about the classic elastic law could be fund in (Callister, 1993) or (Timoshenko and Goodier, 1968) among others.
The differential equation Eq. (4.1) can be expressed in an integral form as

$$\sigma(\varepsilon^{\mathrm{e}}) = \sigma_0 + \int_0^{\varepsilon^{\mathrm{e}}} E\mathrm{d}\tau, \tag{4.2}$$

where σ_0 represents the stress initial condition, while 0 and ε^{e} are the integration limits.

Taking into account the integral form of the classic elastic law Eq. (4.2), the proposed extension is obtained introducing a new kernel function in the integral,

$$\sigma(\varepsilon^{\mathrm{e}}, \boldsymbol{\alpha}) = \sigma_0 + \int_0^{\varepsilon^{\mathrm{e}}} \mathsf{K}(\tau, \boldsymbol{\alpha})\, E\mathrm{d}\tau, \tag{4.3}$$

where $\mathsf{K}(\cdot)$ represents the new kernel function, which is dependent of the integration variable τ and it can be also dependent of state variables, $\boldsymbol{\alpha}$.

As a particular case, when the kernel takes the unit value $\mathsf{K}(\tau, \boldsymbol{\alpha}) \equiv 1$, the extended elastic law Eq. (4.3) results in the classical elastic law shown in Eq. (4.2).

On the other hand, if the kernel function is dependent on the accumulated plastic strain $\mathsf{K}(\tau, \boldsymbol{\alpha}) = f(\bar{\varepsilon}^{\mathrm{p}})$, the extended elastic law represents a linear elastic behaviour where the elastic modulus evolves with the accumulated plastic strain. This kind of models are widely used in damage theories (e.g., Halilovic et al., 2007) as well as in the

previously reviewed equivalent elastic modulus models (e.g., Yu, 2009; Yoshida et al., 2002).

Otherwise, introducing a kernel dependent on the integration variable τ and other external variables $\boldsymbol{\alpha}$, $\mathsf{K}(\tau, \boldsymbol{\alpha}) = f(\boldsymbol{\alpha}, \tau)$, a non-linear elastic behaviour is achieved.

Analysing the range of values of the introduced kernel, the following conclusions are obtained:

- On the one hand, if the kernel function takes the zero value $\mathsf{K} = 0$, then the stress value will remains equal to the stress initial condition for any value of elastic strain, $\sigma(\varepsilon^{\mathrm{e}}) = \sigma_0, \quad \forall\, \varepsilon^{\mathrm{e}}$.
- On the other hand, if the kernel function takes the unit value $\mathsf{K} = 1$, as it has been previously mentioned the extended elastic law leads to the same expression as the classic elastic law, where the stress and elastic strain are related with the Young's modulus, $\mathrm{d}\sigma(\varepsilon^{\mathrm{e}}) = E\,\mathrm{d}\varepsilon^{\mathrm{e}}$.
- Otherwise, if the kernel function takes a value different to zero and one, $0 \neq \mathsf{K} \neq 1$, the extended elastic law represents an elastic behaviour where the relation between the stress and elastic strain will be defined with the product of the kernel value and the Young's modulus, $\mathrm{d}\sigma(\varepsilon^{\mathrm{e}}) = (E \cdot \mathsf{K})\,\mathrm{d}\varepsilon^{\mathrm{e}}$. Therefore, a reduction of the elastic modulus is represented with a kernel value lower than one but greater than zero, $0 < \mathsf{K} < 1$. Representing an elastic modulus hardening with a kernel value greater than one, $\mathsf{K} > 1$.

In some cases, the elastic behaviour to be represented follows a symmetric condition between loading and unloading, e.g. the elastic behaviour of the TRIP 700 shown[1] in Fig. 4.1. Therefore, in order to take advantage of this property, the previously presented general form of the extended elastic law is modified.

A new spacial variable ξ is introduced. This new spacial variable is related with the shape of the behaviour path and it is non-negative,

$$\xi \geq 0. \tag{4.4}$$

Consequently, the extended elastic law Eq. (4.3), results

$$\sigma(\xi, \boldsymbol{\alpha}) = \sigma_0 \pm \int_0^{\xi} \mathsf{K}(\tau, \boldsymbol{\alpha})\, E\, \mathrm{d}\tau, \tag{4.5}$$

[1] In Chapter 3 is concluded that the unloading and loading paths are not perfectly symmetric but this hypothesis will be stated in this chapter in order to facilitate the modelling procedure.

where $\xi = |\varepsilon_1^{\mathrm{e}} - \varepsilon_0^{\mathrm{e}}|$, and where if it is a loading process, $\varepsilon_1^{\mathrm{e}} > \varepsilon_0^{\mathrm{e}}, \quad \dot{\varepsilon}^{\mathrm{e}} > 0$, the sign of the integral is positive,

$$\sigma(\xi, \boldsymbol{\alpha}) = \sigma_0 + \int_0^{\xi} \mathsf{K}(\tau, \boldsymbol{\alpha})\, E \, \mathrm{d}\tau, \tag{4.6}$$

and if it is an unloading process, $\varepsilon_1^{\mathrm{e}} < \varepsilon_0^{\mathrm{e}}, \quad \dot{\varepsilon}^{\mathrm{e}} < 0$, the sign of the integral is negative,

$$\sigma(\xi, \boldsymbol{\alpha}) = \sigma_0 - \int_0^{\xi} \mathsf{K}(\tau, \boldsymbol{\alpha})\, E \, \mathrm{d}\tau. \tag{4.7}$$

Therefore, the extended elastic law satisfies,

$$\sigma(\xi, \boldsymbol{\alpha}) = \sigma_0 + \operatorname{sign}(\dot{\varepsilon}^{\mathrm{e}}) \int_0^{\xi} \mathsf{K}(\tau, \boldsymbol{\alpha})\, E \, \mathrm{d}\tau, \tag{4.8}$$

where the $\operatorname{sign}(a)$ function represents,

$$\operatorname{sign}(a) = \begin{cases} +1 & \text{if } a > 0, \\ -1 & \text{if } a < 0. \end{cases} \tag{4.9}$$

By means of this modifications, it is taken advantage of the symmetry of the behaviour without losing the capability of the model to represent the classical linear elastic behaviour. If the kernel takes the unit value $\mathsf{K}(\tau, \boldsymbol{\alpha}) \equiv 1$, the extended elastic law still represents the classic behaviour Eq. (4.2).

Kernel identification

In this section, the methodology to identify the expression of the kernel of the extended elastic law from experimental data is exposed. The identification methodology outlined in this section is based on the kernel search technique exposed in (Luchko et al., 2010) in the population dynamic field.

The kernel search process starts from the numerical values of the experimentally obtained elastic strain-stress pairs $[\varepsilon^{\mathrm{e}}, \sigma]$. This data pairs could be obtained from a loading-unloading cyclic test presented in Chapter 3.
The extended elastic law Eq. (4.3), can be resumed as,

$$\sigma(\varepsilon^{\mathrm{e}}, \boldsymbol{\alpha}) = \sigma_0 + E\, \mathrm{I}_{\varepsilon^{\mathrm{e}}}, \tag{4.10}$$

where,

$$\mathrm{I}_{\varepsilon^{\mathrm{e}}} = \int_0^{\varepsilon^{\mathrm{e}}} \mathsf{K}(\tau, \boldsymbol{\alpha})\, \mathrm{d}\tau. \tag{4.11}$$

The expression Eq. (4.10) can be regrouped as,

$$\frac{\sigma(\varepsilon^{\mathrm{e}}, \boldsymbol{\alpha}) - \sigma_0}{E} = \mathrm{I}_{\varepsilon^{\mathrm{e}}}, \tag{4.12}$$

where the left hand side terms being already known, only the integral value remains as unknown.

From a practical point of view, the Eq. (4.11) integral is evaluated using a quadrature method. Among all the quadratures existing in the literature, in this work the simple midpoint integration rule is used (Press et al., 1992). The schematic representation of this integration rule is shown in Fig. 4.2. Applying the midpoint integration rule

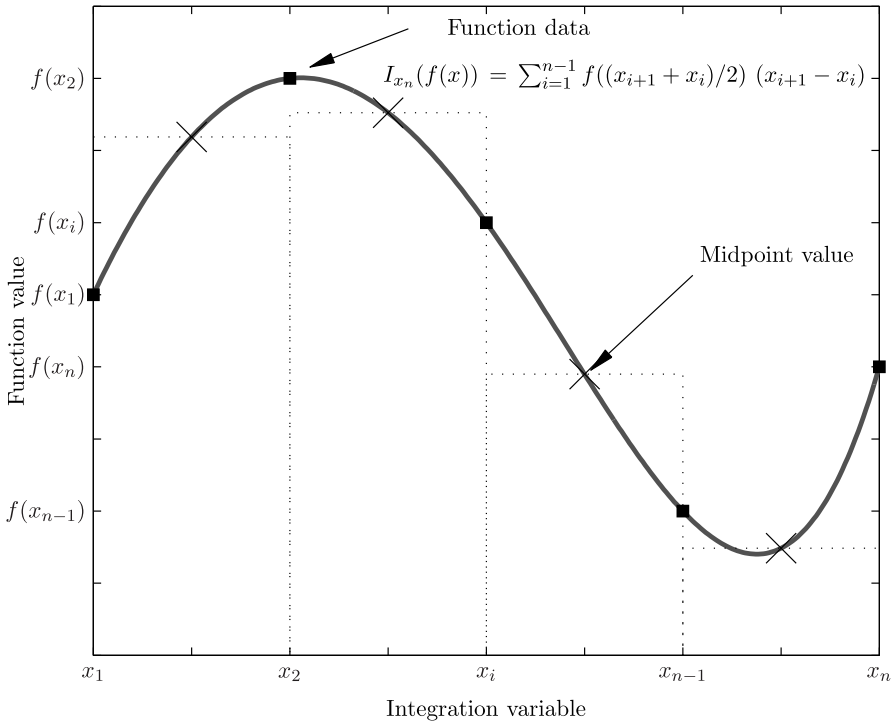

Figure 4.2. Schematic representation of the midpoint integration rule.

to the Eq. (4.11) integral, this can be evaluated as

$$\mathrm{I}_{\varepsilon^{\mathrm{e}}_n} = \sum_{i=1}^{n-1} \mathsf{K}((\tau_{i+1} + \tau_i)/2, \boldsymbol{\alpha})\,(\tau_{i+1} - \tau_i), \tag{4.13}$$

where $\tau_n = \varepsilon^{\mathrm{e}}_n$ and $\tau_1 = \varepsilon^{\mathrm{e}}_0$.
In the case of equispaced data, the expression above is reduced to

$$\mathrm{I}_{\varepsilon^{\mathrm{e}}_n} = \sum_{i=1}^{n-1} \mathsf{K}((i-1)h_{\varepsilon^{\mathrm{e}}} + h_{\varepsilon^{\mathrm{e}}}/2, \boldsymbol{\alpha})\, h_{\varepsilon^{\mathrm{e}}}, \tag{4.14}$$

where $h_{\varepsilon^{\mathrm{e}}}$ is the step of the equispaced data.

Using this quadrature technique, based on elastic strain-stress data pairs, $[\varepsilon^{\mathrm{e}}, \sigma]$, at $[\varepsilon^{\mathrm{e}}_1, \varepsilon^{\mathrm{e}}_2, ..., \varepsilon^{\mathrm{e}}_N]$ position, it is possible to obtain the value of the kernel at the $[(\varepsilon^{\mathrm{e}}_1 + \varepsilon^{\mathrm{e}}_2)/2, (\varepsilon^{\mathrm{e}}_2 + \varepsilon^{\mathrm{e}}_3)/2, ..., (\varepsilon^{\mathrm{e}}_{N-1} + \varepsilon^{\mathrm{e}}_N)/2]$ positions.

Once the value of the kernel is obtained in those positions, is possible to fit an analytical function to the cloud of the kernel's data points, obtaining by this way the kernel function that particularises the analysed material extended elastic law.

4.3 Elastoplastic formulation

In this section, the theoretical basis of an elastoplastic behaviour with isotropic hardening and with the previously presented extended elastic law one-dimensional model is exposed.

Then, the basis laws with compose the elastoplastic one-dimensional model are established.

Elastoplastic decomposition of the strain

The elastoplastic decomposition of the strain supposes that the total strain ε^{t} can be decomposed in the recoverable elastic strain ε^{e} and the permanent plastic strain ε^{p},

$$\varepsilon^{\mathrm{t}} = \varepsilon^{\mathrm{e}} + \varepsilon^{\mathrm{p}}. \tag{4.15}$$

Extended elastic law

The extended elastic law is defined with the expression in Eq. (4.8), which leads,

$$\sigma(\varepsilon^{\mathrm{e}}, \alpha) = \sigma_0 + \mathrm{sign}(\dot{\varepsilon}^{\mathrm{e}}) \int_0^{\xi} \mathsf{K}(\tau, \boldsymbol{\alpha})\, E \,\mathrm{d}\tau,$$

where $\xi = |\varepsilon^{\mathrm{e}}_1 - \varepsilon^{\mathrm{e}}_0|$, and the sign of the integral depends on the nature of the process, i.e. loading nature of contrary unloading nature.

Yield function and yield criteria

The yield function Φ limits the elastic zone and defines if in a particular state the behaviour is purely elastic or on the contrary it is elastoplastic. In a one-dimensional particular case, the yield function is defined as

$$\Phi(\sigma, \sigma_{\mathrm{y}}) = |\sigma| - \sigma_{\mathrm{y}}, \tag{4.16}$$

where, $|\sigma|$ represents the absolute value of the stress, and σ_y is the yield stress at which the plastic mechanisms are triggered. This signifies that the absolute value of the stress is below the yield stress, the material is under purely elastic behaviour

$$|\sigma| < \sigma_{\mathrm{y}}. \tag{4.17}$$

However, when the stress reaches the yield stress,

$$|\sigma| = \sigma_{\mathrm{y}}, \tag{4.18}$$

the plastic mechanisms are triggered.

It should be noted that, at any stage, the stress never overcome the yield stress, because the yield surface, represented in the one-dimensional case by the yield function, expands with the increasing plastic deformations, maintaining the stress on the yield surface during all the elastoplastic loading. This property of the yield surface allows to define the plastically admissible stress as:

$$\Phi(\sigma, \sigma_{\mathrm{y}}) \leq 0, \tag{4.19}$$

$$\begin{aligned}
&\text{If } \Phi(\sigma, \sigma_{\mathrm{y}}) > 0 \implies \text{Inadmissible},\\
&\text{If } \Phi(\sigma, \sigma_{\mathrm{y}}) < 0 \implies \dot{\varepsilon}^{\mathrm{p}} = 0,\\
&\text{If } \Phi(\sigma, \sigma_{\mathrm{y}}) = 0 \implies \dot{\varepsilon}^{\mathrm{p}} = 0 \text{ for elastic unloading},\\
&\text{If } \Phi(\sigma, \sigma_{\mathrm{y}}) = 0 \implies \dot{\varepsilon}^{\mathrm{p}} \neq 0 \text{ for plastic loading}.
\end{aligned} \tag{4.20}$$

Plastic flow rule, loading/unloading conditions

The plastic flow rule for a one-dimensional case leads

$$\dot{\varepsilon}^{\mathrm{p}} = \dot{\gamma}\,\mathrm{sign}(\sigma), \tag{4.21}$$

where $\dot{\gamma}$ is the plastic multiplier, which is defined as non-negative, $\dot{\gamma} \geq 0$.

Taking into account the non-negative property of the plastic multiplier and the plastically admissible yield functions values, the consistency condition can be expressed as

$$\Phi\,\dot{\gamma} = 0. \tag{4.22}$$

Hardening law

The hardening law establishes the relation between the yield surface expansion and the elastoplastic state.
In this particular case, an isotropic hardening law in function of the accumulated plastic strain $\bar{\varepsilon}^{\mathrm{p}}$ is given by

$$\sigma_{\mathrm{y}} = \sigma_{\mathrm{y}}(\bar{\varepsilon}^{\mathrm{p}}), \tag{4.23}$$

where the accumulated plastic strain $\bar{\varepsilon}^{\mathrm{p}}$ is defined as

$$\bar{\varepsilon}^{\mathrm{p}} = \int_0^t |\dot{\varepsilon}^{\mathrm{p}}| \mathrm{d}t, \tag{4.24}$$

where t is a pseudo-time process variable.
As it has been previously advanced, in a monotonic tensile test

$$\bar{\varepsilon}^{\mathrm{p}} = \varepsilon^{\mathrm{p}}, \tag{4.25}$$

whereas in a monotonic compression test

$$\bar{\varepsilon}^{\mathrm{p}} = -\varepsilon^{\mathrm{p}}. \tag{4.26}$$

For practical purposes, the evolution of the accumulated plastic strain is defined as

$$\dot{\bar{\varepsilon}}^{\mathrm{p}} = |\dot{\varepsilon}^{\mathrm{p}}| = \dot{\gamma}. \tag{4.27}$$

The Table 4.1 summarises the elastoplastic model presented in this section.

Table 4.1
One-dimensional elastoplastic model summary.

Constitutive equation	Equation
Elastoplastic strain decomposition	$\varepsilon^{\mathrm{t}} = \varepsilon^{\mathrm{e}} + \varepsilon^{\mathrm{p}}$
Elastic extender new law	$\sigma(\varepsilon^{\mathrm{e}}) = \sigma_0 + \mathrm{sign}(\dot{\varepsilon}^{\mathrm{e}}) \int_0^{\xi} \mathsf{K}(\tau, \boldsymbol{\alpha})\, E\, \mathrm{d}\tau;\ \xi = \lvert\varepsilon_1^{\mathrm{e}} - \varepsilon_0^{\mathrm{e}}\rvert$
Yield function	$\Phi(\sigma, \sigma_y) = \lvert\sigma\rvert - \sigma_{\mathrm{y}}$
Plastic flow	$\dot{\varepsilon}^{\mathrm{p}} = \dot{\gamma}\,\mathrm{sign}(\sigma)$
Hardening law	$\sigma_{\mathrm{y}} = \sigma_{\mathrm{y}}(\bar{\varepsilon}^{\mathrm{p}})$
	$\dot{\bar{\varepsilon}}^{\mathrm{p}} = \dot{\gamma}$
Loading unloading conditions	$\Phi \leq 0 \quad \dot{\gamma} \geq 0, \quad \dot{\gamma}\Phi = 0$

4.4 Numerical implementation

In this section the numerical implementation methodology of the elastoplastic model summarised in the Table 4.1 is presented. The main objective of this numerical implementation procedure is to include the elastoplastic model with the extended elastic law into a general computing software, as Matlab® or into finite element software as Abaqus®.

The numerically implemented scheme has to star knowing the variable's values in the initial state n, $(\cdot)_n$, and taking into account the elastoplastic model, given by Table 4.1, and the imposed strain increment $\Delta\varepsilon^{\mathrm{t}}$ (which from now on is represented as $\Delta\varepsilon$), it has to be able to predict the variable's values at the end of the increment, $(\cdot)_{n+1}$.

Before detailing the numerical implementation of the elastoplastic model, the numerical implementation of the extended elastic law (4.8) is presented.

4.4.1 Numerical implementation of the extended elastic law

In order to facilitate the numerical implementation of the extended elastic law, a new process nature variable CD is introduced. This new variable indicates the nature of the process, differentiating between loading processes and unloading processes.

When the imposed strain increment involves a loading process, the CD variable takes the unit positive value,

$$\Delta\varepsilon^{\mathrm{e}} > 0 \rightarrow CD = 1, \tag{4.28}$$

however, if the imposed strain increment involves an unloading process, the CD variable takes the unit negative value,

$$\Delta\varepsilon^{\mathrm{e}} < 0 \rightarrow CD = -1. \tag{4.29}$$

Consequently, the sign of the integral in the extended elastic law expression, Eq. (4.5), can be replaced by the process nature variable, CD,

$$\sigma(\xi, \bar{\varepsilon}^{\mathrm{p}}) = \sigma_0 + (CD) \int_0^{\xi} \mathsf{K}(\tau, \boldsymbol{\alpha})\, E \, \mathrm{d}\tau. \tag{4.30}$$

It should be noted that the new spacial variable ξ is sensitive to process nature changes. That means that when a change occurs in the process nature, the new spacial variable ξ is initialised. This phenomenon can be shown in the Fig. 4.3.

In the Fig. 4.3, two different unloading-loading cycles are shown. These cycles are both taken from the experimental results from the Chapter 3. The first figure, Fig. 4.3(a), shows the nature change at a totally relaxed point, where $\varepsilon_0^{\mathrm{e}} = 0$ and $\sigma = 0$. But Fig. 4.3(b) illustrates that the nature change occurs in a different point where neither the elastic strain nor the stress have zero value is shown, $\varepsilon_0^{\mathrm{e}} \neq 0$ and $\sigma_0 \neq 0$. Both nature changes have the consequence of the behaviour path change from concave to convex, which is controlled initially with the new spacial variable ξ, and therefore has to be defined that the new variable ξ, is sensitive to the process nature change, to be able to change from the unloading concave shape to loading convex shape and viceversa.

Consequently, being the new spacial variable sensible to the process nature change, if the imposed increment implies a process with different nature as the previous, the spacial variable is initialised,

$$\xi_{n+1} = |\Delta\varepsilon^{\mathrm{e}}|. \tag{4.31}$$

While if the new process nature is the same as the previous increment's process' nature, the spacial variable takes as start point the value at the start of the increment and continues growing,

$$\xi_{n+1} = \xi_n + |\Delta\varepsilon^{\mathrm{e}}|. \tag{4.32}$$

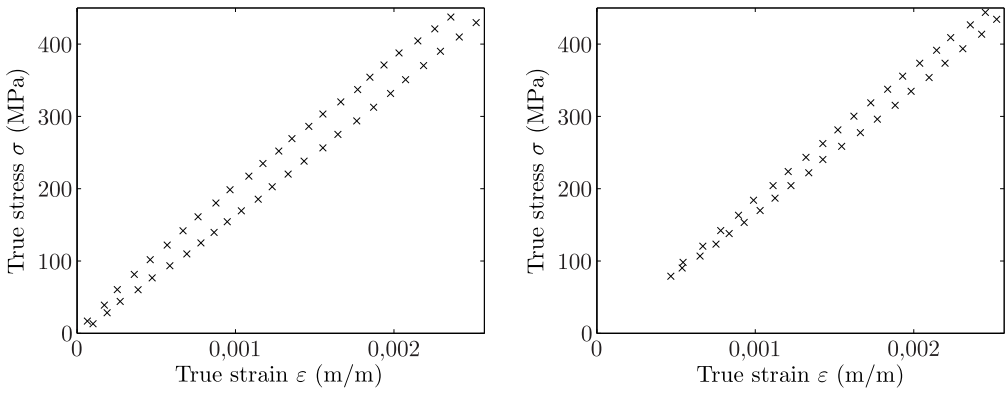

Figure 4.3. Initialisation property of the spacial variable ξ, two different unloading-loading cycles taken from the experimental results of the Chapter 3: (a) complete unloading test data; (b) partial unloading test data.

On the other hand, the integral of the extended elastic law, Eq. (4.30), has to be numerically analysed, and in the same way as for the kernel function identification, the midpoint integration rule is used with this purpose.
Unlike in the kernel function identification where the experimental non-equispaced points where used, now the integration points can be arbitrary defined. Therefore, N equispaced points are defined for the numerical evaluation of the integral, $\Delta\xi = |\Delta\varepsilon^{\mathrm{e}}/N|$, (the more points are defined, more accurate is the integral calculation but it implies more numerical effort). In this way, as is shown in the Fig. 4.2, the kernel has to be evaluated in the following points:

$$\xi = \left(\xi_{n+1} - (\Delta\xi\,(j-1)) - \frac{\Delta\xi}{2}\right), \tag{4.33}$$

starting at $j = 1$, and finishing at $j = N$.

The algorithm to evaluate the stress at the end of imposed elastic strain increment $\Delta\varepsilon^{\mathrm{e}}$ is summarised in the Algorithm Table 1.

4.4.2 Numerical implementation of the elastoplastic model

An elastic predictor/plastic corrector algorithm is used in order to implement the elastoplastic model defined in Section 4.3. This kind of algorithms are widely developed in

Algorithm Table 1 Numerical implementation of the extended elastic law.

1: Known variables

$$\sigma_n,\, \xi_n,\, CD_n, \boldsymbol{\alpha}_n, \boldsymbol{\alpha}_{n+1}$$

2: Imposed elastic strain increment, and the number of equispaced points to the integral evaluation

$$N,\, \Delta\varepsilon^{\mathrm{e}}$$

3: Evaluate the internal variable increment

$$\Delta\boldsymbol{\alpha} \,=\, \boldsymbol{\alpha}_{n+1} - \boldsymbol{\alpha}_n$$

4: Verify the nature of the process

5: **if** $\Delta\varepsilon^{\mathrm{e}} > 0$ **then**

6: $$CD_{n+1} = 1$$

7: **else**

8: $$CD_{n+1} = -1$$

9: **end if**

10: Evaluate the value of the spacial variable ξ

11: **if** $CD_{n+1} = CD_n$ **then**

12: $$\xi_{n+1} = \xi_n + |\Delta\varepsilon^{\mathrm{e}}|$$

13: **else**

14: $$\xi_{n+1} = |\Delta\varepsilon^{\mathrm{e}}|$$

15: **end if**

16: Define le integral discretisation increment

$$\Delta\xi \,=\, |\Delta\varepsilon^{\mathrm{e}}|/N$$

17: Define the internal variable increments for each spacial variable increment $\Delta\xi$

$$\Delta\boldsymbol{\alpha} \,=\, \Delta\boldsymbol{\alpha}/N$$

18: Compute the integral

$$I = \sum_{j=1}^{N} \mathsf{K}\left(\xi_{n+1} - (\Delta\xi\,(j-1)) - \frac{\Delta\xi}{2}, \boldsymbol{\alpha}_n + (j\,\Delta\boldsymbol{\alpha})\right)\,\Delta\xi$$

19: Update stress

$$\sigma_{n+1} = \sigma_n \,+\, (CD_{n+1})\,E\,I$$

the literature, where it can be found from simple elastoplastic model's implementation, e.g. perfect plastic model, to complex behaviour's model's implementation, e.g. models including mixed hardening, anisotropy, fracture, damage or viscoplasticity.

The elastic predictor/plastic corrector algorithms are divided into two steps. One first purely elastic assumption and the second one the plastic corrector of the purely elastic. The algorithms start knowing the value of the variables at the initial sate $(\cdot)_n$ and the

imposed strain increment $\Delta\varepsilon$. First, the elastic predictor step is performed, where the assumption of a purely elastic increment without plastic mechanisms is done,

$$\Delta\varepsilon^{\mathrm{e}} = \Delta\varepsilon. \tag{4.34}$$

Based on the purely elastic increment assumption, the value of the variables at the end of the increment are calculated, $(\cdot)_{n+1}^{\mathrm{trial}}$.

$$(\cdot)_n \rightarrow \Delta\varepsilon^{\mathrm{e}} \rightarrow (\cdot)_{n+1}^{\mathrm{trial}}. \tag{4.35}$$

Once the trial variables are calculated, it has to be evaluated the admissibility of the yield criteria Eq. (4.19).

If the obtained state, $(\cdot)_{n+1}^{\mathrm{trial}}$, is admissible from a yield function point of view, that means that the stated hypothesis of purely elastic increment is confirmed and the final state variables are those calculated under purely elastic assumption, leading to

$$(\cdot)_{n+1} = (\cdot)_{n+1}^{\mathrm{trial}}. \tag{4.36}$$

However, if the obtained final trial state $(\cdot)_{n+1}^{\mathrm{trial}}$ is not plastically admissible, the assumption of purely elastic increment is not correct and a plastic correction has to be performed.

The plastic corrector step has as a main objective to obtain the plastic strain increment,

$$\Delta\varepsilon = \Delta\varepsilon^{\mathrm{e}} + \Delta\varepsilon^{\mathrm{p}}, \tag{4.37}$$

following the behaviour defined for the elastoplastic model.

Many variation of the plastic corrector step are found in the literature, each one being particularised to a specific elastoplastic model. All of them have in common the objective of minimising the computational effort taking advantage of the already performed calculus in the elastic predictor step (de Souza Neto et al., 2008).

Then, the elastic predictor and plastic corrector steps are defined for the elastoplastic model defined in the previous Section 4.3.

Elastic predictor

To start the elastic predictor step, the variables at the start of the increment $(\cdot)_n$ and the imposed strain increment $\Delta\varepsilon$ have to be known. In the particular case of the elastoplastic model defined in Section 4.3, the variables can be differentiated into two groups.

On the one hand, the physical meaning variables as the total strain ε^{t}, elastic strain ε^{e}, plastic strain ε^{p}, or the stress variable σ. On the other hand, the state variables or internal variables as, the accumulated plastic strain, $\bar{\varepsilon}^{\mathrm{p}}$, spacial variable, ξ, the process nature variable, CD, and the internal variables, $\boldsymbol{\alpha}$.

The main hypothesis of the elastic predictor step is to be a purely elastic step, and therefore as plastic mechanisms are not involved, the accumulated plastic strain internal variable $\bar{\varepsilon}^{\mathrm{p}}$ and the internal variables[2], $\boldsymbol{\alpha}$, remains constant through the increment,

$$\bar{\varepsilon}^{\mathrm{p}\,\mathrm{trial}}_{n+1} = \bar{\varepsilon}^{\mathrm{p}}_{n}, \tag{4.38}$$

$$\boldsymbol{\alpha}^{\mathrm{trial}}_{n+1} = \boldsymbol{\alpha}_{n}. \tag{4.39}$$

Then, once the accumulated plastic strain $\bar{\varepsilon}^{\mathrm{p}\mathrm{trial}}_{n+1}$ and the elastic strain increment $\Delta\varepsilon^{\mathrm{e}}$ are known, the strain physical variables are evaluated,

$$\varepsilon^{\mathrm{t}\,\mathrm{trial}}_{n+1} = \varepsilon^{\mathrm{t}}_{n} + \Delta\varepsilon, \tag{4.40}$$

$$\varepsilon^{\mathrm{e}\,\mathrm{trial}}_{n+1} = \varepsilon^{\mathrm{e}}_{n} + \Delta\varepsilon^{\mathrm{e}}, \tag{4.41}$$

$$\varepsilon^{\mathrm{p}\,\mathrm{trial}}_{n+1} = \varepsilon^{\mathrm{p}}_{n}. \tag{4.42}$$

Once the strain configuration is known, taking into account the hardening law, the yield stress, $\sigma_{\mathrm{y}}(\bar{\varepsilon}^{\mathrm{p}}_{n+1})$ at the end of the increment, is computed

$$\sigma^{\mathrm{trial}}_{\mathrm{y}\,n+1} = \sigma_{\mathrm{y}}(\bar{\varepsilon}^{\mathrm{p}\,\mathrm{trial}}_{n+1}). \tag{4.43}$$

By means of the extended elastic law, summarised in the Algorithm Table 1, the stress value at the end of the increment can be related with the elastic strain increment,

$$\sigma^{\mathrm{trial}}_{n+1} = \sigma(\Delta\varepsilon^{\mathrm{e}}, N, \xi_n, CD_n, \sigma_n, \boldsymbol{\alpha}^{\mathrm{trial}}_{n+1}, \boldsymbol{\alpha}_n). \tag{4.44}$$

At this point, where the stress at the end of the increment σ_{n+1} and the characteristic yield stress $\sigma_{\mathrm{y}\,n+1}$ are known, the yield function Φ defined in Eq. (4.16) as,

$$\Phi(\sigma, \sigma_{\mathrm{y}}) = |\sigma| - \sigma_{\mathrm{y}}$$

can be evaluated. In the elastic predictor step, the yield function leads

$$\Phi = |\sigma^{\mathrm{trial}}_{n+1}| - \sigma^{\mathrm{trial}}_{\mathrm{y}\,n+1}. \tag{4.45}$$

[2] In this formulation, the hypothesis that the internal variables of the elastic behaviour only evolves during plastic deformation is established.

After calculating the yield function value, it has to be verified the hypothesis of purely elastic increment. If the resultant yield function value Eq. (4.45) is lower than zero

$$\Phi < 0, \tag{4.46}$$

the hypothesis of purely elastic increment is confirmed and the physical and state variables at the end of the increment can be updated with those calculated as elastic trial, $(\cdot)_{n+1} = (\cdot)^{\text{trial}}_{n+1}$,

$$\begin{aligned}
\varepsilon^{\text{t}}_{n+1} &= \varepsilon^{\text{t trial}}_{n+1}, && (4.47)\\
\varepsilon^{\text{e}}_{n+1} &= \varepsilon^{\text{e trial}}_{n+1}, && (4.48)\\
\varepsilon^{\text{p}}_{n+1} &= \varepsilon^{\text{p trial}}_{n+1} && (4.49)\\
\sigma_{n+1} &= \sigma^{\text{trial}}_{n+1}, && (4.50)\\
\bar{\varepsilon}^{\text{p}}_{n+1} &= \bar{\varepsilon}^{\text{p trial}}_{n+1}, && (4.51)\\
CD_{n+1} &= CD^{\text{trial}}_{n+1}, && (4.52)\\
\boldsymbol{\alpha}_{n+1} &= \boldsymbol{\alpha}^{\text{trial}}_{n+1}, && (4.53)\\
\xi_{n+1} &= \xi^{\text{trial}}_{n+1}. && (4.54)
\end{aligned}$$

However, if the yield function value is not lower than zero, so the stress is not plasticity admissible, the hypothesis of purely elastic increment is not confirmed and the plastic corrector step has to be executed.

Plastic corrector

The plastic corrector step starts from the premise that the increment is an elastoplastic increment and then the strain increment can be divided into both elastic and plastic strains, as it has been defined in the elastoplastic model definition Eq. (4.37),

$$\Delta\varepsilon = \Delta\varepsilon^{\text{e}} + \Delta\varepsilon^{\text{p}}\,.$$

In order to simplify the plastic corrector algorithm, the plastic multiplier increment is introduced $\Delta\gamma$ wherefrom the elastic increment leads

$$\Delta\varepsilon^{\text{e}} = \Delta\varepsilon - \operatorname{sign}(\sigma_{n+1})\,\Delta\gamma. \tag{4.55}$$

The main objective of the plastic corrector step is to find the value of the plastic multiplier increment $\Delta\gamma$, in order to solve the following equation system:

$$\begin{aligned}
\varepsilon^{\mathrm{t}}_{n+1} &= \varepsilon^{\mathrm{t}}_{n} + \Delta\varepsilon, && (4.56)\\
\varepsilon^{\mathrm{e}}_{n+1} &= \varepsilon^{\mathrm{e}}_{n} + \Delta\varepsilon - \mathrm{sign}(\sigma_{\mathrm{n+1}})\,\Delta\gamma, && (4.57)\\
\varepsilon^{\mathrm{p}}_{n+1} &= \varepsilon^{\mathrm{p}}_{n} + \mathrm{sign}(\sigma_{\mathrm{n+1}})\,\Delta\gamma, && (4.58)\\
\bar{\varepsilon}^{\mathrm{p}}_{n+1} &= \bar{\varepsilon}^{\mathrm{p}}_{n} + \Delta\gamma, && (4.59)\\
\boldsymbol{\alpha}_{n+1} &= \boldsymbol{\alpha}_{n} + \boldsymbol{\alpha}(\Delta\gamma), && (4.60)\\
\sigma_{\mathrm{y}\,n+1} &= \sigma_{\mathrm{y}}(\bar{\varepsilon}^{\mathrm{p}}_{n+1}), && (4.61)\\
\sigma_{n+1} &= \sigma(\Delta\varepsilon^{\mathrm{e}}, N, \xi_n, CD_n, \sigma_n, \bar{\varepsilon}^{\mathrm{p}}_{n+1}, \bar{\varepsilon}^{\mathrm{p}}_{n}), && (4.62)\\
\Phi(\sigma, \sigma_{\mathrm{y}}) &= |\sigma_{n+1}| - \sigma_{\mathrm{y}\,n+1}, && (4.63)\\
\Phi &= 0. && (4.64)
\end{aligned}$$

To solve the non-linear equation system, a Newton-Raphson method is applied, where the plastic multiplier increment, $\Delta\gamma$, is the unknown of the system.

As it is shown in the Fig. 4.4, where the Newton-Raphson method is graphically summarised, the method starts with the null plastic multiplier increment value guess,

$$\Delta\gamma^{(1)} = 0. \tag{4.65}$$

In this way, having been this guess already calculated in the trial step, the same values can be used.

Once the yield function value $\Phi^{(1)}$ under the first guess is evaluated, the distance between the current yield function value and the objective function value, a zero value in this case, is calculated,

$$r^{(1)} = \Phi^{(1)} - 0. \tag{4.66}$$

Then, the slope of the function has to be evaluated in order to obtain the new plastic multiplier increment guess,

$$d^{(1)} = \frac{\mathrm{d}\Phi^{(1)}}{\mathrm{d}\Delta\gamma^{(1)}}, \tag{4.67}$$

$$\Delta\gamma^{(2)} = \Delta\gamma^{(1)} + \frac{-r^{(1)}}{d^{(1)}}. \tag{4.68}$$

With this new plastic multiplier increment guess, the new yield function is calculated,

$$\Phi^{(2)} = \Phi(\Delta\gamma^{2}), \tag{4.69}$$

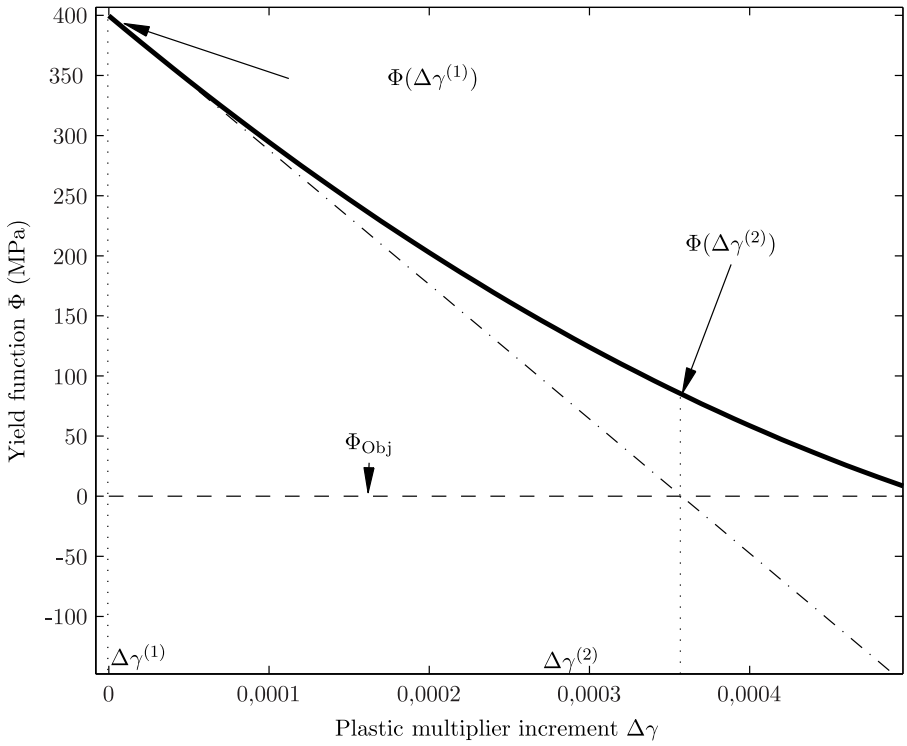

Figure 4.4. Graphically summary of the Newton-Raphson method.

and if it is not close enough to validate the $\Phi = 0 \pm \epsilon_{\mathrm{tol}}$ solution, the procedure is repeated until validation.

When the value of the plastic multiplier increment that satisfies the non-linear equation system is known, the physical and state variables are updated $(\cdot)_{n+1}$, and the next increment can be analysed.

In the Algorithm Table 2, the methodology to calculate the slope of the yield function, $\mathrm{d}\Phi^{(n)}/\mathrm{d}\Delta\gamma^{(n)}$, is exposed. The yield function Eq. (4.16) is composed by two terms, therefore its derivative can be expressed as

$$\frac{\mathrm{d}\Phi}{\mathrm{d}\Delta\gamma} = D - h, \tag{4.70}$$

where D is the derivative of the absolute value of the stress with respect to the plastic multiplier increment,

$$D = \frac{\mathrm{d}|\sigma|}{\mathrm{d}\Delta\gamma}, \tag{4.71}$$

and h is the slope of the hardening law,

$$h = \frac{\mathrm{d}\sigma_{\mathrm{y}}}{\mathrm{d}\Delta\gamma}. \tag{4.72}$$

Focusing in the D derivative calculation: the expression of D derived form the extended elastic law's Eq. (4.30) is given by

$$\frac{\mathrm{d}|\sigma|}{\mathrm{d}\Delta\gamma} = \frac{\mathrm{d}|\sigma|}{\mathrm{d}\xi}\frac{\mathrm{d}\xi}{\mathrm{d}\Delta\gamma}, \tag{4.73}$$

which leads to

$$\frac{\mathrm{d}|\sigma|}{\mathrm{d}\Delta\gamma} = (CD)\,\mathsf{K}(\xi,\boldsymbol{\alpha})\,E\,(-1) \tag{4.74}$$

when $\sigma > 0$, and

$$\frac{\mathrm{d}|\sigma|}{\mathrm{d}\Delta\gamma} = -\,(CD)\,\mathsf{K}(\xi,\boldsymbol{\alpha})\,E\,(-1) \tag{4.75}$$

when $\sigma < 0$.

In short,

$$D = \pm\,(CD)\,\mathsf{K}(\xi,\boldsymbol{\alpha})\,E\,(-1). \tag{4.76}$$

Algorithm Table 2 Yield function's slope calculation algorithm.

1: Known variables

$\Delta\gamma$, ξ, $CD, \boldsymbol{\alpha}_n$, σ_n

2: Internal variable value

$\boldsymbol{\alpha} = \boldsymbol{\alpha}_n + \boldsymbol{\alpha}(\Delta\gamma)$

3: Evaluate h, for a specific $\bar{\varepsilon}^{\mathrm{p}}$

$h = \dfrac{\mathrm{d}\sigma_{\mathrm{y}}}{\mathrm{d}\Delta\gamma}$

4: Evaluate D

5: **if** $\sigma_n > 0$ **then**

6: **return** $D = (CD)\,\mathsf{K}(\xi,\boldsymbol{\alpha})\,E\,(-1)$

7: **else**

8: **return** $D = -\,(CD)\,\mathsf{K}(\xi,\boldsymbol{\alpha})\,E\,(-1)$

9: **end if**

10: Compute the slope

$d = D - h$

In the Algorithm Table 3, the elastoplastic model summarised in Table 4.1 is exposed. This algorithm make use of the extended elastic law algorithm, Algorithm Table 1, and the yield function's slope evaluation algorithm, Algorithm Table 2.

Algorithm Table 3 Elastic predictor/Plastic corrector algorithm summary.

1: Known variables

$$\varepsilon_n^{\mathrm{t}}\,,\ \varepsilon_n^{\mathrm{e}}\,,\ \varepsilon_n^{pl}\,,\ \bar{\varepsilon}_n^{\mathrm{p}}\,,\ \sigma_n\,,\ \xi_n\,,\ CD_n\,,\ \boldsymbol{\alpha}_n$$

2: ELASTIC PREDICTOR

3: Evaluate the trial strain variables

$$\begin{aligned}
\Delta\varepsilon^{\mathrm{e}} &= \Delta\varepsilon \\
\varepsilon_{n+1}^{\mathrm{t\,trial}} &= \varepsilon_n^{\mathrm{t}} + \Delta\varepsilon \\
\varepsilon_{n+1}^{\mathrm{e\,trial}} &= \varepsilon_n^{\mathrm{e}} + \Delta\varepsilon^{\mathrm{e}} \\
\varepsilon_{n+1}^{\mathrm{p\,trial}} &= \varepsilon_n^{\mathrm{p}} \\
\bar{\varepsilon}_{n+1}^{\mathrm{p\,trial}} &= \bar{\varepsilon}_n^{\mathrm{p}} \\
\boldsymbol{\alpha}_{n+1}^{\mathrm{trial}} &= \boldsymbol{\alpha}_n
\end{aligned}$$

4: Evaluate the trial stress values

$$\begin{aligned}
\sigma_{\mathrm{y}\,n+1}^{\mathrm{trial}} &= \sigma_{\mathrm{y}}(\bar{\varepsilon}_{n+1}^{\mathrm{p}}) \\
\sigma_{n+1}^{\mathrm{trial}} &= \sigma(\Delta\varepsilon^{\mathrm{e}}, N, \xi_n, CD_n, \sigma_n, \boldsymbol{\alpha}_{n+1}^{\mathrm{trial}}, \boldsymbol{\alpha}_n)\ \textbf{GOTO Alg.Sum. } 1
\end{aligned}$$

5: Compute the yield function Φ^{trial}

$$\Phi = |\sigma_{n+1}^{\mathrm{trial}}| - \sigma_{\mathrm{y}\,n+1}^{\mathrm{trial}}$$

6: Check for admissibility

7: **if** $\Phi^{\mathrm{trial}} \leq 0$ **then**

8: **return** $(\cdot)_{n+1} = (\cdot)_{n+1}^{\mathrm{trial}}$ and **END**

9: **else**

10: **GOTO** 12

11: **end if**

12: PLASTIC CORRECTOR

13: First guess

$$\Delta\gamma^{(1)} = 0$$

14: Compute the yield function value

$$\Phi^{(1)} = \Phi(\Delta\gamma^{(1)}) = \Phi^{\mathrm{trial}}$$

15: Check for convergence

16: **while** $\Phi > 0 + \epsilon_{\mathrm{tol}}$ **do**

17: Evaluate the residue

18: **return** $r^{(k)} = \Phi^{(k-1)} - 0$

19: Slope value calculation

20: **return** $d^{(k)}$ **GOTO** 2

21: New guess

22: **return** $\Delta\gamma^{(k)} = \Delta\gamma^{(k-1)} + \dfrac{-r^{(k)}}{d^{(k)}}$

23: Compute the new yield function value

$$\Phi^{(k)} = \Phi(\Delta\gamma^{(k)})$$

24: **end while**

4.5 Parameter identification

In this section, the parameter identification of the elastic law for the previously characterised TRIP 700 steel is carried out. From the literature review it has been shown that three different modelling techniques are used to represent the elastic behaviour of AHSS steels. On the one hand, the classical elastic law, where the relation between the stress increment and elastic strain increment is defined with the Young's modulus.

On the other hand, the linear elastic laws with variable elastic modulus, such as those of Yu (2009) or Yoshida et al. (2002).

The extended elastic law with a kernel dependent of both elastic and plastic strain, defines the third modelling technique.

4.5.1 Classic elastic law

The classical elastic law summarised in Eq. (4.1) is defined with the initial elastic modulus, i.e. Young's modulus. From the tensile test performed in the previous chapter it is concluded that the Young's modulus for the TRIP 700 steel is 204 GPa.

In terms of extended elastic law, the classical elastic behaviour is defined with the value of the kernel equal to one and the Young's modulus. The summary of the classic elastic law in terms of extended elastic law is shown in Table 4.2.

Table 4.2
Kernel summary table for the classic elastic law.

Model	Equation	Evolution of the coefficients
K	1	$\forall \varepsilon^{e}, \bar{\varepsilon}^{p}$

4.5.2 Linear elastic behaviour with variable elastic modulus

Yu (2009) and Yoshida et al. (2002) proposed analytical functions to describe the evolution of the elastic modulus with the accumulated plastic strain (equal to the plastic strain in a tensile test). The parameter identification is carried out taking into account the results exposed in Fig. 3.14. The parameter identification could be carried out using the loading elastic modulus represented in Fig. 3.11, but as the main objective of these models is to improve the elastic behaviour representation for springback simulations, most of the authors use the chord modulus as a representative elastic modulus (Yu,

2009; Eggertsen and Mattiasson, 2009; Perez et al., 2005).

Yoshida et al. proposed an exponential analytical equation for the elastic modulus evolution,

$$E = E_0 - (E_0 - E_{\text{sat}}) \cdot (1 - \mathrm{e}^{-q\,\bar{\varepsilon}^{\text{p}}}), \tag{4.77}$$

where E_0 represents the initial elastic modulus (Young's modulus), and E_{sat} and q are material parameters.

By curve fitting, using the *fminsearch* algorithm implemented in Matlab®, the parameter identification of the Yoshida's model for the TRIP 700 gives a q parameter value of 22.65 and E_{sat} parameter value of 139.92 GPa.

In terms of extended elastic law, the Yoshida's equation, Eq. (4.77) could be defined as

$$\mathsf{K}(\bar{\varepsilon}^{\text{p}}) = \frac{E_0 - (E_0 - E_{\text{sat}}) \cdot (1 - \mathrm{e}^{-q\,\bar{\varepsilon}^{\text{p}}})}{E_0}, \tag{4.78}$$

because in this case E_0 is equal to the Young's modulus, with which the kernel function will be multiplied. Therefore the Yoshida kernel expression can be simplified as

$$\mathsf{K}(\bar{\varepsilon}^{\text{p}}) = 1 - (1 - E_{\text{sat}}/E_0) \cdot (1 - \mathrm{e}^{-q\,\bar{\varepsilon}^{\text{p}}}). \tag{4.79}$$

On the other hand, the expression proposed by Yu leads

$$E = A_{\text{y}} \cdot (\bar{\varepsilon}^{\text{p}})^2 + B_{\text{y}} \cdot \bar{\varepsilon}^{\text{p}} + E_0, \tag{4.80}$$

where A_{y} and B_{y} are material parameters. Using the same curve fitting method than in the Yoshida's model the Yu's parameters leads to $A_{\text{y}} = 3358$ GPa and $B_{\text{y}} = -933.4$ GPa. In terms of extended elastic law kernel, the Eq. (4.82) expression leads to

$$\mathsf{K}(\bar{\varepsilon}^{\text{p}}) = \frac{A_{\text{y}} \cdot (\bar{\varepsilon}^{\text{p}})^2 + B_{\text{y}} \cdot \bar{\varepsilon}^{\text{p}} + E_0}{E_0}, \tag{4.81}$$

which once simplified results

$$\mathsf{K}(\bar{\varepsilon}^{\text{p}}) = A_{\text{y}}/E_0 \cdot (\bar{\varepsilon}^{\text{p}})^2 + B_{\text{y}}/E_0 \cdot \bar{\varepsilon}^{\text{p}} + 1. \tag{4.82}$$

In Fig. 4.5 the value of the kernel function for the Yu model and Yoshida et al. model are shown. It can be pointed out, that even if until 15% of plastic strain both models represent a decreasing value of the kernel, the Yu's model starts augmenting the kernel

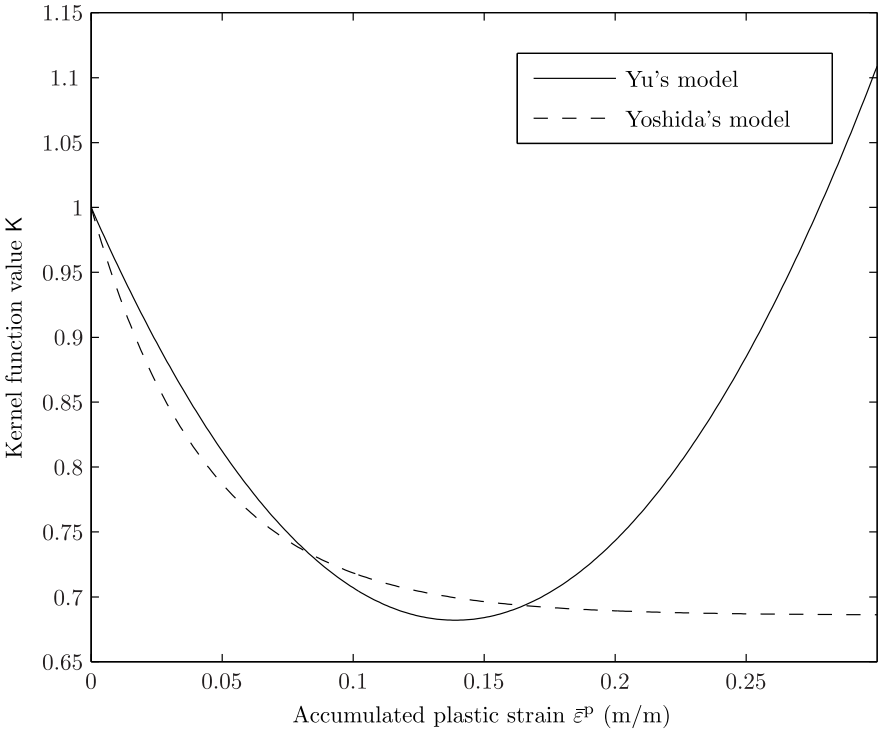

Figure 4.5. Differences between the kernel value of the Yu's model and the value of the Yoshida et al.'s model.

value for higher strains. The experimental results that are obtained in Chapter 3 are only until the 12% of strain but it seams reasonable to expect an decreasing of the elastic modulus when the strain is augmented. This hypothesis contradicts the Yu's model's prediction witch proposes an augmentation even more than E_0 for $0.3 < \bar{\varepsilon}^{\mathrm{p}}$. Therefore, hereafter only the Yoshida et al.'s model will be used to represent the linear elastic behaviour with variable elastic modulus. The summary of the Yoshida's elastic law in terms of extended elastic law is shown in Table 4.3.

4.5.3 Extended elastic law with a kernel dependent of both elastic and plastic strain

Following the identification technique exposed in Section 4.2.1, two different analytical expressions to fit the cloud of kernel's data points are proposed. On the one hand, a power function is proposed. On the other hand, a second polynomial function is proposed. Both kernel propositions are summarised in Table 4.4. In that table it can be shown how the coefficients of the functions evolve with the plastic strain but they remain constant

Table 4.3
Kernel summary table for Yoshida's elastic law.

Model	Equation	Evolution of the coefficients
$\mathsf{K}_1(\bar{\varepsilon}^{\mathrm{p}})$	$1-(1-E_{\mathrm{sat}}/E_0)\cdot(1-\mathrm{e}^{-q\,\bar{\varepsilon}^{\mathrm{p}}})$	$E_0 = 204$ GPa
		$E_{\mathrm{sat}} = 139.92$ GPa
		$q = 22.62$

during purely elastic unloading-loading cycles. In Fig. 4.6 a comparative between the accuracy of each model presented in Table 4.4 is shown.

Table 4.4
Kernel function summary for the complete extended elastic law.

Model	Equation	Evolution of the coefficients
$\mathsf{K}_1(\xi,\bar{\varepsilon}^{\mathrm{p}})$	$A_1+B_1\,(\xi)^{C_1}$	$A_1 = -1.7605\,\bar{\varepsilon}^{\mathrm{p}} + 1.1297$
		$B_1 = 133.91\,\bar{\varepsilon}^{\mathrm{p}} - 34.156$
		$C_1 = 0.75$
$\mathsf{K}_2(\xi,\bar{\varepsilon}^{\mathrm{p}})$	$A_2\,(\xi)^2 + B_2\,(\xi) + C_2$	$A_2 = 0.01$
		$B_2 = 497.29\,\bar{\varepsilon}^{\mathrm{p}} - 175.83$
		$C_2 = -1.5167\,\bar{\varepsilon}^{\mathrm{p}} + 1.1144$

It can be pointed out, that both models are confounded because they leads to very close results. That is why hereafter only the power kernel[3] will be used to represent the non linear elastic behaviour of the TRIP 700 steel.

[3]The power kernel is chosen arbitrary, the same procedure could be followed with the polynomial kernel.

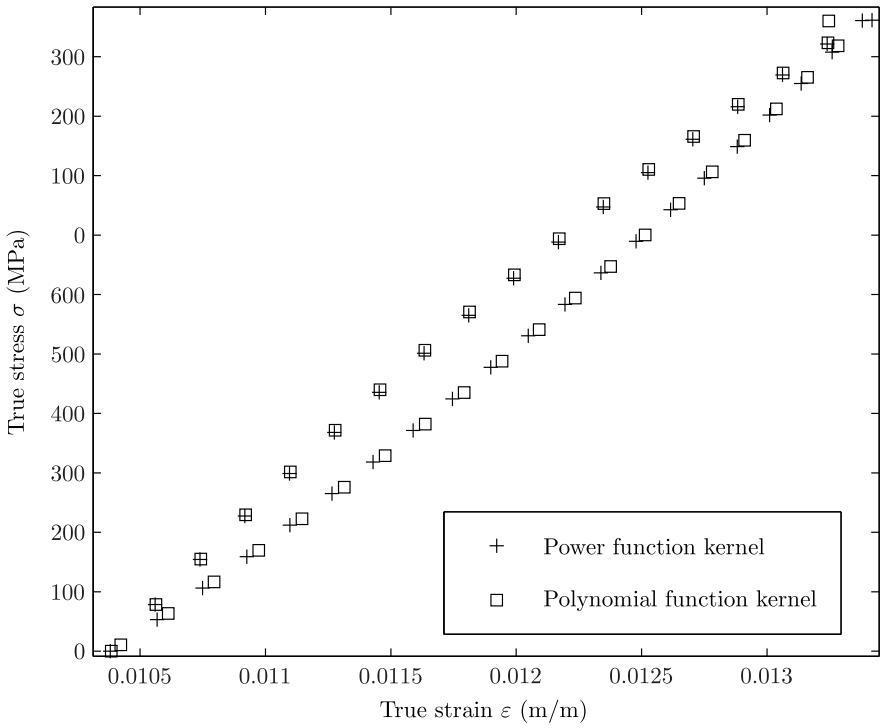

Figure 4.6. Comparative between power and polynomial kernel functions.

4.5.4 Accuracy of each elastic law

Once the parameter identification for the three modelling techniques is done, in this section the accuracy of each modelling technique is evaluated.

In order to analyse the accuracy of each model, the loading-unloading cyclic test is performed numerically with the commercial software Matlab® with the three modelling techniques and compared with the experimental data obtained in the previous chapter.

In Fig. 4.7 experimental data of two elastic unloading-loading cycles are exposed. In the same figure the response predicted for the three modelling techniques is also shown. In the same context, in Fig. 4.8 the same comparison but this time with the non completely relaxed unloading-loading cycle is presented.

From Fig. 4.7 and Fig. 4.8 can be pointed out that when the unloading occurs until complete relaxed point ($\sigma = 0$), both linear elastic with variable elastic modulus and non-linear elastic behaviours leads to the same point even if only the second one follows the experimental data.

Nevertheless, when the unloading does not reach the complete relaxed point, the linear elastic with variable elastic modulus behaviour is not able to fit the experimental data as accurately as the non-linear elastic behaviour.

On the contrary, the classical linear elastic behaviour does not fit neither the case of complete unloading nor the case with partial unloading.

However, due to the complex formulation of the model, the computational effort needed to solve an elastoplastic problem with the extended elastic law is higher than using the classical law.

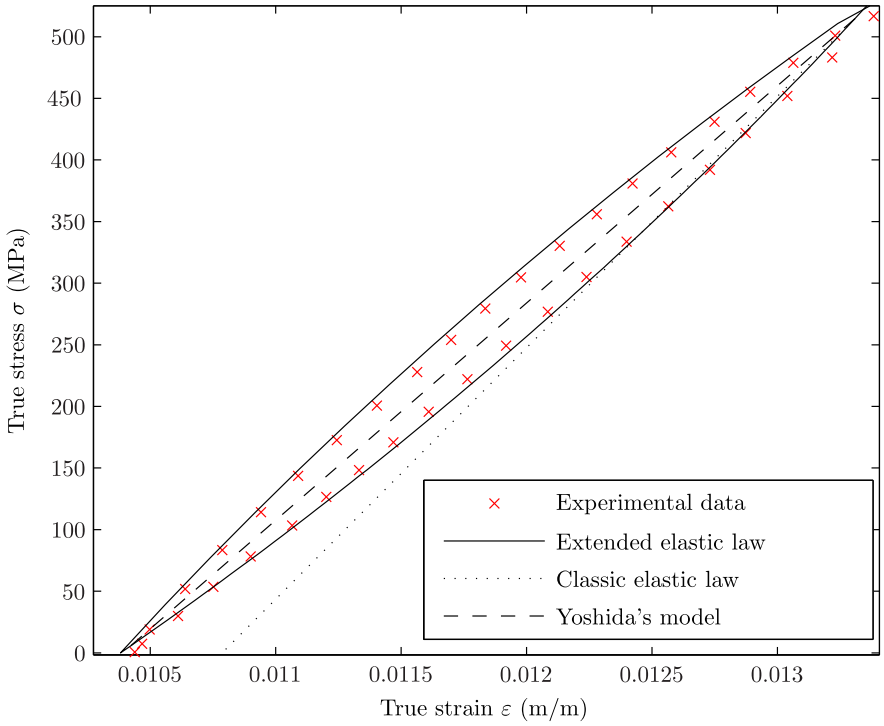

(a)

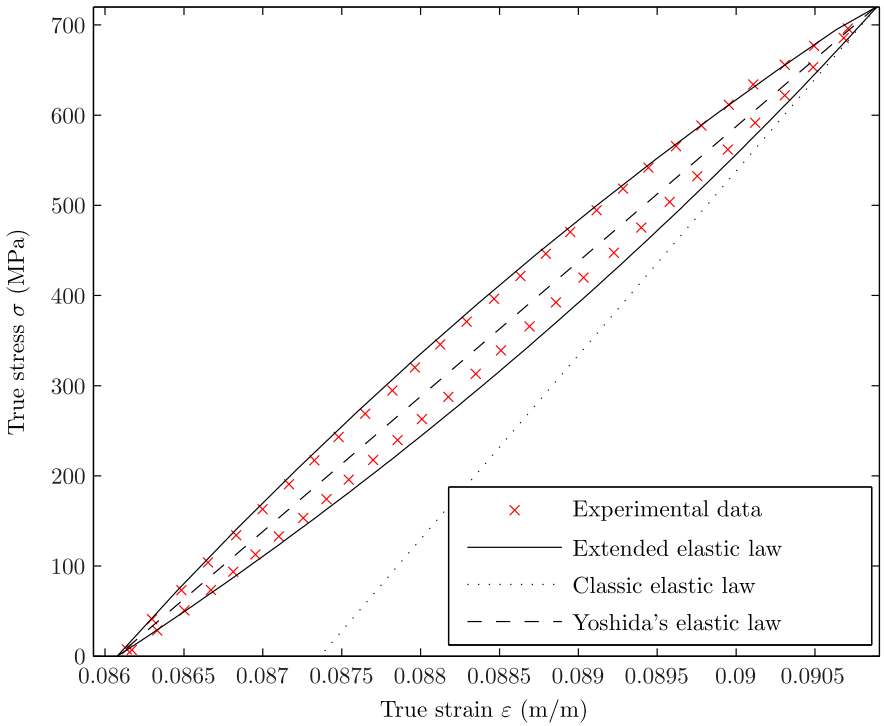

(b)

Figure 4.7. Experimental data of two elastic unloading-loading cycles with the response of the three elastic behaviour modelling techniques: (a) unloading-loading cycle 1.3% pre-strain; (b) unloading-loading cycle after 9.1% pre-strain.

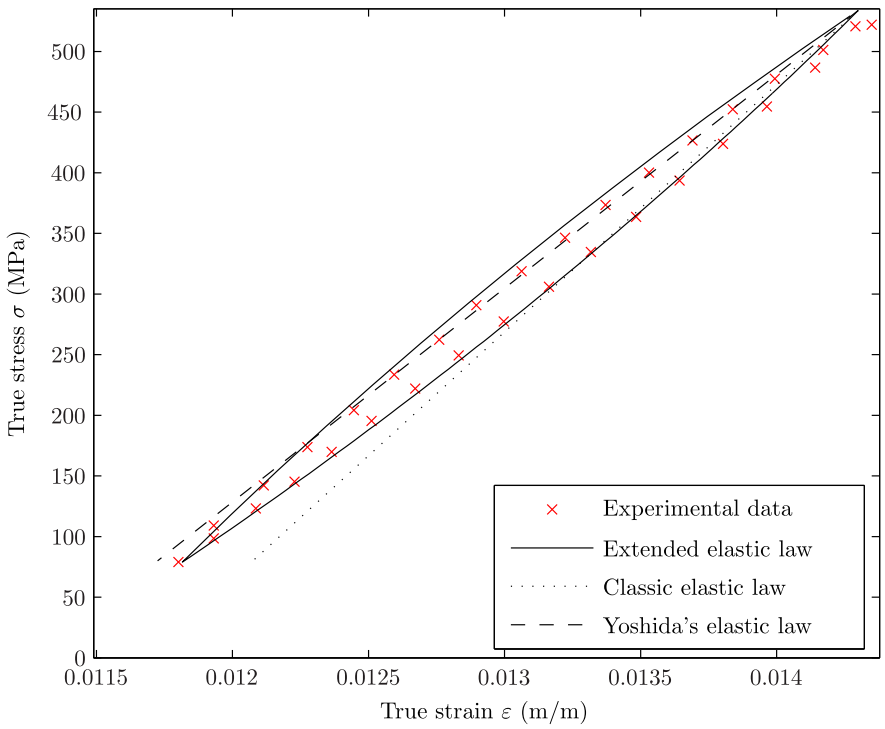

(a)

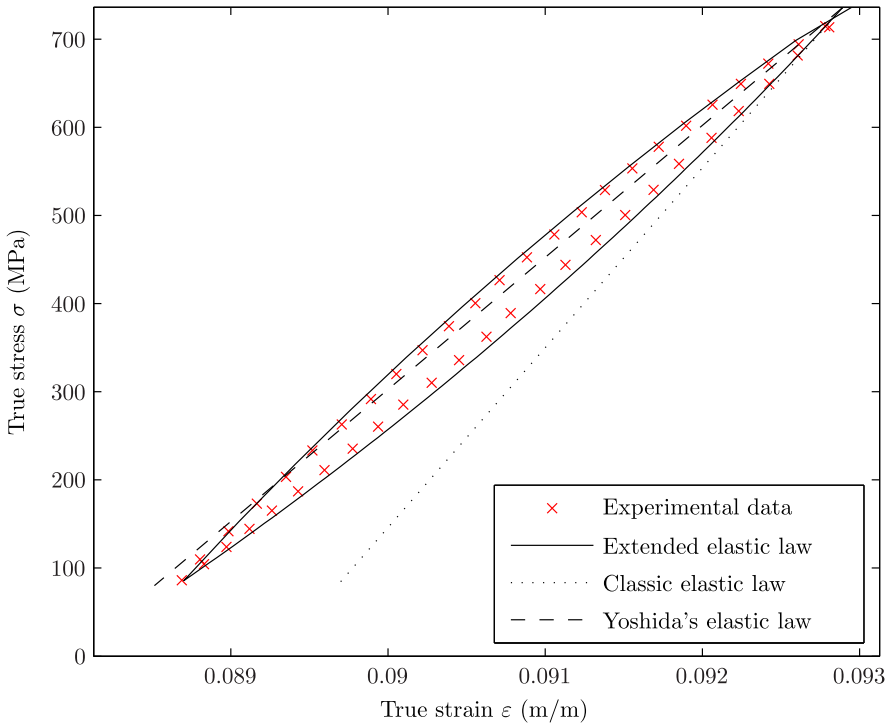

(b)

Figure 4.8. Experimental data of two elastic no completely relaxed unloading-loading cycles with the response of the three elastic behaviour modelling techniques: (a) unloading-loading cycle 1.4% pre-strain; (b) unloading-loading cycle 9.3% pre-strain.

4.6 Pseudo-analytical bending test

In order to analyse the influence of the elastic behaviour accuracy model on the springback prediction, a pseudo-analytical theoretical bending test has been performed.

The selected pseudo-analytical test consist on a first pure bending step and a consequent springback step of a thin sheet. The test is based on the Numisheet2002 Benchmark simplification, where the anticlastic (Li et al., 2002a) phenomenons are neglected, and a thin shell theory is used.

4.6.1 Analytical development

The main idea of the pseudo-analytical test is to study the resultant shape after elastic unloading of a bended TRIP 700 thin sheet. In order to analyse the influence of the elastic law, the numerical simulation is computed with the three elastic laws.

In Fig. 4.9 the schematic representation of the metal sheet is exposed. The $\vec{x}$ direction corresponds to the rolling direction. The $\vec{y}$ direction is the transversal direction, while the $\vec{z}$ direction is the direction in the thickness.

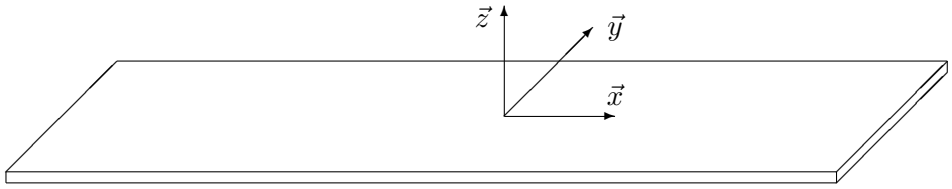

Figure 4.9. Schematic representation of the metal sheet.

During the forming step (the first step), the sheet is bent until 25 mm of curvature radius in the $(\vec{x}, \vec{z})$ plane. In the springback step, the forming loads are removed and the resultant radius is compared between the different elastoplastic formulations.

The first hypothesis of the test is that the midline plane in the $\vec{z}$ direction remains undeformed during all the process. Therefore, the relation between strain and curvature radius satisfies,

$$\varepsilon_{xx}(z) = \frac{-z}{R}, \tag{4.83}$$

where R represents the curvature radius of the midline plane, and z represents the distance in the $\vec{z}$ direction taking the midline plane as $z = 0$. Taking into account this coordinate system, the upper plane of the sheet is at $z = h/2$, while the lower plane is

at $z = -h/2$, being h the thickness of the sheet.

Taking advantage of the second hypothesis of the test, which states that the anticlastic (Li et al., 2002a) phenomena are neglected, the expression of the resultant momentum leads,

$$M_f = \int_{-h/2}^{h/2} b_{\text{with}}\, \sigma_{xx}(z)\, \mathrm{d}z, \tag{4.84}$$

where b_{with}, is the width of the sheet in the $\vec{y}$ direction.
The expression of the momentum Eq. (4.84) is numerically evaluated subdividing the thickness in N segments,

$$M_f = \sum_{i=1}^{N} b_{\text{with}}\, (h/N)\, \sigma_{xx}(z_i), \tag{4.85}$$

where $\sigma_{xx}(z_i)$ represents the stress value in the middle of the segment. In this work the thickness is divided in 2000 segments.

To compute the first step, bending step, a bending radius is imposed $R_{\text{b}} = 25\,\text{mm}$, and the stress distribution along the thickness and the resultant momentum are evaluated. In Fig. 4.10 the stress distributions along the thickness after forming are shown. In that figure can be appreciated how a critical value of z exist where the transition between elastic behaviour to elastoplastic behaviour occurs.

Once the stress distribution for a bending radius is evaluated, the elastic recovery until a stable zero resultant momentum is calculated, $M_f = 0$.

4.6.2 Results

The resultant stress distributions using the different elastic laws are shown in Fig. 4.11. In this figure the existing difference between the use of the different elastic laws is shown.

The resultant radii after springback step calculated with the three elastic laws are exposed in Table 4.5. In Table 4.6, the recovered angle values assuming a 90º bending with 25 mm bending radius computed with the different elastic laws are shown.

By means of this pseudo-analytical test, it is shown how the use of the extended elastic law predicts higher springback angles than the Yoshida's and classic elastic laws. Taking the classical elastic law as a reference, under 90º bending assumption differences of 2º-4º have been found between modelling the elastic behaviour with different levels of accuracy.

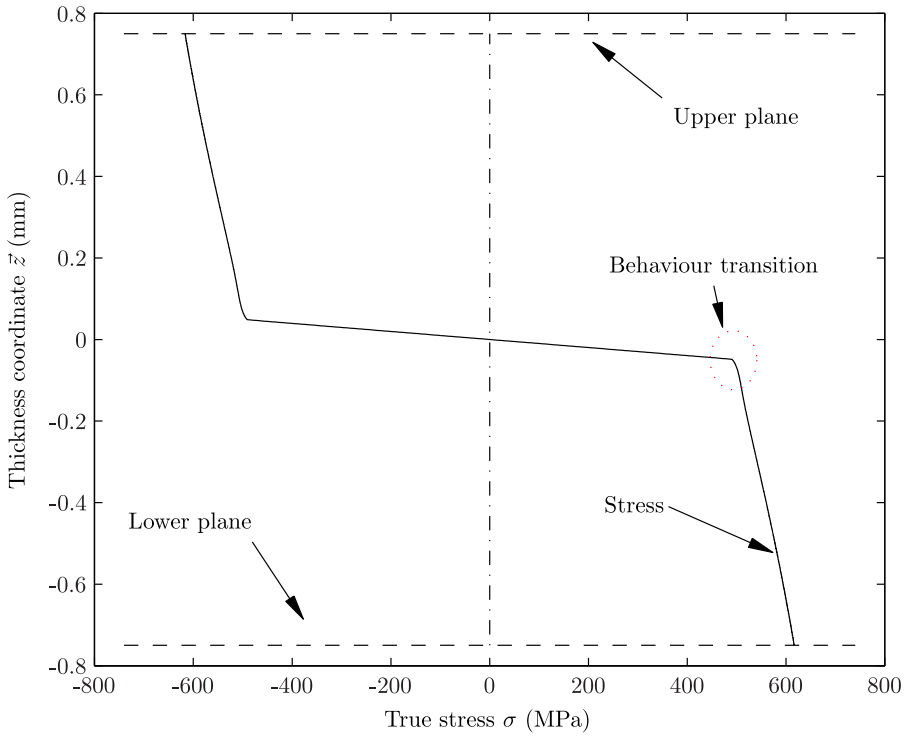

Figure 4.10. Stress distribution along the thickness after forming step.

Table 4.5
Resultant radius after springback step.

Classic elastic law	Yoshida's elastic law	Extended elastic law
29.05 mm	29.62 mm	30 mm

Table 4.6
Recovered angles values after springback assuming a 90° bending with 20 mm bending radius.

Classic elastic law	Yoshida's elastic law	Extended elastic law
14.6°	16.6°	18.0°

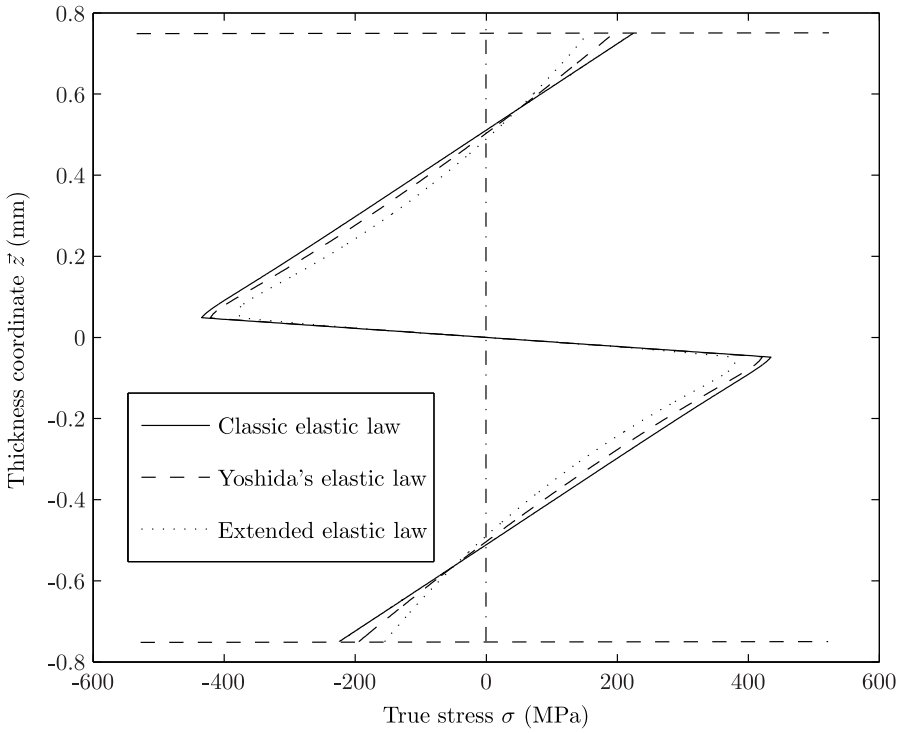

Figure 4.11. Stress distribution along the thickness after elastic unloading.

4.7 Conclusions

In this chapter an extension of the classical elastic law has been proposed in order to augment the capability of the elastic law to represent non-linear elastic behaviours, e.g. the behaviour of the TRIP 700 steel.

- By means of this extension, an elastic law able to represent both classical and non-classic elastic behaviours is formulated.
- In Section 4.2 how the extended elastic law can be particularised by means of the loading-unloading cyclic tests is shown. Using this testing technique the extended elastic law has been particularised for the TRIP 700 steel.
- In this context, the loading-unloading cyclic tests are performed in order to emphasise the differences of using the extended, Yoshida's and classical elastic laws. Based on the results, it can be concluded that there are appreciable differences between the springback results when the final stress differs from zero.
- Nevertheless, it has to be taken into account the limitations of the presented elasto-

plastic model. The kinematic hardening and the anisotropic yielding phenomena are not taken into account. Therefore, the model is not going to be able to accurately represent processes that involve a cyclic plasticity or highly anisotropic yielding.

- However, by means of the pseudo-analytical test it has been illustrated the influence of the elastic behaviour modelling accuracy on a springback prediction.

Chapter 5

Three-dimensional extended elastic law

Synopsis

In this chapter the three-dimensional elastic law is developed. In the previous chapter, the one-dimensional model has been presented and in this section the extension of this model to the three-dimensional space is performed. In order to provide a useful tool, during the chapter, apart from the three-dimensional elastic law, an isotropic hardening von Mises elastoplastic formulation is detailed and its numerical implementation is explained.

An isotropic elastic behaviour as well as an isotropic plasticity model are chosen in this work to build the elastoplastic model. The numerical implementation follows the same elastic predictor/plastic corrector algorithm defined in the previous chapter. Therefore, in this chapter only the particularities of the three-dimensional model are detailed. Within the different possibilities of representing a three-dimensional process by finite elements, the implementation for full three-dimensional elements as well as the implementation for shell elements are shown.

The numerical algorithm are introduced into a V-free bending finite element simulation with solid elements in order to compare the sensitivity of the springback prediction in function of the introduced elastic law: linear elastic, linear elastic with variable elastic modulus or non-linear elastic behaviour.

5.1 Introduction

In this chapter, the three-dimensional behaviour model is developed. First the extended elastic law presented in the previous chapter is extended to the three-dimensional scenario supposing an isotropic elastic behaviour. In the extrapolation of one-dimensional behaviour to three-dimensional behaviour processes, some hypothesis have to be stated in order to determine the homogeneousness of the three-dimensional behaviour. In the literature review some elastically anisotropic models are found, but in this work the assumption of an isotropic elastic behaviour is stated.

Once the extended elastic law is defined in the three-dimensional space an elastoplastic behaviour model is presented. The presented elastoplastic model is an isotropic hardening von Mises model. As in Chapter 4, the theoretical basis laws involved in this elastoplastic model are detailed, i.e. yield function, elastic law, hardening model and plastic flow rule.

The objective of this chapter is to provide a useful elastoplastic model to simulate springback process. Therefore, after detailing the elastoplastic model, its numerical implementation is presented. The numerical implementation follows the same elastic predictor/plastic corrector algorithm exposed in the Chapter 4. That is why in this chapter only the particularities of the three-dimensional implementation are discussed. Then, a numerical simulation of springback prediction of a V-free bending process is carried out with the new extended elastic law. By means of this simulation the influence of the accuracy of the elastic law on the springback prediction is analysed.

5.2 Theoretical basis

In this section, the theoretical basis of the three-dimensional extended elastic law are presented. In Chapter 4, the theoretical basis of the one-dimensional extended elastic law have been exposed. In order to develop the three-dimensional model, the same extension technique by introducing a kernel function is applied in the classical three-dimensional elastic law.

In this work, a Cauchy's elastic material model is developed using the extended elastic law.

The Cauchy's elastic material establishes a relation between the stress and the strain

as

$$\boldsymbol{\sigma} = \boldsymbol{F}(\boldsymbol{\varepsilon}^{\mathrm{e}}), \tag{5.1}$$

where $\boldsymbol{\sigma}$ represents the stress tensor, and $\boldsymbol{F}(\boldsymbol{\varepsilon}^{\mathrm{e}})$ represents the elasticity tensor function dependent on the elastic strain tensor. This kind of material formulations define the stress independency on the strain path. Therefore, the stress is defined only dependent on the instantaneous material state.

The general form of the three dimensional elastic law is given by

$$\sigma_{ij} = D_{ijkl}\, \varepsilon^{\mathrm{e}}_{kl}, \tag{5.2}$$

where D_{ijkl} represents the $[i,j,k,l]$ term of the fourth order elasticity tensor $\mathbf{D}$. Due to the symmetry of the stress and elastic strain tensor, the elasticity tensor $\mathbf{D}$ can be composed of a maximum of 36 independent constants for its general form.

On the one hand, if an ortotropic elastic behaviour is supposed, only nine independent constants will define the elasticity tensor. On the other hand, if a transversal anisotropy is supposed, the tensor is defined with only five independent constants. Nevertheless, when an elastic isotropic material is supposed, the whole elasticity tensor is defined with only two independent constants.

5.2.1 Isotropic linear elastic material

The most general expression for the isotropic linear elasticity is defined by the Hooke's law as

$$\sigma_{ij} = \lambda\, \varepsilon^{\mathrm{e}}_{kk}\, \delta_{ij} + 2\,\mu\, \varepsilon^{\mathrm{e}}_{ij}, \tag{5.3}$$

where the elasticity constants λ and μ are the Lamé coefficients and δ_{ij} is the identity tensor (Kronecker delta).

In terms of Young's modulus and Poisson's ratio, the Lamé coefficients satisfy

$$\lambda = \frac{\nu E}{(1+\nu)(1-2\nu)}, \tag{5.4}$$

$$\mu = \frac{E}{2(1+\nu)}, \tag{5.5}$$

where ν represents the Poisson's ratio.

5.2.2 Isotropic extended elastic material

The extended three dimensional elastic law proposed in this thesis work is based on the isotropic linear elastic law presented before.

The Hooke's law equation (5.3) could be modified according to Eq. (5.4) and Eq. (5.5),

$$\sigma_{ij} \;=\; E\left[\frac{\nu}{(1+\nu)(1-2\nu)}\varepsilon^{\mathrm{e}}_{kk}\delta_{ij} \;+\; \frac{1}{(1+\nu)}\varepsilon^{\mathrm{e}}_{ij}\right]. \tag{5.6}$$

Therefore, a new strain definition is introduced defined as,

$$\varphi_{ij} \;=\; \frac{\nu}{(1+\nu)(1-2\nu)}\varepsilon^{\mathrm{e}}_{kk}\delta_{ij} \;+\; \frac{1}{(1+\nu)}\varepsilon^{\mathrm{e}}_{ij}, \tag{5.7}$$

where $\boldsymbol{\varphi}$ represents the new strain tensor, called hereafter extended elastic strain.

Taking advantage of the extended elastic strain definition, the Hooke's law Eq. (5.3) yields

$$\sigma_{ij} \;=\; E\,\varphi_{ij}. \tag{5.8}$$

The one-dimensional extended elastic law is based on the integral representation of the classical one-dimensional elastic law Eq. (4.2),

$$\sigma(\varepsilon^{\mathrm{e}}) \;=\; \sigma_0 \;+\; \int_0^{\varepsilon^{\mathrm{e}}} E\mathrm{d}\tau,$$

extended subsequently to the extended elastic law Eq. (4.3),

$$\sigma(\varepsilon^{\mathrm{e}},\boldsymbol{\alpha}) \;=\; \sigma_0 \;+\; \int_0^{\varepsilon^{\mathrm{e}}} \mathsf{K}(\tau,\boldsymbol{\alpha})\,E\mathrm{d}\tau.$$

In the three-dimension space the extension is based on the Eq. (5.8) assuming a relation of the form

$$\sigma_{ij}(\varphi_{ij},\boldsymbol{\alpha}_{ij}) \;=\; (\sigma_0)_{ij} \;+\; \int_0^{\varphi_{ij}} \mathsf{K}_{ij}(\tau,\boldsymbol{\alpha}_{ij})\,E\mathrm{d}\tau, \tag{5.9}$$

taking into account the introduction of the new spacial variable ξ, the previous equation leads

$$\sigma_{ij}(\xi_{ij},\boldsymbol{\alpha}_{ij}) \;=\; (\sigma_0)_{ij} \;+\; \mathrm{sign}(\dot{\varphi}_{ij})\int_0^{\xi_{ij}} \mathsf{K}_{ij}(\tau,\boldsymbol{\alpha}_{ij})\,E\mathrm{d}\tau, \tag{5.10}$$

where the tensor $\boldsymbol{\xi}$ is defined as $\boldsymbol{\xi} = |\boldsymbol{\varphi_1} - \boldsymbol{\varphi_0}|$.

During the uni-axial tensile test, the strains in thickness and in width are related to the principal longitudinal stress by means of the Poisson's ratio,

$$\varepsilon_{\mathrm{t}} \;=\; \varepsilon_{\mathrm{w}} \;=\; -\nu\,\varepsilon_{\mathrm{l}}, \tag{5.11}$$

where $\varepsilon_{\mathrm{t}}, \varepsilon_{\mathrm{w}}$ and ε_{l} are the thickness strain, width strain and longitudinal strain respectively. Hence, representing the tensile test from a three-dimensional point of view, the strain tensor results

$$\boldsymbol{\varepsilon} = \begin{bmatrix} \varepsilon_{11} & \varepsilon_{12} & \varepsilon_{13} \\ \varepsilon_{21} & \varepsilon_{22} & \varepsilon_{23} \\ \varepsilon_{31} & \varepsilon_{32} & \varepsilon_{33} \end{bmatrix} = \begin{bmatrix} \varepsilon_{11} & 0 & 0 \\ 0 & \varepsilon_{22} & 0 \\ 0 & 0 & \varepsilon_{33} \end{bmatrix} = \begin{bmatrix} \varepsilon_{11} & 0 & 0 \\ 0 & -\nu\varepsilon_{11} & 0 \\ 0 & 0 & -\nu\varepsilon_{11} \end{bmatrix}, \tag{5.12}$$

the longitudinal direction being represented as 11, and the transversal and width directions as 22 and 33, respectively. Therefore, the φ_{11} extended elastic strain results

$$\varphi_{11} = \varepsilon_{11}. \tag{5.13}$$

By this result, it can be concluded that the kernel function obtained for the unidimensional model is valid for the three-dimensional extension.

5.3 Elastoplastic formulation

In this section the three dimensional extended elastic law, Eq. (5.10), is introduced in an elastoplastic formulation.

Elastoplastic decomposition of the strain

In the three-dimensional space the total strain tensor is the addition of the elastic and the plastic strain tensors,

$$\boldsymbol{\varepsilon}^{\mathrm{t}} = \boldsymbol{\varepsilon}^{\mathrm{e}} + \boldsymbol{\varepsilon}^{\mathrm{p}}, \tag{5.14}$$

where $\boldsymbol{\varepsilon}^{\mathrm{t}}, \boldsymbol{\varepsilon}^{\mathrm{e}}$ and $\boldsymbol{\varepsilon}^{\mathrm{p}}$ are the total, elastic and plastic strain tensors, respectively.

Extended elastic law

The three dimensional extended elastic law is defined with the Eq. (5.10). In this context, a new hypothesis is introduced in the elastoplastic formulation; the state variables that influence the elastic behaviour are independent of the material orientation. Therefore, the Eq. (5.10) results

$$\sigma_{ij}(\xi_{ij}, \boldsymbol{\alpha}) = (\sigma_0)_{ij} + \operatorname{sign}(\dot{\varphi}_{ij}) \int_0^{\xi_{ij}} \mathsf{K}_{ij}(\tau, \boldsymbol{\alpha})\, E \mathrm{d}\tau. \tag{5.15}$$

Yield function and yield criteria

In contrast to the one-dimensional yield criteria, in the three-dimensional space, a relation has to be established between the three-dimensional stress state and its equivalent uni-axial stress.

In this thesis work, an isotropic von Mises theory is used to relate the three-dimensional stress state and its equivalent monotonic stress (de Souza Neto et al., 2008). The von Mises equivalent stress is defined as

$$\sigma_{\mathrm{q}} \equiv \sqrt{(3J_2(\boldsymbol{s}(\boldsymbol{\sigma})))}, \tag{5.16}$$

where σ_{q} represents the von Mises equivalent stress and $J_2(\boldsymbol{s}(\boldsymbol{\sigma}))$ is the second invariant of the deviatoric stress, $\boldsymbol{s}(\boldsymbol{\sigma})$.

The kinematic hardening is not going to be taken into account. Thus, the yield function leads

$$\Phi(\boldsymbol{\sigma}, \sigma_{\mathrm{y}}) = \sigma_{\mathrm{q}} - \sigma_{\mathrm{y}}, \tag{5.17}$$

resulting in

$$\Phi(\boldsymbol{\sigma}, \sigma_{\mathrm{y}}) = \sqrt{(3J_2(\boldsymbol{s}(\boldsymbol{\sigma})))} - \sigma_{\mathrm{y}}. \tag{5.18}$$

Hardening law

As it has been previously stated, in this model only isotropic hardening is taken into account. A plasticity model is said to be isotropic hardening if the evolution of the yield surface is such that, at any state of hardening, it corresponds to a uniform expansion of the initial yield surface, without transition. For a multi-axial plasticity model with a von Mises yield surface, isotropic hardening corresponds to the increase in radius of the von Mises cylinder in principal stress state (de Souza Neto et al., 2008).
Strain hardening approach is chosen in this work, where the accumulated plastic strain is defined as

$$\bar{\varepsilon}^{\mathrm{p}} \equiv \int_0^t \sqrt{\frac{2}{3}\dot{\boldsymbol{\varepsilon}}^{\mathrm{p}} : \dot{\boldsymbol{\varepsilon}}^{\mathrm{p}}}\ \mathrm{d}t = \int_0^t \sqrt{\frac{2}{3}}\, ||\dot{\boldsymbol{\varepsilon}}^{\mathrm{p}}||\ \mathrm{d}t. \tag{5.19}$$

The evolution of the the yield surface is defined with the data obtained from the tensile test Eq. (4.23),

$$\sigma_{\mathrm{y}} = \sigma_{\mathrm{y}}(\bar{\varepsilon}^{\mathrm{p}}).$$

Plastic flow rule

The Prandtl-Reuss plasticity law is the flow rule obtained by taking the von Mises yield function Eq. (5.18) as the flow potential. The corresponding flow vector is given by

$$\boldsymbol{N} \equiv \frac{\partial \Phi}{\partial \boldsymbol{\sigma}} = \frac{\partial}{\partial \boldsymbol{\sigma}} \left[\sqrt{3\, J_2(\boldsymbol{s})} \right] = \sqrt{\frac{3}{2}} \frac{\boldsymbol{s}}{|\boldsymbol{s}|}, \tag{5.20}$$

and the flow rule results in

$$\dot{\boldsymbol{\varepsilon}}^{\mathrm{p}} = \dot{\gamma} \sqrt{\frac{3}{2}} \frac{\boldsymbol{s}}{|\boldsymbol{s}|}. \tag{5.21}$$

Table 5.1 summarises the three dimensional elastoplastic model presented in this section.

Table 5.1
Three-dimensional elastoplastic model summary.

Constitutive Equation	Equation
Elastoplastic strain decomposition	$\boldsymbol{\varepsilon}^{\mathrm{t}} = \boldsymbol{\varepsilon}^{\mathrm{e}} + \boldsymbol{\varepsilon}^{\mathrm{p}}$
Elastic extender new law	$\sigma_{ij}(\xi_{ij}, \boldsymbol{\alpha}) = (\sigma_0)_{ij} + \mathrm{sign}(\dot{\varphi}_{ij}) \int_0^{\xi_{ij}} \mathsf{K}_{ij}(\tau, \boldsymbol{\alpha})\, E \mathrm{d}\tau$
	$\boldsymbol{\xi} = \lvert \boldsymbol{\varphi_1} - \boldsymbol{\varphi_0} \rvert$
Yield function	$\Phi(\boldsymbol{\sigma}, \sigma_{\mathrm{y}}) = \sqrt{(3 J_2(\boldsymbol{s}(\boldsymbol{\sigma})))} - \sigma_{\mathrm{y}}$
Plastic flow	$\dot{\boldsymbol{\varepsilon}}^{\mathrm{p}} = \dot{\gamma} \sqrt{\frac{3}{2}} \frac{\boldsymbol{s}}{\lvert \boldsymbol{s} \rvert}$
Hardening law	$\sigma_{\mathrm{y}} = \sigma_{\mathrm{y}}(\bar{\varepsilon}^{\mathrm{p}})$
	$\bar{\varepsilon}^{\mathrm{p}} = \int_0^t \sqrt{\frac{2}{3}}\, \lVert \dot{\boldsymbol{\varepsilon}}^{\mathrm{p}} \rVert \, \mathrm{d}t$
Loading unloading conditions	$\Phi \leq 0 \quad \dot{\gamma} \geq 0, \quad \dot{\gamma} \Phi = 0$

5.4 Numerical implementation

In this section, the numerical implementation of the elastoplastic model summarised in Table 5.1 is explained. For the three-dimensional case, the same elastic predictor/plastic corrector technique used for the one-dimensional case is applied.

The theoretical basis of the elastic predictor/plastic corrector algorithm have been exposed in Chapter 4. The three-dimensional implementation follows the same basis but taking into account that the stress and strain are composed by different components, six in the general form. Therefore, in this section only the particularities of the three-dimensional case are presented. On the one hand, the numerical implementation of the three-dimensional extended elastic law. On the other hand, the plastic corrector is solved by a single non-linear equation in the one-dimensional case, will be solved by a non-linear equation system in the three-dimensional case.

Vectorial representation

Due to the symmetry property of the strain and stress tensors, they can be given by column vectorial representation,

$$\boldsymbol{\varepsilon} = \begin{bmatrix} \varepsilon_{11} \\ \varepsilon_{22} \\ \varepsilon_{33} \\ \varepsilon_{12} \\ \varepsilon_{13} \\ \varepsilon_{23} \end{bmatrix} \qquad \boldsymbol{\sigma} = \begin{bmatrix} \sigma_{11} \\ \sigma_{22} \\ \sigma_{33} \\ \sigma_{12} \\ \sigma_{13} \\ \sigma_{23} \end{bmatrix} \tag{5.22}$$

5.4.1 Numerical implementation of the three-dimensional extended elastic law

Even if an isotropic elastic model has been chosen, each direction may has different kernel K_{ij}, with which to model different elastic behaviour evolution. In this thesis work, an isotropic elastic behaviour evolution is assumed, taking as reference the uni-axial kernel,

$$\mathsf{K} = \mathsf{K}_{ij} = \mathsf{K}_{11}, \qquad \forall i, j. \tag{5.23}$$

Consequently, the extended elastic law results

$$\sigma_{ij}(\xi_{ij}, \boldsymbol{\alpha}_{ij}) = (\sigma_0)_{ij} + \operatorname{sign}(\dot{\varphi}_{ij}) \int_0^{\xi_{ij}} \mathsf{K}(\tau, \boldsymbol{\alpha})\, E \mathrm{d}\tau. \tag{5.24}$$

Introducing the process nature variable CD, the previous equation leads

$$\sigma_{ij}(\xi_{ij}, \boldsymbol{\alpha}_{ij}) = (\sigma_0)_{ij} + CD_{ij} \int_0^{\xi_{ij}} \mathsf{K}(\tau, \boldsymbol{\alpha})\, E \mathrm{d}\tau, \tag{5.25}$$

where now the process nature variable is dependent on the extended elastic strain increment as

$$\Delta\varphi_{ij} > 0 \rightarrow CD_{ij} = \quad 1 \tag{5.26}$$

and

$$\Delta\varphi_{ij} < 0 \rightarrow CD_{ij} = -1. \tag{5.27}$$

Therefore, in the three-dimensional case, the extended elastic law is implemented following the Algorithm Table 1, for each stress, σ_{ij}.

5.4.2 Plastic corrector

In the one-dimensional case the plastic corrector is performed solving one non-linear equation using the Newton-Raphson method, Algorithm Table 2 and 3. However, in the three-dimension scenario, where the stress and strain tensors are now composed by six independent components (Eq. (5.22)), the resolution of the plastic corrector leads to a m non-linear equation system (this value varies in function of the three-dimensional space hypothesis).

Therefore, the derivative of the yield function Φ with respect to the plastic multiplier increment $\Delta\gamma$, is not longer the direction of the solution. In the three dimensional context, the jacobian matrix J of the objective functions with respect to the variables of the system defines the solution direction,

$$J = \begin{bmatrix} \dfrac{\partial f_1}{\partial u_1} & \cdots & \dfrac{\partial f_1}{\partial u_m} \\ \vdots & \ddots & \vdots \\ \dfrac{\partial f_m}{\partial u_1} & \cdots & \dfrac{\partial f_m}{\partial u_m} \end{bmatrix}, \tag{5.28}$$

where f_i are the objective functions, and u_i are the variables of the system.

Full three-dimensional element case

For the full three-dimensional case, the order of the non-linear equation system is equal to seven, $m = 7$. In this work the plastic multiplier increment $\Delta\gamma$ and the six independent

components of the deviatoric stress tensor s_{ij} are taken as variables of the system,

$$\mathbf{u} = \begin{bmatrix} \Delta\gamma \\ s_{11} \\ s_{22} \\ s_{33} \\ s_{12} \\ s_{13} \\ s_{23} \end{bmatrix}, \tag{5.29}$$

while, as objective functions, the calculated deviatoric stress values (not mandatory equal to the system variables) and the yield function's value are taken,

$$\mathbf{f} = \begin{bmatrix} \mathbf{u}(2) - [\sigma_{11} - 1/3(\sigma_{11} + \sigma_{22} + \sigma_{33})] \\ \mathbf{u}(3) - [\sigma_{22} - 1/3(\sigma_{11} + \sigma_{22} + \sigma_{33})] \\ \mathbf{u}(4) - [\sigma_{33} - 1/3(\sigma_{11} + \sigma_{22} + \sigma_{33})] \\ \mathbf{u}(5) - [\sigma_{12}] \\ \mathbf{u}(6) - [\sigma_{13}] \\ \mathbf{u}(7) - [\sigma_{23}] \\ \Phi \end{bmatrix}. \tag{5.30}$$

Shell element case

The shell formulation follows the Kirchhoff's hypothesis that states that the thickness of the solid is close to neglectable in front of the other two dimensions. This hypothesis implies that the stress out of plane[4] remains equal to zero, $\sigma_{33} = 0$. This assumption implies that the shear stress state out of plane has to be equal to zero, $\sigma_{13} = \sigma_{23} = 0$.

Taking these assumptions into account the deviatoric stress out of plane leads

$$s_{33} = -(s_{11} + s_{22}). \tag{5.31}$$

Contrary to the full three-dimensional element case, for the shell element case the non-linear equation system is composed by four $m = 4$ independent equations and variables.

In this work, the plastic multiplier increment, and the three independent components of the deviatoric stresses on plane are taken as variables of the system,

$$\mathbf{u} = \begin{bmatrix} \Delta\gamma \\ s_{11} \\ s_{22} \\ s_{12} \end{bmatrix}, \tag{5.32}$$

[4]In this work the 11 and 22 directions are taken as on plane direction and 33 out of plane direction.

while, as objective functions, the calculated deviatoric stress values on plane and the yield function's value are taken,

$$\mathbf{f} = \begin{bmatrix} \mathbf{u}(2) - [\sigma_{11} - 1/3(\sigma_{11} + \sigma_{22})] \\ \mathbf{u}(3) - [\sigma_{22} - 1/3(\sigma_{11} + \sigma_{22})] \\ \mathbf{u}(3) - [\sigma_{12}] \\ \Phi \end{bmatrix}. \tag{5.33}$$

Convergence tolerance

The Newton-Raphson algorithm converges when the characteristic error value is lower than the specified tolerance, ϵ_{tol}. In the three-dimensional case the characteristic error is defined as the square of the objective function norm, $||\mathbf{f}||^2$.

5.5 Application example: simulation of V-free bending process

In this section, a numerical simulation of a V-free bending process is carried out with the new elastoplastic material model with different elastic behaviour accuracies: the classical linear elastic, the linear elastic with variable elastic modulus and the non-linear behaviour. This comparison has been carried out by simulating the V-free bending process by means of solid finite element model with the new elastoplastic model changing the kernel of the extended elastic law for each case. The formulation of the kernel for each elastic law was defined in Chapter 4. The objective of the current section is to analyse the influence of the elastic behaviour accuracy on springback prediction by means of finite element model.

5.5.1 Finite element model

The V-free bending test is one of the most used tests to analyse springback (Fei and Hodgson, 2006). As it has been previously schematically represented in Fig. 2.1, the metal strip rests on two dies, separated by a specific gap, and the punch goes down forming the metal strip until the desired angle. After the elastic recovery that occurs when the punch is removed, the resultant angle is measured and compared with the imposed angle during forming. In Fig. 5.1 a schematic representation of the V-free bending test performed in this section is illustrated. It has to be pointed out that the friction between the metal strip and the dies have been taken as negligible, supposing bearing dies.

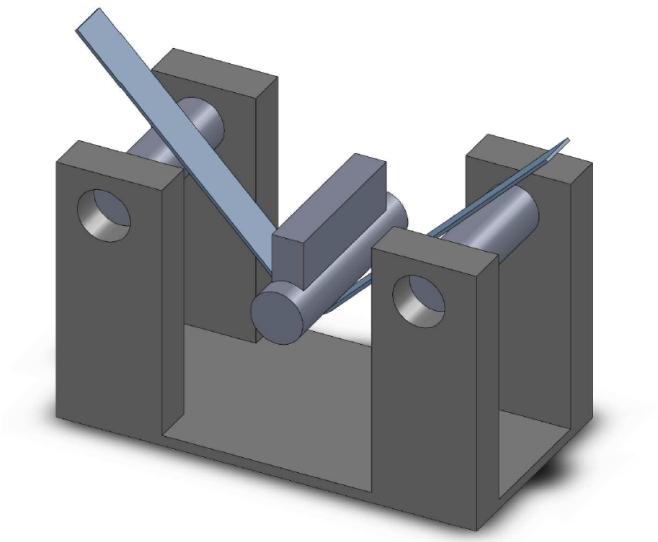

Figure 5.1. Schematic representation of the V-free bending test carried out in this thesis work.

The dies contact cylinders as well as the punch contact cylinder have 25 mm of diameter, while the gap between both dies is 150 mm. During the forming step, the punch has been moved 90 mm down, at 50 mm/min, in the center of both dies, moving it back during the springback step.

The most used technique in industry to simulate springback is to perform the forming step under dynamic explicit algorithms and the springback step under static algorithms. By means of this technique, the powerful contact algorithms characteristics of explicit packages are used during the forming step and vibration issues are avoided in springback step by using static algorithms.

The new elastoplastic material model has been implemented into the commercial finite element software ABAQUS® by means of user material subroutines.

In this thesis work, the new elastoplastic model with the extended elastic law has been implemented in both VUMAT and UMAT user subroutines for three dimensional solid elements.

Due to computational limitations, only three different mesh configurations have been carried out for this model. On the one hand, the V-free bending test has been simulated with two first order elements through the thickness in both reduced integration and complete integration. On the other hand, another model has been created with three first order complete integration solid elements through the thickness. In Fig. 5.2 both mesh

configurations are illustrated. With this configurations, models with two, four and six integration points through the thickness have been created.

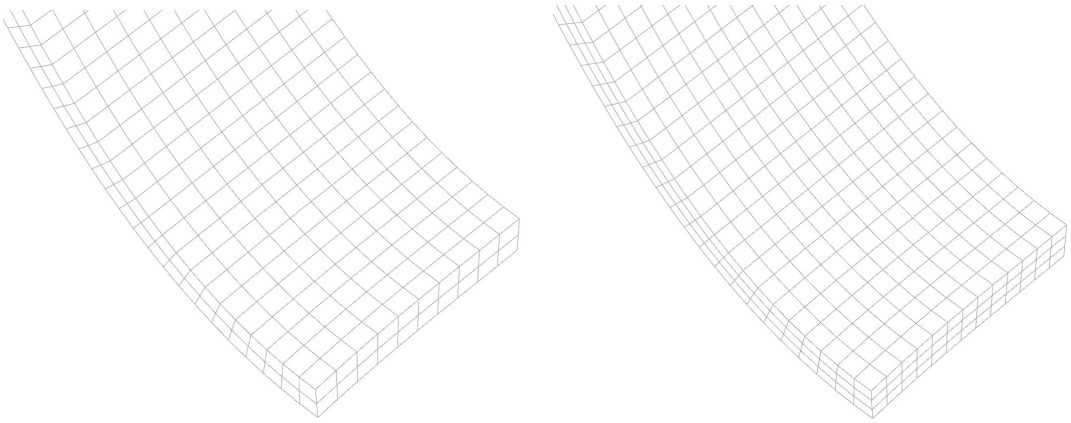

(a) (b)

Figure 5.2. Three dimensional solid element mesh configurations: (a) two element through the thickness mesh; (b) three element through the thickness mesh.

In order to reduce the computational weight of the model, symmetry properties have been used and a quarter of the strip has been modelled, Fig. 5.3. In the same way, a fix mass scaling of 1000 has been used for the forming operation.

5.5.2 Samples and measurement technique

The strip is 300 mm long, 20 mm width and 1.5 mm in thickness. Due to the symmetry condition, the section in the middle of the strip remains vertical during both forming and springback steps. The springback or final angle has been computed selecting only the first group of nodes being in the first 25 mm starting from the free flange edges.

5.5.3 Results and discussion

Figure 5.4 shows the numerical results of the solid elements simulations. Following the same nomenclature used in Chapter 4, in this chapter the linear elastic behaviour model has been referenced as classical model. The linear elastic with evolution of the elastic modulus has been referenced as Yoshida's model and the non-linear elastic model has been referenced as extended.

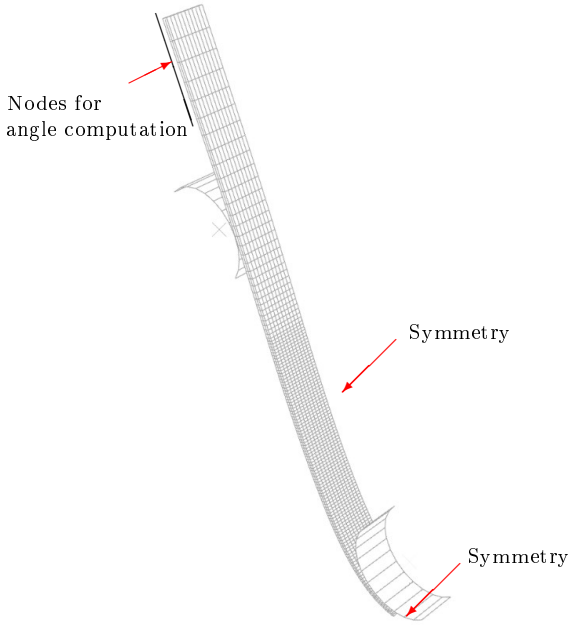

Figure 5.3. V-free bending three dimensional solid model with symmetry conditions.

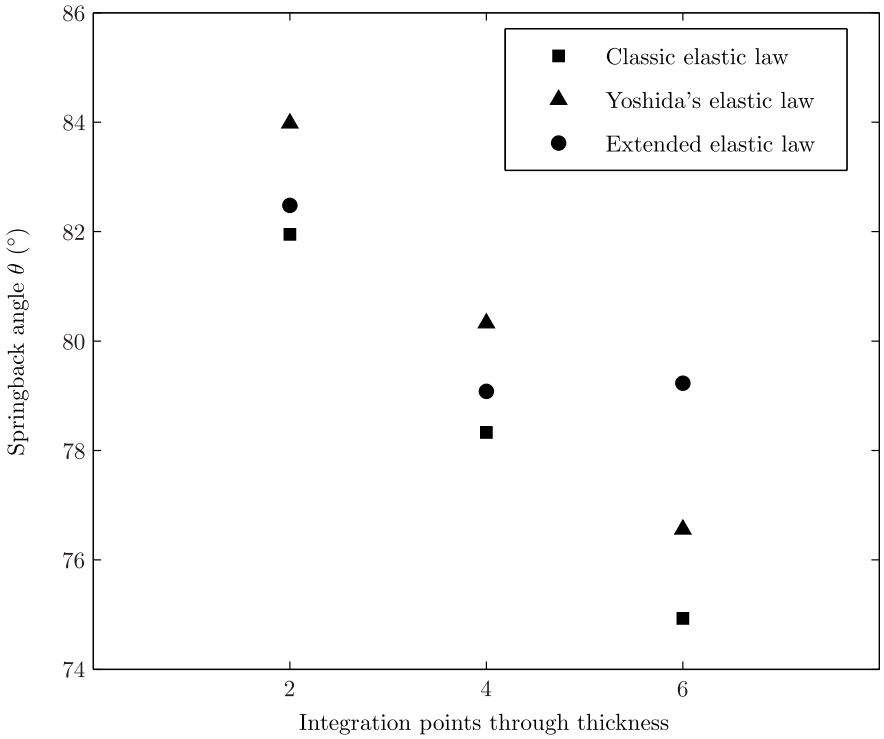

Figure 5.4. Numerical springback angle results for the three material behaviours with solid elements.

From Fig. 5.4 different conclusions can be pointed out. First, it is shown how the convergence of the mesh has not been reached with the six integration points through the thickness mesh model. This conclusion fits with the stated in (Li et al., 2002a) where $15-25$ was concluded as adequate number of integration points through the thickness for accurate springback predictions. In this thesis work, due to computational limitations, the three element through the thickness mesh model has been the finest three dimensional solid element model.

On the other hand, it can be appreciated $2° - 4°$ of difference between the different elastic law's results. Comparing the three elastic behaviour models for the two elements through the thickness meshes, the Yoshida's model predicts more recovery than the extended model, and the extended more than the classic model. But, the six integration points through the thickness model predicts a higher recovery for the extended model than the Yoshida's model. This last results agree with the results showed on the pseudo-analytical test performed in Chapter 4. This is related with the number of integration points through the thickness and the subsequent different level of accuracy of the stress gradient.

During the forming step, the closest surface of the strip to the punch has been compressed while the opposite surface has been tensioned. Therefore, a strain gradient has been imposed through the section of the sample. This strain gradient implies different levels of plasticity at each point on thickness. Consequently, after the springback step a stress gradient remains through the section.

In Fig. 5.5, a characteristic unloading of the analysed TRIP 700 predicted with the three elastic models is exposed. As it has been previously mentioned, when a complete unloading occurs, both Yoshida's and extended models predict the same strain recovery while the classic model predicts less strain recovery than the other two. On the other hand, if the recovery occurs to a different stress value higher than zero, the Yoshida's model predicts more strain recovery than the extended model, and the extended model more than the classic model. Is assumed that, as more strain recovery during the springback step at each point through the thickness, bigger springback angle is predicted.

However, when the unloading is performed to a different stress value than zero going into compression stress state the extended elastic law predicts more recovery than the Yoshida's model, as it can be shown in Fig. 5.6. If both Fig. 5.5 and Fig. 5.6 are analysed, it can be appreciated that for the same stress value in compression and in tension, the strain differences between the Yoshida's model and the extended model are higher at compression than at tension.

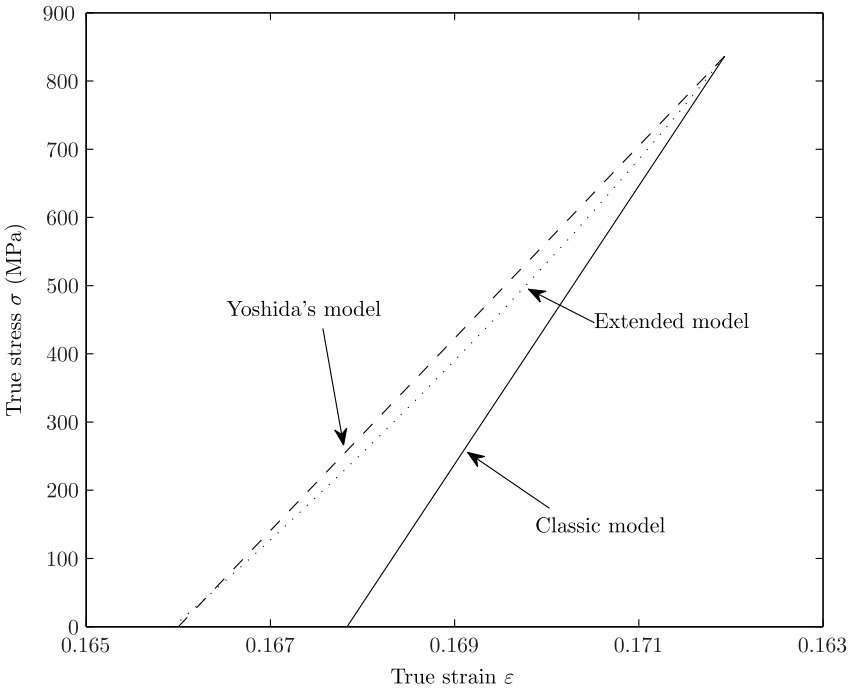

Figure 5.5. Unloading with different elastic models.

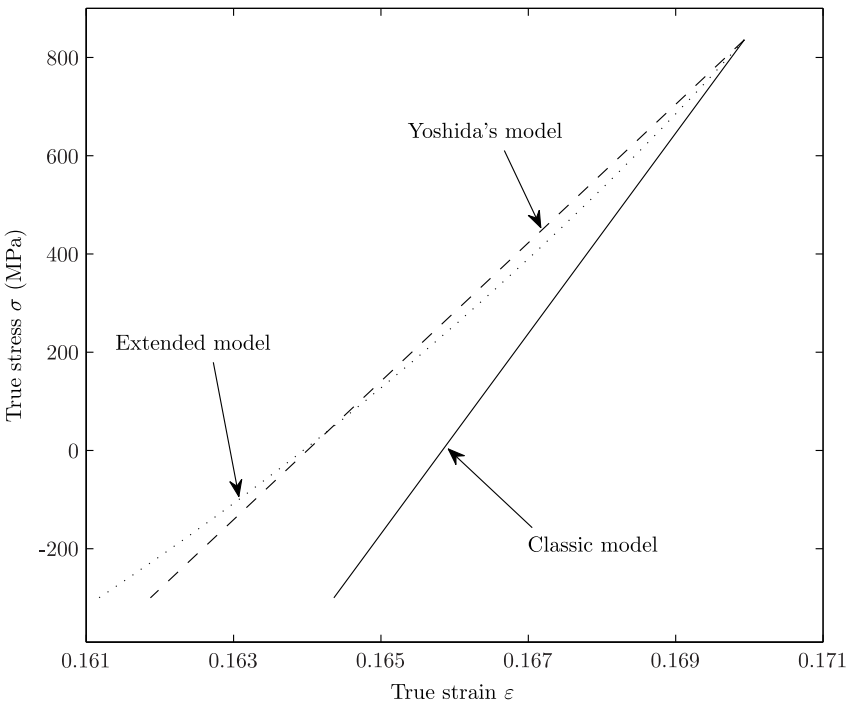

Figure 5.6. Incomplete unloading with different elastic models until compression stress state.

5.6 Conclusions

In this chapter the three dimensional extended law is formulated. In the three dimensional scenario the stress and strain are not longer represented as scalar values but as second order tensors. Therefore, the relation between the stress and the elastic strain should be represented as fourth order tensor. The conducted experimental tests are only uniaxial tests, and even if they have been carried out in three directions a behaviour hypothesis has to be done to extrapolate the uniaxial behaviour to the three-dimensional space. In this work an isotropic behaviour is supposed. Therefore the three-dimensional extension of the extended elastic law is developed from the isotropic Hooke's law.

- The numerical implementation of the three-dimensional model follows the same elastic predictor/plastic corrector algorithm detailed in the one-dimensional model. The biggest difference between the one-dimensional algorithm and the three dimensional algorithm are the use of the vectorial representation instead of the scalar representation. It has to be taken into account that the three-dimensional algorithm uses the jacobian matrix to define the convergence direction.

- The objective functions and variables of the non-linear equation system resultant of the plastic corrector algorithm have been detailed for two different behaviours, the full three-dimensional behaviour, and the shell three-dimensional behaviour. In Chapter 2 it is exposed the range of use of each finite element theory.

- By means of the finite element V-free bending simulation it has been shown that the influence of the elastic model accuracy on springback prediction is between $2° - 4°$. However, due to computational limitations it has been not possible neither to reach the convergence of the model neither to simulate the springback with 25 integration points through the thickness.

Chapter 6

V-bending experimental testing vs numerical simulation

Synopsis

In the previous chapters, a new elastoplastic material model has been developed. In Chapter 5 the implementation of the extended elastic law into V-free bending solid finite element simulation has been carried out. By means of this simulation the influence of the elastic behaviour accuracy on the springback prediction has been stated. However, the convergence of the solid element model has not been reached and the critical number of 25 integration points through the thickness has not been obtained.

Aimed at comparing the numerical predictions with experimental results, in this chapter V-free bending test experiments are carried out and compared with simple elastic behaviour model's predictions using shell elements. In this thesis work the extended elastic law is not implemented on shell finite element theory. That is why, in this chapter only the classical linear elastic and linear elastic with variable elastic modulus behaviours are compared with experimental. At the same time, the hypotheses of no influence of the kinematic hardening and anisotropic yielding are analysed.

On the one hand, the numerical results are compared with the experimental results. From this comparative it is concluded that the springback angle is underestimated by the classic elastic law and overestimated by the Yoshida's elastic law. On the other hand, the hypotheses of no influence of the kinematic hardening and anisotropic yielding are confirmed.

Taking into account the results showed in this chapter and the results of both solid finite element and pseudo-analytical models, it can been assumed that non-linear extended elastic law should predict higher springback angles than the other models, overestimating the real springboard angle.

6.1 Introduction

In the previous chapters, a new elastoplastic material model has been developed. The particularity of this new material model is that it is able to represent both linear and non linear elastic behaviours. The model has been particularised for the TRIP 700 steel with different levels of accuracy on the elastic behaviour representation. On the one hand, the elastic behaviour has been modelled as classic linear behaviour. On the other hand, the evolution of the elastic behaviour under plastic deformations has been taken into account by means of both linear elastic with variable elastic modulus and non-linear elastic behaviours.

In Chapter 5 the implementation of the extended elastic law into V-free bending solid finite element simulation has been carried out. By means of this simulation the influence of the elastic behaviour accuracy on the springback prediction has been stated. However, the convergence of the solid element model has not reached and the critical number of 25 integration points through the thickness has not been obtained.

Aimed at comparing the numerical predictions with experimental results, in this chapter V-free bending experimental tests are carried out and compared with simple elastic behaviour model's predictions using a shell finite elements model. In this thesis work the extended elastic law has not been implemented on shell finite element theory. That is why, in this chapter only the classical linear elastic and linear elastic with variable elastic modulus behaviours are compared with experimental. The former model is already implemented in commercial finite element softwares as linear elastic material and the latter one has been implemented by making the Young's modulus dependent on the accumulated plastic strain.

On the other hand, the shell theory allows the use of 25 integration points through the thickness with less computational effort than the solid element model.

The main objective of this chapter is to analyse the improvement introduced in the springback prediction by representing more accurately the elastic behaviour of the material.

First, the experimental procedure is exposed. Then, the numerical analysis are shown and the comparison between numerical and experimental is performed. Finally, the conclusions of this comparison are carried out.

6.2 V-free bending experiments

In this section the experimental V-free bending tests are presented. This experimental test set up fits the numerical simulation set up performed in Chapter 5.

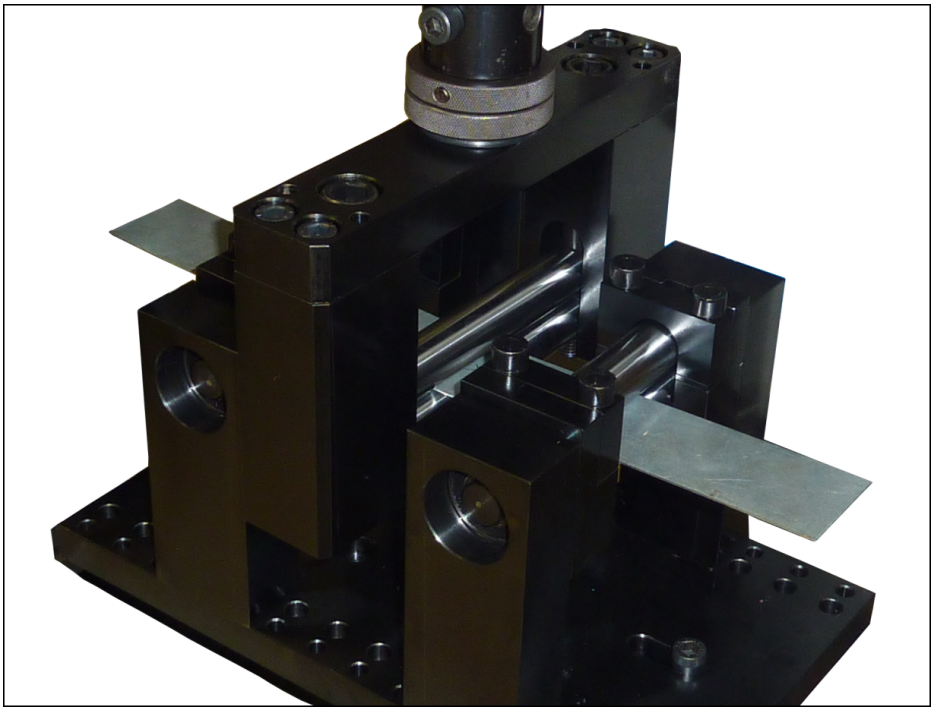

Figure 6.1. V-free bending test set up used in this thesis work.

6.2.1 Experimental procedure

The experimental set up geometry (i.e. gap, die radius, punch radius), as well as the experimental conditions (i.e. punch velocity, stroke limits) agree with the numerical test presented in the previous chapter. The die support are bearings to eliminate the friction phenomenon.

Five strips, 300 mm long and 20 mm width, have been tested. These test samples have been cut in the rolling direction using wire EDM in order to reduce the cutting influence.

After the elastic recovery step, the samples have been measured using a 3D coordinate measuring machine Mititoyo BHN710, Fig. 6.2. From the profile obtained with the 3D coordinate measuring machine, the springback angle has been calculated between both edges of the sample (Fig. 6.3). Straight lines have been fitted to the coordinate data

Figure 6.2. Sample measurement using a 3D coordinate measuring machine Mititoyo BHN710.

in the 25 mm near both edges. The springback angle has been calculated as the angle between both fitted lines.

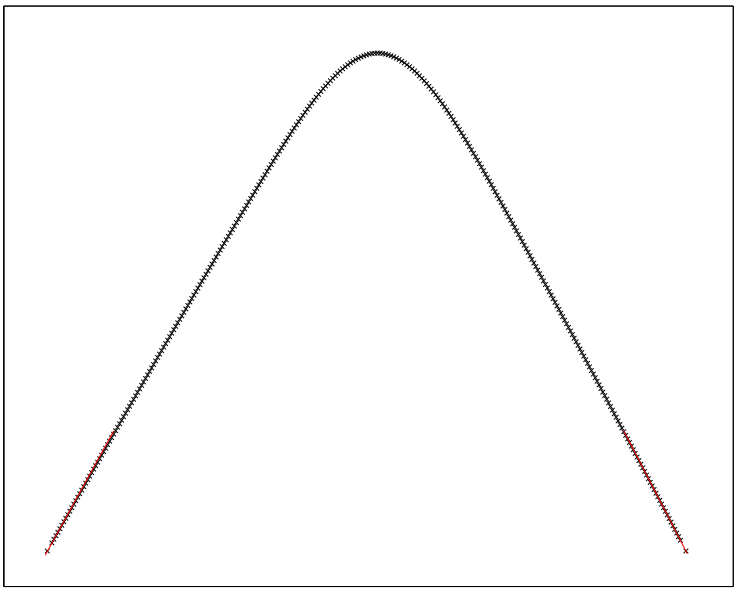

Figure 6.3. Springback angle measurement using the three dimensional profile.

6.2.2 Experimental results

Figure 6.4 shows the experimental springback angle results of the tested five samples. The resultant averaged springback angle is 78.45 ° with a deviation of 0.19 °.

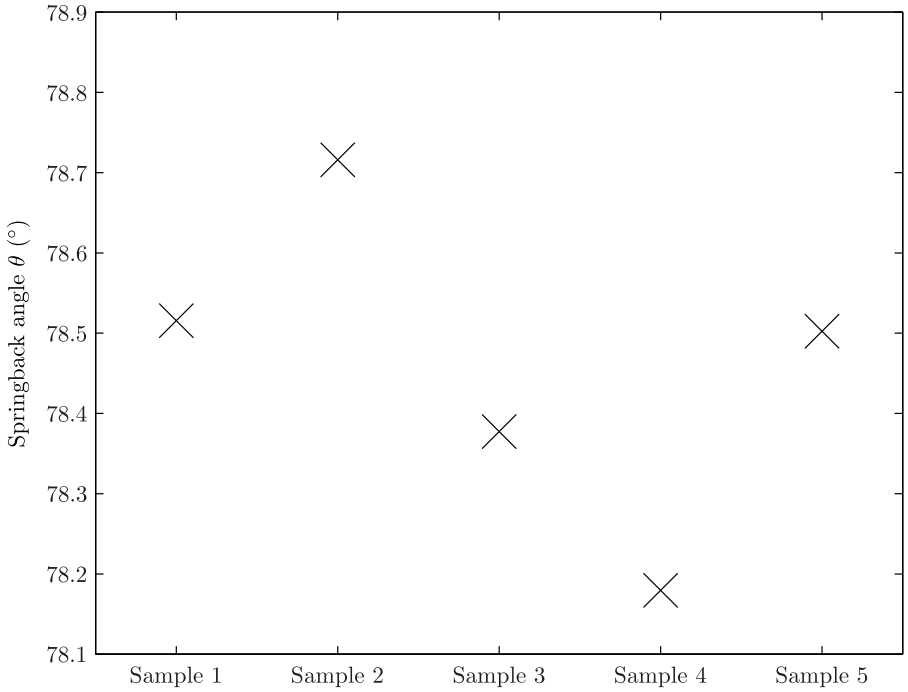

Figure 6.4. Experimental results of the springback angle after V-free bending tests.

6.3 Numerical simulation

In this section, shell finite element simulations are performed and compared with the experimental results. Therefore, two different objectives are analysed in this section:

- Analyse the springback prediction of the shell finite element model with the classical linear elastic and linear elastic with variable elastic modulus and compare these results with experimental data.

- Verify the previously performed hypotheses of no influence of the kinematic hardening and no influence of the anisotropic yielding on the springback prediction.

6.3.1 Shell element model

The shell element three dimensional model is based on the solid element model with three elements through the thickness. A quarter of the sample has been modelled also in this case, and the mesh discretisation on surface is the same as for the three elements through the thickness model. Figure 6.5 shows the shell element mesh model used in this work. This model has been created in the same software as the solid element model. Following

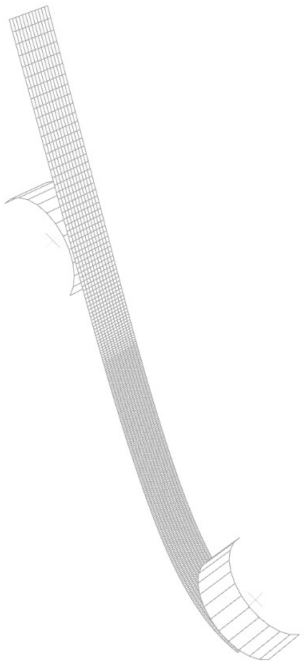

Figure 6.5. V-free bending three dimensional shell model.

an static forming-static springback approach, the V-free bending test has been simulated with reduced integration first order elements with 25 integration points through the thickness. The numerical approach that has been used in this work for implementing the linear elastic with variable elastic modulus behaviour in shell elements only allows to perform both steps (forming and springback) under static algorithms.

In order to introduce the variation of the Young's modulus of the material the USDFLD subroutine has been introduced in the model. By means of this subroutine, it has been possible to analyse both linear elastic and linear elastic with evolution of elastic modulus behaviours.

Table 6.1 shows the numerical results of the shell element models and the experimental

result. The springback angle measurement has been conducted following the same technique as in the solid finite element model.

Table 6.1
Numerical springback angle results with shell elements models and the experimental result.

Elastic model	Springback angle	Experimental angle
Classic elastic law	78.07°	78.45°
Yoshida's elastic law	79.90°	

From Table 6.1 different appreciations can be pointed out. On the one hand, it is confirmed that Yoshida's model predicts higher springback angles than the classic model, this conclusion agrees with the results obtained in both pseudo-analytical and solid finite element predictions.

On the other hand, comparing the numerical results with the experimental ones, it can be concluded that the classical elastic law underestimates the springback angle of the V-free bending test. In the same way, the linear elastic with variable elastic modulus, modelled with the Yoshida's equation, overestimates the springback angle.

6.3.2 Hypothesis validation

The new elastoplastic model has been performed without taking into account neither anisotropic yielding neither kinematic hardening. In the same way, it has been supposed that both phenomena do not have significant influence on V-free bending simulations. Therefore, this section leads with the validation of both hypothesis.

In order to validate these hypothesis, the shell element model has been simulated using the classical elastic law taking into account first the anisotropic yielding and then the kinematic hardening. These results have been compared with the isotropic yielding with isotropic hardening used in this thesis work.

Kinematic hardening

In order to analyse the influence of the kinematic hardening in the V-free bending simulation, the Chaboche mixed hardening model parameters obtained in Chapter 3 have been

used. First, a springback simulation has been conducted with the Chaboche's mixed hardening model (M. Chaboche, 1983). Then, in order to compare exactly the same hardening behaviour but under isotropic hardening assumption, an isotropic hardening picewise data has been created using the Chaboche's model's parameters. Finally, the predicted angle using the mixed hardening model and the angle predicted using the new isotropic hardening picewise model have been compared.

Differences lower than 0.03% have been found between both hardening models. The mixed hardening model predicts a springback angle of 78.09° while the new isotropic hardening picewise model predicts an angle of 78.07°. Therefore, it has been validated the hypothesis of not influence of kinematic hardening in the V-free bending test simulation.

Anisotropic yield criteria

In Table 3.3 the Lankford coefficients for the three material orientations, 0°, 45° and 90° have been obtained. Using the material's Lankford coefficients the V-free bending simulation has been conducted under an anisotropic yielding Hill criteria (de Souza Neto et al., 2008).

The result of this simulations has been compared with the result of the isotropic yielding model and a differences lower than 0.2% has been found. The isotropic yielding model predicts 78.07° of springback angle, while taking into account the anisotropic yielding the predicted angle is 77.97°. Consequently, the influence of taking into account the anisotropy of the material during the plastic yielding can be neglected for the V-free bending test analysed in this work.

6.4 Conclusions

In this chapter, V-free bending test experiments and numerical predictions using shell finite elements model has been carried out. In the same way, the hypotheses validation has been performed. Different conclusion can be stated:

- First, it can be concluded that as well as in the solid simulations, the Yoshida's elastic law predicts higher springback angles than the classic elastic law.
- Then, the numerical results have been compared with the experimental results. From this comparative it has been concluded that the springback angle is underestimated by the classic elastic law and overestimated by the Yoshida's elastic law.

- Finally, the hypotheses of no influence of the kinematic hardening and anisotropic yielding have been confirmed.

Taking into account the results showed in this chapter and the results of both solid finite element and pseudo-analytical models, it can been assumed that the non-linear extended elastic law should predict higher springback angles than the other models, overestimating the real springboard angle.

Chapter 7

Conclusions and future work

7.1 Concluding remarks

The main objective of the present thesis work has been to improve the current numerical algorithms and material modelling techniques allowing the industry to reach more accurate springback predictions in sheet metal forming. In order to achieve this objective, the improvement introduced in springback predictions by representing more accurately the elastic behaviour of the material has been analysed.

In Chapter 3 the material characterisation of the AHSS TRIP 700 steel has been performed. The material characterisation has covered the most important aspects for springback simulations, i.e. tensile behaviour, anisotropic behaviour, kinematic hardening and elastic behaviour during plastic deformation. The main conclusions drawn from this characterisation are:

- The hardening behaviour of the material is closer to a pure kinematic hardening than a pure isotropic hardening. Therefore, the selection of an appropriated hardening model seams to be crucial for simulating complex industrial processes with reverse strain paths.
- An important decrease of the elastic modulus under plastic deformation has been found. If this change is not taken into account in the numerical simulations, it will lead to big differences between predicted and real springback. However, due to the non-linearity of the unloading, the classical linear unloading using the Young's modulus doesn't assure a good prediction for processes implying incomplete unloadings. Therefore, including this phenomenon in the numerical models is very important to obtain reliable predictions.

The characterisation of the material has stated the non-linear elastic behaviour of the analysed TRIP 700 steel. In order to be able to represent more accurately this non-linear behaviour, in Chapter 4, an extension of the classical elastic law has been proposed in order to augment the capability of the elastic law to represent a non-linear elastic behaviour. The most relevant points of the presented work in this area are:

- By means of the pseudo-analytical test the influence of modelling the non-linearity of the elastic behaviour has been quantified. I is clearly demonstrated that not taking into account this effect could lead to big differences in industrial processes with large blanks.

In order to extrapolate the one-dimensional extended elastic law to the three-dimensional space, in Chapter 5, the three dimensional extended elastic law has been formulated. In the same way, a three dimensional elastoplastic model has been created. The numerical implementation of the model has been detailed for both solid and shell elements and numerical V-free solid element simulations have been carried out. The main conclusions of this study are:

- The new elastic law is suitable to be developed as anisotropic elastic model. This can be interesting for other material sciences.

- Due to computational cost associated to the use of the model, it has been not possible to reach the convergence of a solid element model. Therefore, it seams necessary the implementation of the model into shell element is necessary for simulating complex industrial processes.

In Chapter 6, the V-free bending test experiments have been carried out and compared with simple elastic behaviour model's predictions using shell elements with the classical linear elastic law and the linear elastic with variable elastic modulus. In the same way the hypotheses of no influence of the kinematic hardening and the anisotropic yielding have been analysed.

- First, it has concluded that as well as in the solid simulations, the Yoshida's elastic law predicted higher springback angles than the classic elastic law.

- Secondly, the numerical results have been compared with the experimental results. From this comparative, it has been concluded that the springback angle has been underestimated by the classic elastic law and overestimated by the Yoshida's elastic law.

Therefore, the main conclusion of this thesis work is that even if the elastic behaviour of the material has been represented more accurately with the extended elastic law, the obtained elastic model overestimates the experimental data. This erroneous prediction can came from the following assumptions:

- The elastic behaviour under compression has not been analysed in this work. Therefore, suitability of the process to compression states has not been proved.

- Furthermore, the anisotropic yielding and the kinematic hardening have not be taken into account in the new elastoplastic model.

Although, the hypothesis of neglecting the kinematic hardening and the anisotropic yielding have been validated in the previous chapter, the overestimation of the springback angle by using the extended elastic model can be related with the incomplete characterisation of the elastic behaviour, since after recovery, some material fibres are driven to compression states.

7.2 Future work

The present work has analysed the improvement of the springback predictions by representing more accurately the elastic behaviour of the material. Nevertheless, further research work is suggested in order to improve this accurate elastic behaviour modelling.

Every material model is based on the mechanics of the phenomenon to be modelled. Therefore, a deep analysis of the phenomenon is suitable for the correct model development. In this thesis work, the loading-unloading cyclic test has been used in order to characterise the elastic behaviour under plastic deformations. Even if it has been proved that this test is a valid methodology for a detailed characterisation of the elastic behaviour under tension conditions, the transition from tension to compression characteristic of springback steps in sheet metal forming it should be analysed to develop a more accurate elastic model.

Likewise, it should be also analysed the time dependence of the elastic behaviour, since it is related with dislocation movements. In the same way, depending on the application range of the model, an analysis of the temperature and strain ratio parameters should be conducted.

In the present work, the developed elastoplastic model has been simplified with the classical von Mises isotropic yield criteria and by introducing an isotropic hardening model. These two simplifications have been validated for the analysed V-free bending process. However, in order to use the elastoplastic model in different process simulations as stamping or deep drawing, the anisotropic criteria and mixed hardening should be introduced in the elastoplastic formulation.

From the numerical point of view, in this work the new elastoplastic model has been

implemented for solid finite elements. Nevertheless, the implementation of the model for shell elements should be performed for sheet metal forming simulations. Likewise, an optimisation of the implementation numerical code is suitable in order to reduce the numerical cost of simulation.

Appendix A

Publications derived from this work

During the present thesis work different contributions in notional and international scientific congresses and publications in international journals were presented:

International journals

- (Mendiguren et al., 2012a) J. Mendiguren, F. Cortés, L. Galdos (2012). A generalised fractional derivative model to represent elastoplastic behaviour of metals. International Journal of Mechanical Sciences. (//10.1016/j.ijmecsci.2012.08.008).
- (Mendiguren et al., 2012b) J. Mendiguren, F. Cortés, L. Galdos, S. Berveiller (2012). Strain path's influence on the elastic behaviour of the trip 700 steel. Materials Science and Engineering A. (//10.1016/j.msea.2012.09.087).

International congresses

- (Mendiguren et al., 2012d) J. Mendiguren, L. Galdos, E.S. de Argandoña, E. Silvestre (2012). Ludwik model parameter identification for v-bending simulations with Ti64 and MS1200. Key Engineering Materials 504 - 506, 889 - 894.
- (Mendiguren et al., 2012c) J. Mendiguren, L. Galdos, E.S. de Argandoña, E. Silvestre (2012). Influence of material's yield strength on the kinematic hardening of steels. Steel Research International special issue, 967 - 970.
- (Silvestre et al., 2012) E. Silvestre, J. Mendiguren, E.S. de Argandoña, L. Galdos (2012). Roll levelling numerical simulation using a nonlinear mixed hardening material model. Steel Research International special issue, 1295 - 1298.

National congresses

- (Mendiguren et al., 2009) Mendiguren, J., Cortés, F., Galdos, L., 2009. Representación del comportamiento plástico en metales mediante ecuaciones constitutivas fraccionarias. Congreso de Métodos Numéricos en Ingeniería.

ARTICLE IN PRESS

International Journal of Mechanical Sciences ▮ (▮▮▮▮) ▮▮▮–▮▮▮

Contents lists available at SciVerse ScienceDirect

International Journal of Mechanical Sciences

journal homepage: www.elsevier.com/locate/ijmecsci

A generalised fractional derivative model to represent elastoplastic behaviour of metals

Joseba Mendiguren [a,*], Fernando Cortés [b,1], Lander Galdos [a,2]

[a] Department of Mechanical Engineering, Mondragon Unibertsitatea, Loramendi 4, 20500 Mondragón, Spain
[b] Deusto Institute of Technology (DeustoTech), Faculty of Engineering, University of Deusto, Avda. de las Universidades 24, 48007 Bilbao, Spain

ARTICLE INFO

Article history:
Received 16 January 2012
Received in revised form
8 July 2012
Accepted 21 August 2012

Keywords:
Fractional calculus
Model behaviour
Elastoplasticity
Numerical methods
Plasticity

ABSTRACT

In this paper, a one-dimensional elastoplastic model based on fractional calculus is presented. This model is conceived for metal deformation. First, a brief introduction about fractional calculus is exposed. Then, a fractional calculus based general model is proposed, build-up as a series of fractional derivatives. The particular cases of one, two and three terms are discussed. Finally, these three particular cases of the general model are fitted to experimental data and compared with the classical Hollomon and Ramberg–Osgood models. As a result, a model capable of representing the elastoplastic behaviour more precisely than the Hollomon and Ramberg–Osgood models is obtained, despite numerical efforts are enlarged.

1. Introduction

Nowadays, automotive industry is becoming more and more competitive, car safety has to augment while vehicles must be lighter to reduce fuel consumption, reducing prices to be more competitive in the market. Due to this increment in the competitiveness of the market, the automotive engineering needs more accurate material models in order to improve the numerical simulations needed to reach competitive designs.

Among all manufacturing processes used in automotive industry, metal plastic forming is one of the most important. This kind of process exploits the fact that when a metallic material is deformed enough to reach its elastoplastic region, the material remains with this new configuration. In fact, when a material is deformed, it has two regions: a first region of elastic behaviour until reach certain stress value, and when this value of stress is reached, a second elastoplastic region starts, in which permanent deformation occurs.

Materials are usually characterised by tensile test. In this test, the material is stretched in one direction until rupture and elastic and plastic properties of the material are obtained [1]. The elastoplastic behaviour of the material can be represented from a two different point of view. On the one hand, the industrial representation where the objective is to represent the whole behaviour until rupture and even extended to a high strain ranges. On the other hand, from a computational plasticity point of view where the curve is split and the elastic behaviour is represented by means of the elastic modulus and the plastic behaviour is represented with the hardening curve.

In the last years, the representation of the plastic behaviour from a computational plasticity point of view has been deeply developed. New combined hardening models are introduced and new recovering techniques are developed [2–5].

However, the correct representation of these two behaviours (elastic and plastic behaviours) together in a single model is still a challenge. A single model able to describe both behaviours more accurately than current models is a high research due to the exigences of the market. The use of this kind of representations is widely used in industry in order to compare the behaviour of two materials and to extend the tensile test data to get a piecewise data up to the tensile test rupture strain. That is why, the accuracy of the single model and specifically just before necking has become a research interest from an industrial point of view.

Among the different models that can be found in the literature to describe elastoplasticity, both Hollomon and Ramberg–Osgood models are the most used. On the one hand, the Hollomon model satisfies

$$\sigma = K\varepsilon^{n_H}, \tag{1}$$

where K and n_H are the model parameters, σ and ε being the stress and strain, respectively. On the other hand, the Ramberg–Osgood

* Corresponding author. Tel.: +34 943794700; fax: +34 943791536.
E-mail addresses: jmendiguren@mondragon.edu (J. Mendiguren), fernando.cortes@deusto.es (F. Cortés), lgaldos@mondragon.edu (L. Galdos).
[1] Tel.: +34 944139003.
[2] Tel.: +34 943794700; fax: +34 943791536.

0020-7403/$ - see front matter © 2012 Elsevier Ltd. All rights reserved.
http://dx.doi.org/10.1016/j.ijmecsci.2012.08.008

Please cite this article as: Mendiguren J, et al. A generalised fractional derivative model to represent elastoplastic behaviour of metals. Int. J. Mech. Sci. (2012), http://dx.doi.org/10.1016/j.ijmecsci.2012.08.008

Strain path's influence on the elastic behaviour of the TRIP 700 steel

J.Mendiguren[1]*, F.Cortés[2], L.Galdos[1] and S.Berveiller[3]

[1]*Manufacturing Department, Mondragon University, Loramendi 4, 20500 Arrasate-Mondragon (Spain)*

[2]*Deusto Institute of Technology (DeustoTech), Faculty of Engineering, University of Deusto, Avda. de las Universidades 24, 48007 Bilbao (Spain)*

[3]*Laboratoire d'Étude des Microstructures et de Mécanique des Matériaux (LEM3, UMR CNRS 7239), Arts et Métiers ParisTech, 4 rue Augustin Fresnel, 57078 Metz Cedex 03 (France)*

Corresponding author:

E-mail: jmendiguren@mondragon.edu

Fax number: +34 943 79 47 00

Telephone number: +34 943 73 15 36

Abstract

This paper deals with the analysis of the strain path's influence on the elastic behaviour of TRIP 700 steel; it aims to validate the cyclic testing method to characterise inelastic behaviour of advanced high strength steels (AHSS). Different cyclic tests are done, where the strain path is changed from test to test. Large deformation strain gages are used to determine the inelastic behaviour of the specimens at macro level. At a lower scale, stress measurements are carried out using the XRD technique during an in-situ tensile test: ferrite and austenite phases' stresses are measured before unloading and after loading again to study the strain path's influence.

By means of this work it is confirmed that the elastic strain path has no influence on the unloading-loading of this TRIP steel. These results prove that conventional loading-unloading cyclic testing is a valid methodology for a detailed characterisation of the elastic modulus and reliable numerical modelling of springback.

Keywords: *TRIP steel; springback; inelastic behaviour; XRD*

INTRODUCTION AND MOTIVATION

In the last years, and mainly due to the constantly increasing market competitiveness, there has been a trend towards design free and lightweight structures, leading to the use of more complex geometries and new materials. Advanced high strength steels (AHSS) are taking acceptance in the market due to their good mechanical properties to weight ratio [1]. Among these, TRIP steels present a good drawability associated with a high resistance; their good mechanical properties are

Key Engineering Materials Vols. 504-506 (2012) pp 889-894
Online available since 2012/Feb/03 at www.scientific.net

doi:10.4028/www.scientific.net/KEM.504-506.889

Ludwik's model parameter identification for v-bending simulations with Ti64 and MS1200

J. Mendiguren[1,a], L. Galdos[1,b], E. Sáenz de Argandoña[1,c], E. Silvestre[1,d]

[1]Mondragon University – Mechanical and Manufacturing Department – Spain

[a]jmendiguren@mondragon.edu, [b]lgaldos@mondragon.edu, [c]esaenzdeargan@ mondragon.edu, [d]esilvestre@mondragon.edu

Keywords: Hardening, High strength steels, Metal plasticity, Springback, V-bending.

Abstract. Flow curves coming from tensile tests together with constant young modulus are widely used by industry when modelling sheet metal bending processes. Unfortunately this modelling strategy based on previous mentioned variables is not accurate enough and leads to big errors due to the springback of the material. This drawback is even more important when high strength steels are bended. Aiming to reduce the springback errors, Ludwik's hardening material models under v-bending deformation have been obtained for a Ti6Al4V alloy and for a MS1200 martensitic ultra high strength steel and their accuracy has been compared to the classical models obtained from tensile tests. First of all, classical Ludwik's hardening models are obtained from tensile tests. Then, using a v-bending test and inverse simulation, Ludwik hardening model parameters for bending are calculated using a von Mises yielding criteria.
As a result, a model able to represent the bending behaviour of these two materials more accurately without complex code modifications is achieved.

Introduction

In the last years, the automotive industry is becoming more and more competitive, car safety has to augment while vehicles must be lighter to reduce fuel consume, reducing prices to be more competitive in the market. Since the industry attempts to utilize Advanced High Strength Steels (AHSS) and new Ti-alloys for manufacturing their products, springback is becoming a significant issue. Numerical models have become essential tools in order to predict accurately the forming final stress state, which is crucial for the sprinback prediction. Wagoner in 2002 [1], analyzed the influence of different numerical models' variables in the springback prediction. After the wider introduction of these kinds of materials, different authors have worked in the improvement of the numerical models in order to be more accurate [2]. Nowadays, different yield functions [3], elastic modulus variation [4] and hardening models [5], can be combined to achieve optimal numerical models able to predict the behaviour of the materials at each manufacturing process. However, industries usually work with flow curves coming from tensile test together with constant young modulus and von Mises based yield criteria and plastic flow. Unfortunately this modelling strategy is not accurate enough and leads to big errors. This drawback is even more important when high strength steels are bended.

In this context, this work leads with the identification of the material parameters directly from the v-bending test. First the material model is obtained from the tensile test. In this case, a von Mises yield criterion with isotropic Ludwik's hardening model [6], composes the behaviour of the material. This model is selected because it is implemented in almost all the commercial numerical software.

Then, the v-bending tests are performed and the results of the test are compared with those obtained from the numerical simulations launched using the Ludwik's model parameters obtained from the tensile test. As is presented below, differences exist between the v-bending test results and those

Influence of Material's Yield Strength on the Kinematic Hardening of Steels

Joseba Mendiguren, Lander Galdos, Eneko Sáenz de Argandoña, Elena Silvestre

Mondragon University – Mechanical and Manufacturing Department – Spain – jmendiguren@mondragon.edu

Abstract. In the last years, and mainly due to the constantly increasing market competitiveness, there has been a trend towards more and more complex geometries, design free structures and new materials with higher ultimate tensile strengths and consequently lower formability properties. Common problems are premature cracks, high springback, excessive distortion of the parts, bad final surface quality, etc. All these changes make numerical simulation an indispensable tool for process development. Nevertheless, the numerical results are directly linked to the material and contact description, being the Baushinger phenomenon in cyclic plasticity an important factor for sheet metal forming simulations in those processes where material is subjected to compression-tension stress states. In the present work, the influence of the yield strength on the mixed hardening model parameters is analysed. Kinematic hardening parameters are obtained for DC04, TRIP700 and MS1200 steels. First, tensile tests are performed using a conventional uniaxial tensile machine. Then, using inverse simulation, the parameters of the mixed Chaboche1990 hardening model are obtained. As a result, the Chaboche1990 mixed hardening parameters are obtained and compared to the materials´ yield strength. Back-Stress Tensor stabilizes later when using high strength steels and thus long range of cycles is needed before reaching the stable state when using AHSS.

Keywords: Metal forming, Baushinger phenomenon, kinematic hardening, Chaboche

1. INTRODUCTION

In the last years, and mainly due to the constantly increasing market competitiveness, there has been a trend towards more and more complex geometries, design free structures and new materials. Moreover these challenges have been attempted trying in parallel to reduce the number of manufacturing steps due to economical reasons. All the previous changes applied to sheet metal forming processes have concluded into a scenario where the deformations that materials are subjected during the manufacturing processes have raised considerably being much closer to their formability limits.

Furthermore, new problems have appeared such as premature cracks, springback problems, excessive distortion of the parts, bad final surface quality, etc. All these changes make numerical simulation an indispensable tool for process development. Nevertheless, the numerical results are directly linked to the material and contact description, being the Baushinger phenomenon in cyclic plasticity an important factor for sheet metal forming simulations [1].

Strain path reversal is quite common in sheet metal forming processes, e.g bending-unbending or deep drawing. In steel characterization the tension-compression test is commonly used to obtain the hardening behaviour of the material [2]. The problem of the sample´s buckling that appears in this kind of test in metal sheets has been differently overcomed, e.g using the bending test instead of the tensile test, using special tools to block the buckling [3]. Due to the buckling problem, the kinematic hardening characterization in metal sheets is still a big challenge.

In this work, experimental tension/compression tests are performed in three different steel sheets using a tooling that avoids the buckling. Then, an elastoplastic model with mixed isotropic/kinematic hardening model is fitted to the experimental results to found the hardening parameters for each steel.

Finally, the obtained results are discussed and the influence of the quasi-static material parameters in the hardening parameters are analysed.

2. MATERIAL MODEL

The behaviour law used in this study is a unidimensional elastoplastic associative behaviour law with mixed hardening. The basic equations which compose the material model are presented in the following lines.

The main hypothesis underlying the small strain theory of plasticity is the decomposition of axial strain:

$$\varepsilon = \varepsilon^e + \varepsilon^p, \tag{1}$$

where ε, is the axial strain , ε^e, is the elastic strain and ε^p, represents the plastic strain.

Following the above definition of the strain, the constitutive law for the axial stress can be presented as:

$$\sigma = E\,\varepsilon^e, \tag{2}$$

where σ, is the axial stress, and E is the material's Young's modulus.

In this unidimensional model with mixed hardening the yield function leads:

$$\Phi(\sigma, X, \sigma_y) = |\sigma - X| - \sigma_y, \tag{3}$$

where Φ, represents the yield function, while X, is the backstress tensor characteristic of the kinematic hardening and σ_y, is the size of the yield surface defined by the isotropic hardening.

The plastic flow rule for this unidimensional elastoplastic formulation can be expressed as:

$$\dot{\varepsilon}^p = \dot{\gamma}\, sign(\sigma), \tag{4}$$

Roll Levelling Numerical Simulation Using a Nonlinear Mixed Hardening Material Model

Elena Silvestre, Joseba Mendiguren, Eneko Sáenz de Argandoña, Lander Galdos

Mondragon University – Mechanical and Manufacturing Department – Spain – esilvestre@mondragon.edu

Abstract. Roll levelling is a forming process used to remove the residual stresses and imperfections of metal strips by means of plastic deformations. During the process the metal fibers are subjected to cyclic tension-compression deformations leading to a flat product. The process is especially important to avoid final geometrical errors when coils are cold formed or when thick plates are cut by laser. In the last years, and due to the appearance of high strength materials such as Ultra High Strength Steels, machine design engineers are demanding a reliable tool for the dimensioning of the levelling facilities. In response to this demand, Finite Element Analysis is becoming an important technique able to lead engineers towards facilities optimization through a deeper understanding of the process. Nevertheless, the most commonly used material models, isotropic hardening models, are not able to reproduce the material´s Bauschinger effect and the final numerical results are not accurate enough. Aiming to study the influence of the material model in roll levelling simulation, a mixed isotropic-kinematic hardening formulation, firstly introduced by Armstrong and Frederick and subsequently modified by Chaboche, has been used in the present work. A MS1200 high strength steels and a DC04 mild steel are analyzed. Both materials are characterized, using uniaxial tensile tests and uniaxial cyclic tension-compression tests. Finally the influence of the material model in the numerical results is analyzed by comparing a pure isotropic model and a mixed Chaboche hardening model.

Keywords: Roll levelling, kinematic hardening, ultra high strength steels, tension/compression test, parameter identification

1. INTRODUCTION

With the introduction of new high performance steel grades, efficient and sophisticated forming techniques of thin sheets are required. Specifically, the automotive industry is becoming more and more competitive in this area. In this context, High-Strength-Steels (HSS) and Ultra-High-Strength-Steel (UHSS) offer great possibilities for weight and fuel consumption reduction and safety improvement.

Roll levelling is a forming process that aims at correcting flatness defects and minimizing residual stresses where sheets are bent in alternate directions by a certain number of rolls. During this process, materials are subjected to elasto-plastic deformations within the levelling machines leading to complex behaviours of the material. As an initial step in order to improve the control of the process, several attempts have been carried out in order to better understand the behaviour of the material. This way, Doege et al. [1] carried out an analysis of the levelling process based on a one-dimensional analytical model. This model needs a very short calculation time and uses bending theory to find the optimal set up for the rolls. Dratz et al [2] developed three different models (a finite element approach, an analytical approach and a semi-analytical approach) to determine the loading modes experienced by the material in roll levelling operations. Other authors have proposed finite element models to simulate the sheet behaviour, taking into account cyclic elasto-plasticity and the Bauschinger effect in their own code. Analytical models have the advantage that they need a shorter computational time than EF method. However they require several assumptions in the model which restrict the accuracy of the results significantly.

From the material point of view, different yield functions and hardening models [3] can be combined to achieve optimal numerical models able to consider the phenomena that occur during cyclic loading, such as the Bauschinger effect, the transient behaviour, the permanent softening and the work hardening stagnation. These effects are defined by the hardening law. In all the processes where cyclic plasticity performance occurs, an isotropic-kinematic hardening model seems to be the most appropriate. A pure isotropic model provides poorly accurate results, but combined with a kinematic model significant improvements can be achieved. The complexity of the model depends on the number of material parameters which have to be identified.

At the present research a von Mises yield criterion with the Chaboche nonlinear mixed (isotropic + kinematic) hardening law with four parameters is chosen to model the material behaviour. The model is obtained from the tension/compression test. This test is the simplest one because an inverse method in order to calculate the parameters is not necessary. However, there is a tendency of the strip to buckle under compression load during the test. At the present research, an experimental equipment for cyclic testing has been successfully developed to avoid the buckling effect.

This way, the tension/compression tests are directly carried out to identify the material parameters by means of an optimization technique. Finally, numerical results of a levelling process are compared when using a mixed material model and a pure isotropic model.

2. MIXED HARDENING MODEL

The selected model is a mixed isotropic-kinematic hardening formulation introduced by Chaboche and Lemaitre [4, 5]. A proper hardening law must describes the movement of the yield surface corresponding to the kinematic hardening and the change in the size of the yield surface corresponding to the isotropic hardening.

In this unidimensional model with mixed hardening the yield function leads

$$\Phi(\sigma, X, \sigma_y) = |\sigma - X| - \sigma_y, \quad (1)$$

Congreso de Métodos Numéricos en Ingeniería 2009
Barcelona, 29 junio al 2 de julio 2009

MODELIZACIÓN DEL COMPORTAMIENTO PLÁSTICO DE METALES MEDIANTE ECUACIONES CONSTITUTIVAS FRACCIONARIAS

Joseba Mendiguren[1*], Fernando Cortés[1] y Lander Galdos[1]

1: Departamento de Mecánica y Producción Industrial
Escuela Politécnica Superior
Mondragon Unibertsitatea
Loramendi 4, 20500 Mondragon, Spain
e-mail: jmendiguren,fcortes,lgaldos@eps.mondragon.edu, web: http://www.mondragon.edu

Palabras clave: Plasticidad, Cálculo Fraccionario, Modelos de Material, Ajuste de modelos

Resumen. *En esta comunicación se presentan leyes constitutivas fraccionarias para la modelización del comportamiento plástico de metales. Estos modelos de material, a diferencia de los modelos clásicos que se formulan en base a relaciones tensión-deformación no lineales, se enuncian mediante ecuaciones diferenciales fraccionarias lineales, con el fin de simplificar el tratamiento numérico en aplicaciones estructurales. Así mismo, se analiza la influencia de los parámetros del modelo en el comportamiento representado, de modo que seleccionando el número adecuado de parámetros se consigue mejorar la representación del comportamiento experimental de metales. Este hecho se pone de manifiesto comparando los ajustes realizados sobre mediciones de la aleación A608o para diferentes temperaturas, con los aportados por el modelo de Hollomond.*

1. INTRODUCCIÓN

La historia de la plasticidad como ciencia tiene por origen los primeros trabajos de Tresca en los que formula su famoso criterio de fluencia. Unos años más tarde, basándose en los resultados experimentales obtenidos por Tresca, Saint-Venant y Lévy desarrollan los fundamentos de la teoría de plasticidad moderna. Sin embargo, no es hasta aproximadamente 1945 cuando una teoría de plasticidad unificada comienza a emerger (para una revisión histórica mas profunda véanse, por ejemplo, las monografías [1] y [2]).

La teoría de la plasticidad se puede clasificar en dos categorías: la teoría física y la teoría matemática. Por un lado, la teoría física, tiene como objetivo explicar los mecanismos de deformación plástica, analizando tanto el material microscópicamente como el comportamiento de los átomos y las redes cristalinas antes, durante y después de la deformación

Bibliography

Andersson, A., 2005. Numerical and experimental evaluation of springback in a front side member. Journal of Materials Processing Technology 169 (3), 352 – 356.

Andersson, A., 2007. Numerical and experimental evaluation of springback in advanced high strength steel. Journal of Materials Engineering and Performance 16 (3), 301 – 307.

Asgari, A., Pereira, M., Rolfe, B., Dingle, M., Hodgson, P., 2005. Design of experiments and springback prediction for AHSS automotive components with complex geometry. No. 778. USA, pp. 215 – 20.

Asgari, S., Pereira, M., Rolfe, B., Dingle, M., Hodgson, P., 2008. Statistical analysis of finite element modeling in sheet metal forming and springback analysis. Journal of Materials Processing Technology 203 (1-3), 129 – 136.

B. Osgurg, G. Lengfeld, O. S., 2012. Innovation and globalization as a factor of success for global hotstamping growth. In: Liewald, M. (Ed.), New Developments in Sheet Metal Forming. pp. 79–92.

Berrahmoune, M., Berveiller, S., Inal, K., Moulin, A., Patoor, E., 2004. Analysis of the martensitic transformation at various scales in TRIP steel. Materials Science and Engineering A 378, 304 – 307.

Berveiller, S., Inal, K., Kubler, R., Eberhardt, A., Patoor, E., 2004. Experimental approach of the martensitic transformation in shape-memory alloys and TRIP steels. Journal de Physique IV 115, 261 – 8.

Bramfitt, B., Benscoter, A., 2002. Metallographer's guide: practice and procedures for irons and steels. ASM International.

Callister, W., 1993. Materials science and engineering: an introduction. John Wiley & Sons, New York.

Carden, W., Geng, L., Matlock, D., Wagoner, R., 2002. Measurement of springback. International Journal of Mechanical Sciences 44 (1), 79 – 101.

Chatti, S., 2010. Effect of the elasticity formulation in finite strain on springback prediction. Computers and Structures 88, 769 – 805.

Chatti, S., Hermi, N., 2011. The effect of non-linear recovery on springback prediction. Computers and Structures 89 (13-14), 1367 – 1377.

Chun, B., Jinn, J., Lee, J., 2002. Modeling the Bauschinger effect for sheet metals, part I: Theory. International Journal of Plasticity 18 (5), 571 – 595.

Cleveland, R., Ghosh, A., 2002. Inelastic effects on springback in metals. International Journal of Plasticity 18 (6), 769 – 785.

de Souza Neto, E., Peric, D., Owen, D., 2008. Computational methods for plasticity. Wiley.

Doege, E., Kulp, S., Sunderkotter, C., 2002. Properties and application of TRIP-steel in sheet metal forming. Steel Research 73 (6-7), 303 – 308.

Eggertsen, P.-A., Mattiasson, K., 2009. On the modelling of the bending-unbending behaviour for accurate springback predictions. International Journal of Mechanical Sciences 51 (7), 547 – 563.

Eggertsen, P.-A., Mattiasson, K., 2011. On the identification of kinematic hardening material parameters for accurate springback predictions. International Journal of Material Forming 4 (2), 103 – 120.

Farías, D., 2006. Bake hardening response of DP800 and the influence on the 'In Service Performance'. Master's thesis, Technische Universiteit Eindhoven.

Fei, D., Hodgson, P., 2006. Experimental and numerical studies of springback in air v-bending process for cold rolled TRIP steels. Nuclear Engineering and Design 236 (18), 1847 – 1851.

Firat, M., Mete, O. H., Kocabicak, U., Ozsoy, M., 2010. Stamping process design using fea in conjunction with orthogonal regression. Finite Elements in Analysis and Design 46 (11), 992 – 1000.

Foreman, A. J. E., 1967. The bowing of a dislocation segment. Philosophical Magazine 15 (137), 1011 – 1021.

Galdos, L., García, C., Aginagalde, A., Esnaola, J. A., 2006. Influence of the lubrication in tube hydroforming processes. Method for the determination of the friction coefficients and modelling of the process. In: Advances in Materials Processing Technologies, AMPT2006 (Las Vegas).

Gan, W., Babu, S., Kapustka, N., Wagoner, R., 2006. Microstructural effects on the springback of advanced high-strength steel. Metallurgical and Materials Transactions A: Physical Metallurgy and Materials Science 37 (11), 3221 – 3231.

Gelin, J., Thibaud, S., Boudeau, N., 2005. Modelling and simulation of the influence of forming processes on the structural behavior of high strength steels. Vol. 778. USA, pp. 101 – 106.

Gomes, C., Onipede, O., Lovell, M., 2005. Investigation of springback in high strength anisotropic steels. Journal of Materials Processing Technology 159 (1), 91 – 98.

Greisert, C., Wesemann, J., 2002. Influence of constant and variable restraining force on springback of TRIP 700 and stainless steel grades. Steel Research 73 (6-7), 309 – 313.

Haddag, B., Balan, T., Abed-Meraim, F., 2007. Investigation of advanced strain-path dependent material models for sheet metal forming simulations. International Journal of Plasticity 23 (6), 951 – 979.

Halilovic, M., Vrh, M., Stok, B., 2007. Impact of elastic modulus degradation on springback in sheet metal forming. AIP Conference Proceedings 908 (1), 925 – 30.

Hauk, V., 1997. Structural and residual stress analysis by non-destructive methods. Elsevier, Amsterdam.

Huh, H., Kim, S., Song, J., Lim, J., 2008. Dynamic tensile characteristics of TRIP-type and DP-type steel sheets for an auto-body. International Journal of Mechanical Sciences 50 (5), 918 – 931.

Ingarao, G., Di Lorenzo, R., Micari, F., 2009. Analysis of stamping performances of dual phase steels: a multi-objective approach to reduce springback and thinning failure. Materials and Design 30 (10), 4421 – 4433.

Jatczak, C. F., 1980. Retained austenite and its measurement by X-ray difraction. SAE Preprints (800426).

Kilbas, A., Srivastava, H., Trujillo, J., 2006. Theory and applications of fractional differential equations. Elsevier Science Ltd.

Koc, M., Chen, P., 2007. Simulation of springback variation in forming of advanced high strength steels. Journal of Materials Processing Technology 190 (1-3), 189 – 198.

Kouznetsova, V., Geers, M., 2008. A multi-scale model of martensitic transformation plasticity. Mechanics of Materials 40 (8), 641 – 657.

Laurent, H., Greze, R., Oliveira, M., Menezes, L., Manach, P., Alves, J., 2010. Numerical study of springback using the split-ring test for an AA5754 aluminum alloy. Finite Elements in Analysis and Design 46, 751 – 759.

Li, K., Carden, W., Wagoner, R., 2002a. Simulation of springback. International Journal of Mechanical Sciences 44 (1), 103 – 122.

Li, L., Tikun, S., 2011. Effect of transformation on springback for TRIPsteel stamping. Vol. 221. Qingdao, China, pp. 405 – 410.

Li, X., Yang, Y., Wang, Y., Bao, J., Lo, S., 2002b. Effect of the material-hardening mode on the springback simulation accuracy of V-free bending. Journal of Materials Processing Technology 123 (2), 209 – 211.

Luchko, Y., Rivero, M., Trujillo, J., Velasco, M., 2010. Fractional models, non-locality, and complex systems. Computers and Mathematics with Applications 59 (3), 1048 – 1056.

M. Chaboche, G. R., 1983. On the plastic and viscoplastic constitutive equations- part i: Rules developed with internal variable concept. Transaction of ASME 105, 153 – 158.

Madej, L., Muszka, K., Perzynski, K., Majta, J., Pietrzyk, M., 2011. Computer aided development of the levelling technology for flat products. CIRP Annals - Manufacturing Technology 60 (1), 291 – 294.

Maki, T., 2012. Sheet hydroforming of aluminum body panels. In: Liewald, M. (Ed.), Hydroforming of Sheets, Tubes und Profiles. Vol. 7. pp. 41–56.

Marretta, L., Di Lorenzo, R., 2010. Influence of material properties variability on springback and thinning in sheet stamping processes: a stochastic analysis. The International Journal of Advanced Manufacturing Technology 51, 117–134.

Matlock, D., Hilditch, T., Speer, J., 2007. Influence of low-strain deformation characteristics of high strength sheet steel on curl and springback in bend-under-tension tests. Journal of Materials Processing Technology 182 (1-3), 84 – 94.

Mendiguren, J., Cortés, F., Galdos, L., 2009. Representación del comportamiento plástico en metales mediante ecuaciones constitutivas fraccionarias. In: Congreso de Métodos Numéricos en Ingeniería.

Mendiguren, J., Cortés, F., Galdos, L., 2012a. A generalised fractional derivative model to represent elastoplastic behaviour of metals. International Journal of Mechanical Sciences. (//10.1016/j.ijmecsci.2012.08.008).

Mendiguren, J., Cortés, F., Galdos, L., Berveiller, S., 2012b. Strain path's influence on the elastic behaviour of the TRIP 700 steel. Materials Science & Engineering A. (//10.1016/j.msea.2012.09.087).

Mendiguren, J., Galdos, L., de Argandoña, E. S., Silvestre, E., 2012c. Influence of material's yield strength on the kinematic hardening of steels. Steel Research International special issue, 967 – 970.

Mendiguren, J., Galdos, L., de Argandoña, E. S., Silvestre, E., 2012d. Ludwik model parameter identification for v-bending simulations with Ti64 and MS1200. Key Engineering Materials 504 - 506, 889 – 894.

Morestin, F., Boivin, M., 1996. On the necessity of taking into account the variation in the Young modulus with plastic strain in elastic-plastic software. Nuclear Engineering and Design 162 (1), 107 – 116.

NC, W., 2010. Instruction bulletin B-129-8: Surface preparation for strain gage bonding. Micro-Measurements® of Vishay Precision Group, Inc.

Oliveira, M., Alves, J., Chaparro, B., Menezes, L., 2007. Study on the influence of work-hardening modeling in springback prediction. International Journal of Plasticity 23 (3), 516 – 543.

Panthi, S., Ramakrishnan, N., Ahmed, M., Singh, S. S., Goel, M., 2010. Finite element analysis of sheet metal bending process to predict the springback. Materials and Design 31 (2), 657 – 662.

Pereira, M., Asgari, A., De Souza, T., Rolfe, B., Dingle, M., Hodgson, P., 2005. Sheet forming simulation and springback prediction for AHSS automotive components. Materials Science and Technology 4, 51 – 62.

Perez, R., Benito, J., Prado, J., 2005. Study of the inelastic response of TRIP steels after plastic deformation. ISIJ International 45 (12), 1925 – 1933.

Press, W., Teukolsky, S., Vetterling, W., Flannery, B., 1992. Numerical recipes in FORTRAN: the art of scientific computing. Cambridge Univ Pr.

Rivero, M., Rodriguez-Germa, L., Trujillo, J. J., Pilar Velasco, M., 2010. Fractional operators and some special functions. Computers and Mathematics with Applications 59 (5), 1822 – 1834.

Schwarze, M., Vladimirov, I. N., Reese, S., 2011. Sheet metal forming and springback simulation by means of a new reduced integration solid-shell finite element technology. Computer Methods in Applied Mechanics and Engineering 200 (5-8), 454 – 476.

Shan, T., Liu, L., 2011. Springback prediction of the TRIP sheet steel stamping. Advanced Materials Research 221, 152 – 158.

Silvestre, E., Mendiguren, J., de Argandoña, E. S., Galdos, L., 2012. Roll levelling numerical simulation using a nonlinear mixed hardening material model. Steel Research International special issue, 1295 – 1298.

Souza, T. D., Rolfe, B., 2010. Characterising material and process variation effects on springback robustness for a semi-cylindrical sheet metal forming process. International Journal of Mechanical Sciences 52 (12), 1756 – 1766.

Sun, L., Wagoner, R., 2011. Complex unloading behavior: Nature of the deformation and its consistent constitutive representation. International Journal of Plasticity 27 (7), 1126 – 1144.

Taherizadeh, A., Ghaei, A., Green, D., Altenhof, W., 2009. Finite element simulation of springback for a channel draw process with drawbead using different hardening models. International Journal of Mechanical Sciences 51 (4), 314 – 25.

Thibaud, S., Boudeau, N., Gelin, J., 2002. Influence of initial and induced hardening in sheet metal forming. Int. J. Damage Mech 13, 107 – 122.

Timoshenko, S., Goodier, Y., 1968. Teoría de la elasticidad. Urmo.

Tomita, Y., Iwamoto, T., 1995. Constitutive modeling of TRIP steel and its application to the improvement of mechanical properties. International Journal of Mechanical Sciences 37 (12), 1295–1305.

Vrh, M., Halilovic, M., tok, B., 2008. Impact of Young's modulus degradation on springback calculation in steel sheet drawing. Journal of Mechanical Engineering 54 (4), 288 – 296.

Wagoner, R., Geng, L., 2002. Role of plastic anisotropy and its evolution on springback. International Journal of Mechanical Sciences 44 (1), 123 – 148.

Weidner, A., Glage, A., Biermann, H., 2010. In-situ characterization of the microstructure evolution during cyclic deformation of novel cast TRIP steel. Procedia Engineering 2 (1), 1961 – 1971.

Yanagimoto, J., Oyamada, K., 2006. Springback-free isothermal forming of high-strength steel sheets and aluminum alloy sheets ander warm and hot forming conditions. ISIJ International 46 (9), 1324 – 1328.

Yoshida, F., Uemori, T., Fujiwara, K., 2002. Elastic plastic behaviour of steel sheets under in plane cyclic tension compression at large strain. International Journal of Plasticity 18, 633 – 659.

Yu, H. Y., 2009. Variation of elastic modulus during plastic deformation and its influence on springback. Materials and Design 30 (3), 846 – 850.

Zhou, C., Liao, J., Zhu, Y., Chen, Z., 2010. A method of springback prediction and tool shape compensation for multi-curvature sheet metal bending. AIP Conference Proceedings 1252, 868 – 874.